Molecular basis for the enzymatic macrocyclization of multiply backbone N-methylated peptides

Emmanuel Matabaro3#, Haigang Song1,2#, Fabio Gherlone3, Lukas Sonderegger3, Andrew Giltrap1, Sam Liver1, Alvar Gossert4, Markus Künzler3*, James H Naismith1,2*

[1] Structural Biology, The Rosalind Franklin Institute, Harwell Science & Innovation Campus, Didcot, UK. OX11 0QS
[2] Division of Structural Biology, University of Oxford, The Wellcome Centre for Human Genetics, Headington, Oxford, UK. OX3 7BN
[3] Institute of Microbiology, Department of Biology, ETH Zürich, Vladimir-Prelog-Weg 4, CH-8093 Zürich, Switzerland
[4] Biomolecular NMR Spectroscopy Platform, Department of Biology, ETH Zürich, Otto-Stern-Weg 5, CH-8093 Zürich, Switzerland

#equal contribution
*correspondence to (MK for protein and peptide production and function, JHN for protein structure and molecular mechanism)

Abstract

OphP is an essential enzyme for the biosynthesis of the macrocyclic peptide natural product omphalotin A. The enzyme has been proposed to proteolytically release a peptide intermediate from the precursor protein OphMA and to macrocyclize the multiply α-N-methylated core of this intermediate to produce omphalotin A. Our *in vitro* experiments demonstrate that OphP does not process OphMA but shows robust macrocyclase activity on pre-processed α-N-methylated peptides. We conclude that *in vivo,* an as yet, unidentified fungal protease liberates the peptide substrate from OphMA. OphP tolerates sequence promiscuity in the substrate but has a preference for highly α-N-methylated substrates and for N-methylated glycine residue at the catalytic site. The promiscuity of OphP is explained by structural analysis of co-complexes which reveals a predominantly hydrophobic substrate binding cleft with few interactions between substrate side chains and OphP. These structures also describe a small and hydrophobic P1 pocket that we propose rationalizes the preference for N-methylated glycine. Our data suggests a substrate entry path that is different from other members of the POP family. Since macrocyclic peptides with multiple backbone N-methylations such as omphalotin A possess potent biological activity, exploitation of enzymes to produce such compounds is highly desirable.

Introduction

Despite violating Lipinski's rule of five[1], some peptide macrocycles show potent biological activity. This is because the macrocyclization restricts the bond rotations of the peptide backbone and, thus, the favourable conformation of the peptide has a much lower entropic penalty for target engagement[2,3]. In addition, peptide macrocycles are metabolically more stable as they are intrinsically resistant to proteases, and generally show an improved membrane permeability and oral availability when compared to linear peptides[4]. Macrocycles are in clinical use against G-protein coupled receptors and protein-protein interfaces, targets of which the latter are traditionally challenging for small (Lipinski compliant) molecules[5,6]. Peptide macrocycles are particularly attractive for drug development due to their modular structure and potential chemical diversity arising from the flexible choice of building blocks (natural and unnatural amino acids, α-N-methylated amino acids, D-amino acids, β-amino acids, heterocyclised amino acids and thioamides). Macrocyclization of peptides can be accomplished by linking two or more functional groups together forming amide, lactone, ether, thioether, or disulfide bonds[7–9]. There are powerful routes to synthetic peptide macrocycles with simple amino acids, but synthesis with more complex building blocks that can significantly improve the potency and pharmacokinetics are challenging. As a consequence, natural products remain the main sources of marketed peptide macrocycle drugs[10].

Naturally occurring peptide macrocycles are produced by two broad pathways, resulting in non-ribosomal peptides (NRPs) and ribosomally synthesized and post-translationally modified peptides (RiPPs). In the case of NRPs, multidomain megaenzymes, non-ribosomal peptide synthetases (NRPS), catalyse the synthesis of the linear peptides from proteinogenic and non-proteinogenic amino acids using linearly arranged, amino acid specific modules in an assembly line fashion. The macrocylization of NRPs is mediated by a final thioesterase domain of the NRPS in bacteria or a condensation-like domain in fungi[11–13]. Several enzyme classes catalyse macrocyclization of RiPPs, including PatG in patellamide biosynthesis[14,15], GmPOPB in fungal amatoxin[16,17], and PCY1 in plant orbitide[18,19,20]. Mechanistically, these enzymes first cleave off a C-terminal sequence (the follower peptide) from the ribosomally synthesized precursor peptide, forming an acyl enzyme intermediate which is then decomposed intramolecularly by the nucleophilic attack of the free amino terminus of the peptide substrate to form the macrocycle. The macrocyclase domain of PatG belongs to the S8 family of subtilisin-type serine peptidases (https://www.ebi.ac.uk/merops/) and recognizes a four-residue follower peptide and a preceding heterocyclic ring residue[15,21,22]. PatG tolerates a wide range of peptide substrates but is slow[23–25]. PCY1 and GmPOPB belong to post-proline cleaving prolyl oligopeptidases (POP) of the S9A family of serine peptidases (https://www.ebi.ac.uk/merops/). GmPOPB is a dual function macrocyclase as it sequentially catalyses the removal of a leader and follower sequence from the same peptide substrate (precursor peptide)[16,17,26]. PCY1 relies on an additional protease to first remove the leader sequence to create the substrate for macrocyclisation[18]. Structural and biophysical analysis shows that both PCY1 and GmPOPB recognise the residues in the follower region for substrate binding and catalysis[19,20]. Butelase 1, a fast and promiscuous cyclase from the asparaginyl endopeptidase (AEP) family, has been reported to recognize the C-terminal Asn/Asp-His-Val motif of its substrate peptide, cleave off C-terminus and ligate the exposed Asn/Asp to the N-terminus of substrate[27,28].

A considerable fraction of naturally occurring macrocyclic peptides is backbone N-methylated at one or multiple amino acids. The function of backbone N-methylation of peptides is to enhance their conformational rigidity, membrane permeability, protease

resistance and – most relevant in their use as drugs – oral availability[29,30]. GmPOPB and PCY1 have been shown to catalyse the macrocyclization of singly backbone N-methylated linear peptides[20,31] but no enzyme has been characterised which can efficiently macrocyclise multiply backbone N-methylated peptides. Synthesis and macrocyclization of peptides with multiple backbone N-methylations by entirely chemical means[2,3,32] is challenging. Yet, they have enormous potential, as demonstrated by the most well-known example, cyclosporin A, an orally available natural product used as an immunosuppressant during organ transplantation[33]. The macrocycle consists of 11 amino acids, 7 of which are backbone N-methylated and 3 are non-proteinogenic[34]. The oral availability is a consequence of its chameleon-like property where the molecule reversibly switches between a non-polar arrangement for membrane transit and a polar arrangement for water solubility[35,36]. The conformational flipping depends on the methylated backbone. Cyclosporin A is synthesised by an NRPS pathway with methylations pre-installed on the building blocks prior to peptide bond formation and ring closure by condensation[37,38].

The peptide natural product at the center of this study is omphalotin A, a 12-residue macrocyclic RiPP with 9 backbone N-methylations. The molecule is produced by the wood-degrading fungus *Omphalotus olearius* and has anti-nematode activity[39]. Two posttranslationally modifying enzymes, a peptide α-N-methyltransferase, OphMA, and a serine peptidase of the S9A family (https://www.ebi.ac.uk/merops/), OphP, contribute to its biosynthesis[40,41]. OphMA catalyses the iterative backbone N-methylation of the amide bonds within the core peptide which is its own C-terminus. The enzyme uses SAM as cofactor and has promiscuity towards both proteinogenic hydrophobic, aromatic, small hydrophilic and also non-proteinogenic amino acid residues[42–44]. Coexpression of OphMA and OphP in the yeast *Pichia pastoris* yielded omphalotin A and swapping of the core peptide in OphMA with sequences for lentinulin A and dendrothelin A led to the production of the respective backbone N-methylated macrocycles, consistent with a promiscuous and functional biosynthetic pathway of the two enzymes[41,45] (**Figure 1a**). Based on these data and the sequence similarity between the two enzymes, it was hypothesized that OphP, like GmPOPB[17], possesses two catalytic activities: (1) cleavage of the OphMA protein at the N-terminus of the backbone N-methylated core peptide (proteinase activity) and (2) cleavage of the released precursor peptide at the C-terminus of the core peptide and formation of an acyl-enzyme intermediate. The chemical difference between macrocyclization and proteolysis is the decomposition of the intermediate by nucleophilic attack of the free N-terminus (macrocyclase activity) or water (protease activity) (**Figure 1a**)[41,45,46]. Consequently, macrocyclases commonly exhibit proteolytic activity[41,45,46].

The promiscuity of OphMA[40–43], and OphP [45] enables biotechnological applications including the generation of libraries of multiply backbone N-methylated macrocyclic peptides[47]. A dual function of OphP – proteinase and macrocyclase – would significantly extend the activity spectrum of the POPB family of dual-function macrocyclases, which to date operate on relatively short peptides (the longest so far is 35 amino acid residues seen in GmPOPB[16,17]). Equally important, OphP would be the first macrocyclase with specificity for backbone N-methylated peptide substrates and the first example of this family which requires a rather short C-terminal recognition sequence. Here, we characterize OphP *in vitro* and find no evidence for its proteinase activity. In addition, in contrast to other macrocyclase systems, the enzyme appears to be insensitive to the sequence of the C-terminal recognition sequence (follower peptide). Structural and biochemical analysis shows that the enzyme rather acts on OphMA-derived, backbone N-methylated peptides and recognizes a backbone N-methylated

137 glycine residue within the OphMA core peptide. This knowledge will enable the exploitation
138 of the pathway for the production of novel methylated peptide macrocycles.
139

Results

OphP does not cleave the precursor protein OphMA

OphP was purified from *P. pastoris* as an N-terminal His_8SUMO* fusion protein (**Figure 1-Figure supplement 1**) and confirmed to be catalytically active using a standard chromogenic substrate for POPs, benzyloxycarbonyl-Gly-Pro-p-nitroanilide (Z-Gly-Pro-4-pNA)[48] (**Figure 1-Figure supplement 2a,b**). OphP showed a maximal activity at 30°C and pH 6.0. This activity was reduced by Z-Pro-prolinal (ZPP), a common covalent inhibitor for POPs, but the enzyme was not inhibited as strongly as other members of the family[49] (**Figure 1-Figure supplement 2c**). Full-length OphMA was expressed in *E. coli* for 72 hours and purified as previously described[40,42,50]. The purified protein is a mixture of different species regarding the degree of backbone N-methylation with the predominant protein species containing 10 methylations (includes one residue in the follower peptide) (**Figure 1a**). Co-incubation of the intact protein with purified and catalytically active OphP showed no detectable peptide product (LC-MS) nor did we observe any mass loss of OphMA (ESI-MALDI-ToF) (**Figure 1-Figure supplement 3**). The experiment was repeated by purifying OphMA with a lower degree of methylation (predominantly zero, one or two methylations) (**Figure 1b**) and again we detected no turnover by OphP. This experiment was repeated in the presence of SAM, where, as expected, OphMA converts itself to the completely methylated state over time. No cleavage of OphMA or generation of omphalotin A was observed (**Figure 1b**). Co-expression of full-length OphMA (N-terminal His_8-tag) and OphP (N-terminal His_8SUMO* fusion) in *Pichia pastoris* was performed as previously described[45,46]. Since both proteins are His-tagged, they co-purified on a metal affinity column, however, on a subsequent size exclusion column, they separated without any evidence for any complex formation (**Figure 1-Figure supplement 4, 5**). Based on these data, we conclude that OphP is not able to cleave the completely methylated OphMA protein at Pro399 or any other position.

OphP macrocyclizes OphMA-derived, multiply backbone N-methylated peptides

To characterize the presumed peptidase and/or macrocyclization activity of OphP, we tested a variety of backbone N-methylated OphMA-derived peptides, consisting of leader, core and follower sequences, for *in vitro* processing by OphP. Since, in our hands, the chemical synthesis of methylated or unmethylated C-terminal peptides of OphMA failed (an issue we attributed to their highly hydrophobic character), we produced variants of recombinant OphMA protein containing cleavage sites for the tobacco etch virus (TEV) protease in the unmethylated leader peptide region in various distances from the core peptide. The OphMA variants were expressed for a sufficient period in *E. coli* to allow backbone N-methylation to proceed, purified and processed by TEV protease and either GmPOPB[17] or ProAlanase (Promega, Madison WI, USA) to remove the leader. The peptides were purified by preparative HPLC (**Figure 2a**). Briefly, Oph-24mer and -21mer contain the follower peptide (S-V-M-S-T-E), the 12-residue core and different portions of the leader peptide. Two additional 21mers, denoted as Led-21mer and Dbi-21mer, contain a short three-residue leader (G-F-P), the 12-residue cores and the follower peptides (S-V-V-S-S-A) of the lentinulin A and dendrothelin A precursor proteins, LedMA and DbiMA1[45,46], respectively (**Figure 2a, Figure 2-Figure supplement 1**). Two Oph-18mers were produced, one containing the core and follower (S-V-M-S-T-E), but no leader peptide (denoted as Oph-18mer^{NL}) and the other one containing a short leader (G-F-P) and the follower (S-V-M-S-T-E), and a truncated core peptide lacking the three C-terminal residues (denoted as Oph-18mer^{Tr}) (**Figure 2a**). Finally, we produced an Oph-15mer containing the G-F-P leader and the 12-residue core but lacking the follower peptide (**Figure 2a**). MS analysis indicated that the Oph-21mer, Oph-24mer, Dbi-21mer, and Led-21mer peptides contained up to ten methylations, both the Oph-18mer^{Tr} and Oph-18mer^{NL} peptides had up to 8 methylations and the Oph-15mer carried 7

methylations (**Figure 2-Figure supplement 1, 2**). All our attempts to produce and purify non-methylated peptide substrates, using either the catalytically inactive R72A mutant of OphMA or maltose-binding protein fusions of C-terminal parts of OphMA, failed due to the insolubility of the peptides.

Incubation of the Oph-24mer, -21mer, -18mer^{Tr} and -15mer with OphP, all produced cyclic peptides but in each case the leader peptides were incorporated into the product (**Figure 2a, 2b**). The linear Oph-24mer peptide yielded a mixture of the cyclic 15-residue cyclo(S-Q-N-G-F-P-W-^{me}V-I-^{me}V-^{me}V-^{me}G-^{me}V-^{me}I-^{me}G) ($[M+H]^+$=1651.958) and the cyclic 18-residue cyclo(S-Q-N-G-F-P-W-^{me}V-I-^{me}V-^{me}V-^{me}G-^{me}V-^{me}I-^{me}G-V-^{me}I-^{me}G) ($[M+H]^+$=1949.163) (^{me} denotes backbone N-methylation (**Figure 2b, Figure 2-Figure supplement 3**). The linear Oph-21mer peptide yielded the cyclic 12-residue cyclo(G-F-P-W-^{me}V-I-^{me}V-^{me}V-^{me}G-^{me}V-^{me}I-^{me}G) ($[M+H]^+$=1322.824) and the cyclic 15-residue cyclo(G-F-P-W-^{me}V-I-^{me}V-^{me}V-^{me}G-^{me}V-^{me}I-^{me}G-V-^{me}I-^{me}G) ($[M+H]^+$=1620.0293) (**Figure 2c, Figure 2-Figure supplement 3**). The linear Oph-18mer^{Tr} and -15mer peptides both produced cyclic dodecapeptide cyclo(G-F-P-W-^{me}V-I-^{me}V-^{me}V-^{me}G-^{me}V-^{me}I-^{me}G) in the LC-MS (**Figure 2d, S7, S9**). Noteworthy, linear peptide product (G-F-P-W-^{me}V-I-^{me}V-^{me}V-^{me}G-^{me}V-^{me}I-^{me}G) is also detected which is typical for peptide macrocyclases and a consequence of the inherent peptidase activity of these enzymes[17] (**Figure 2d**, **Figure 2-Figure supplement 4**). Incubation of OphP with longer linear substrates such as the OphMA C-terminal tryptic fragment (Oph-30mer) were not processed by OphP (**Figure 2a**).

Native cyclopeptides are obtained after proteolytic removal of the leader peptide

Since OphP did not process the leader peptide leading to non-native cyclopeptides, we tested if prior removal of the leader peptide by other proteases would yield native peptide natural products. Indeed, removal of the leader peptide from Oph-24mer (leading to 18mer^{NL}), Oph-21mer (leading to 18mer^{NL}), Led-21mer (leading to Led-18mer^{NL}) and Dbi-21mer (leading to Dbi-18mer^{NL}) by GmPOPB or ProAlanase (**Figure 2a, Figure 2-Figure supplement 4**) and subsequent incubation with OphP led to the formation of omphalotin A, lentinulin A and dendrothelin A, respectively (**Figure 2e**). In contrast, incubation of these peptides with the dual function GmPOPB did not yield any cyclic product (**Figure 2-Figure supplement 4**). Also, incubation of ProAlanase-treated Oph-18mer^{Tr} and Oph-15mer with OphP did not result in any conversion, suggesting that OphP is not able to form macrocycles of 9 rather than 12 residues (**Figure 2a**).

OphP prefers highly methylated peptide species including an α-N-methylated glycine residue at the P1 site

A closer analysis of the data revealed that not all peptides were cyclized equally well, but that highly methylated species were preferred. MS analysis of purified Oph-18mer^{NL} showed predominantly 10 methylations with 4- to 11-fold methylated species being present (11th methylation of the Met414 residue in the follower peptide). Incubation of Oph-18mer^{NL} with OphP showed that OphP converted 10- and 11-fold methylated peptides more readily than 9-fold methylated peptides and failed to convert less methylated peptides (**Figure 3a**). It needs to be noted, that OphMA methylates the core peptide residues in a sequential manner from the N- to the C-terminus[40]. The 9-, 10- and 11-fold methylated species thus all have ^{me}Gly at the cleavage site while the others do not. The Oph-18mer^{Tr} was purified as a mixture of 2- to 8-fold methylated species; the 8-fold methylated species (G-F-P-W-^{me}V-I-^{me}V-^{me}V-^{me}G-^{me}V-^{me}I-^{me}G-S-^{me}V-M-S-T-E) was converted faster than the 7-fold methylated species (G-F-P-W-^{me}V-I-^{me}V-^{me}V-^{me}G-^{me}V-^{me}I-^{me}G-S-V-M-S-T-E) and species lacking ^{me}Gly were not processed (**Figure 3a**). In case of the Oph-15mer substrate, first the 7-fold methylated

peptide species was processed, resulting in cyclo(G-F-P-W-^{me}V-I-^{me}V-^{me}V-^{me}G-^{me}V-^{me}I-^{me}G), and only after its complete consumption, cyclo(G-F-P-W-^{me}V-I-^{me}V-^{me}V-^{me}G-^{me}V-^{me}I-G) from the 6-fold methylated substrate was produced. (**Fig3a, 3b, 3c**). These results show that OphP has a strong preference for an α-N-methylated glycine residue at the P1 site.

OphP has an unusual tunnel that could allow access to the active site

OphP shares 35% and 38% sequence identity to PCY1 from *Saponaria vaccaria* and GmPOPB from *Galerina marginata*, respectively, including conservation of the putative catalytic triad residues Ser580, Asp665 and His701 (**Figure 4-Figure supplement 3**). Despite these similarities, OphP has two remarkable features that distinguish it from these and other members of the POP family; its preference for multiply backbone N-methylated substrates including a ^{me}Gly residue (rather than a proline residue) at the P1 site, and the apparent lack of a site for the recognition of the substrate C-terminus (follower peptide). In order to elucidate the structural basis of these differences, we determined the crystal structures of OphP alone (apo form) and in complex with substrates and inhibitors.

We first determined the structure of the putatively catalytically inactive OphP variant S580A. The structure of the apo form was determined in space group P1 (eight monomers in the asymmetric unit) to 1.9 Å by molecular replacement using GmPOPB structure (PDB entry 5N4C) as the search model. Visual analysis and the PISA server suggest OphP is a monomer in the crystal which is consistent with estimation from gel filtration (**Figure 1-Figure supplement 4**) and other POP enzymes. The eight monomers differ only in flexible loops some of which are involved in crystal contacts. Similar to other POPs, the monomer has two domains, an α/β hydrolase domain (residues 1–82, 453–738) and the seven-bladed β-propeller domain (residues 83–452) (**Figure 4a**). All the monomers in the asymmetric unit adopt a "closed" conformation with the two domains packed against each other. OphP is most similar to GmPOPB (5N4B) with a root-mean-square-deviation (RMSD) of 1.5 Å over 686 residues and closely related to PCY1 (5O3W, RMSD of 1.7 Å over 650 residues) with a more distant relation to porcine muscle POP (1QFS, RMSD of 1.7 Å over 650 residues). Examination of the surface of OphP revealed a large and neutral, hydrophobic tunnel in the middle of the β-propeller domain that connects to the putative active site with its key residue S580 (**Figure 4-Figure supplement 1**). Structure alignment between OphP and GmPOPB confirmed the putative catalytic triad with some deviations regarding the position of its histidine residue (**Figure 4a**). His701 of OphP sits in a flexible loop region (Leu697–Thr707) which is only resolved in two chains (chain A and chain H) where it adopts different conformations (**Figure S11**). Although chain A and H have different arrangements of this loop, in both His701 is around 15 Å away from Ser580 and a structural re-arrangement is required to form the canonical catalytic triad.

We determined the covalent complex structure of OphP with ZPP by soaking wild-type OphP crystals with 5 mM ZPP overnight. The structure of the complex was determined at 2.0 Å resolution. Additional electron density, which we fitted as ZPP covalently linked to S580 (**Figure S11**) was seen in two subunits. The other two subunits had weak electron density suggesting low occupancy. The overall structure of the OphP:ZPP complex is largely unchanged from the apo structure of S580A (0.5 Å over 716 Cα atoms) (**Figure 4-Figure supplement 2**). There are differences in loops Leu139–Ala146, Ser164–Met171, Ser179–Met195, Pro222–Gly230, Leu696–Ser706 and Ala622–Tyr664. As a result, His701 has moved closer (7.6 Å to serine) to both Asp665 and Ser580 to form the catalytic triad (**Figure 4-Figure supplement 2**). The carbonyl at P1 proline of the ZPP(acyl)-enzyme intermediate hydrogen bonds to the backbone amide of Asn581 and the side chain hydroxyl of Tyr499.

The carbonyl at the P2 proline of ZPP interacts with the guanine sidechain of Arg667 which also salt bridges to Asp169 (**Figure 4-Figure supplement 2**). The benzene ring of ZPP is located in an aromatic hydrophobic pocket. These results confirm Ser580 as the key catalytic residue and suggest a structural re-arrangement of active site residues including His701 upon substrate binding.

^{me}Gly is positioned in the active site

To characterize the interactions of OphP with its presumed natural substrate, S580A mutant crystals were soaked with a ten-fold methylated Oph-18mer^{NL} (W1-^{me}V2-I3-^{me}V4-^{me}V5-^{me}G6-^{me}V7-^{me}I8-^{me}G9-V10-^{me}I11-^{me}G12-S13-^{me}V14-M15-S16-T17-E18) and a seven-fold methylated Oph-15mer substrate (G1-F2-P3-W4-^{me}V5-I6-^{me}V7-^{me}V8-^{me}G9-^{me}V10-^{me}I11-^{me}G12-V13-I14-G15) (**Figure 2a**) (both substrates yield dodecameric macrocycles with the underlined residues). The Oph-18mer^{NL} complex was obtained at 2.0 and the Oph-15mer complex at 2.5 Å resolution. The overall structures superimpose well with the apo structure with an RMSD of 0.4 Å over 715 Cα atoms (Oph-18mer^{NL}) and 0.8 Å over 714 Cα atoms (Oph-15mer). The substrate peptide is located at the interface between two domains with its N-terminus extending into the β-propeller domain and its C-terminus contacting the hydrolase domain (**Figure 4b**). Substrate binding has displaced both a glycerol and water molecules found in the apo structure. For Oph-18mer^{NL}, we focus on subunit A which has the clearest density for the substrate (**Figure 4c**). There is some weak electron density for the loop (698–704) which contains the catalytic histidine His701, but we did not model it. Only residues ^{me}I8-^{me}G9-V10-^{me}I11-^{me}G12-S13-^{me}V14 were fitted to the electron density whilst the remainder were presumed to be disordered (**Figure 4c**). The side chain of ^{me}I8 packs against Arg316 whilst ^{me}G9 makes almost no contact; the side chain of V10 interacts strongly with the aromatic ring of Phe617, ^{me}I11 makes a similar interaction with Phe502 whilst its N-methyl group points to solvent (**Figure 4d**). The N-methyl group ^{me}G12 contacts the indole ring of Trp621 and sits in the P1 pocket which is also formed by Ile606 and Phe502. S13 and ^{me}V14 make few interactions. The peptide bond of ^{me}G12 is positioned for nucleophilic attack by Ser580. The hydroxyl of Tyr499 and the backbone amide of Asn581 are well-positioned to function as the canonical oxyanion hole pair to stabilize the tetrahedral intermediate formed by the nucleophilic attack of Ser580.

The P1 binding pocket that accommodates ^{me}G12 is primarily formed by Ile606 and Trp621. To investigate the role of Ile606 and Trp621 on substrate recognition and catalysis, we produced OphP variants I606A and W621A. Incubation with Oph-15mer (in almost exclusively 7-fold methylated form) showed that I606A is only slightly less active than the native enzyme while W621A had no activity, suggesting it is essential (**Figure 4g**). We hypothesised that Ile606 might restrict the volume of the P1 pocket thus introducing selectivity. To test this we explored whether bulkier side chains at P1 could be process by the I606A variant of OphP. Unfortunately, we were unable to purify G12V and G12L substrate variants of Oph-15mer and the variant G12A resulted in a complex mixture that prevented further analysis.

OphP's promiscuity in substrate recognition

In the Oph-15mer complex, residues G1-F2-P3-W4-^{me}V5-I6-^{me}V7-^{me}V8-^{me}G9-^{me}V10-^{me}I11 were located in the electron density in subunit D (**Figure 4e**) but there is evidence of disorder in the peptide. The two complexes overlay with an RMSD of 0.9 Å over 719 residues. In contrast to the Oph-18mer^{NL} complex structure, residue ^{me}G12 which is attacked by Ser580 to generate the macrocycle is not at the P1 pocket (**Figure 4f**). Rather the peptide bond of ^{me}V8 is closest to this residue (**Figure 4f**). The peptide adopts a different conformation in the active site and as a result, the side chains in this complex make different interactions than the

340 18mer^{NL} (**Figure 4f)**. The substrate is not aligned properly for catalysis as the carbonyl of
341 ^{me}Val8 is tilted and no longer hydrogen bonds to the canonical oxyanion hole. The side chain
342 of ^{me}V8 contacts Ile606 and Trp621 in the hydrophobic P1 pocket identified in the 18mer^{NL}
343 complex. **(Figure 4f)**. This complex demonstrates the plasticity of peptide recognition by
344 OphP – rather than disclosing additional mechanistic insights – and perhaps explains its
345 rather broad substrate specificity, as there don't seem to be clearly specific interactions with
346 the substrate except for the P1 pocket residue.

Discussion

The multiply backbone N-methylated peptide macrocycle omphalotin A from *Omphalotus olearius* originates from a RiPP pathway involving a peptide auto-α-N-methylating enzyme OphMA and the serine peptidase OphP[40,41,45]. Similar macrocyclic peptides, lentinulin A and dendrothelin A, both with nine-fold backbone N-methylations have been isolated from *Lentinula edodes* and *Dendrothele bispora* harboring biosynthetic gene clusters containing OphMA and OphP homologs[45] (**Figure 1a**). The simplest model of the biosynthetic pathway is that OphP is a bifunctional enzyme, that (1) cleaves the precursor protein OphMA and (2) cleaves and macrocyclizes the released C-terminal precursor peptide to yield the final product omphalotin A. The active site of OphP is defined by the position of Ser580, the nucleophilic serine, which is conserved in all POP enzymes. It is this residue that formed a covalent complex with the ZPP inhibitor.

An additional protease is required to make omphalotin A

Our *in vitro* experiments with a chromogenic peptide substrate showed peptidase activity of purified OphP. However, in experiments with full-length OphMA, OphP showed no binding to or cleaving of full-length OphMA irrespective of its methylation state (**Figure 1b**). We considered three explanations, firstly our purification protocols have inactivated the protease activity of OphP. We ruled this out because OphP macrocyclase activity, which would seem certain to use the same catalytic residues, was unambiguously demonstrated (**Figure 2**). Moreover, where leader residues were present in the substrate peptides, these were incorporated into the product instead of being removed (**Figure 2a, 2b, 2c**). Finally, we detected no damage to OphP integrity and were able to crystallize the protein. The second explanation we considered was that another protein is required to destabilise the structure of methylated OphMA in such a way to expose the methylated peptide for OphP to cut. The lack of proteolytic activity of OphP on isolated peptides including extensive (12 residues) leader peptides argues against this "disordered" OphMA hypothesis. Further, structural analysis of OphP reveals that the active site is at the centre of the protein, thus binding the C-terminus of OphMA would require very significant conformational changes within the β-propeller domain of OphP. Similarly, the dual function macrocyclase GmPOPB also processes a smaller peptide and not a large protein. Methylation activity is similar in both highly purified OphMA and *in vivo*, thus it would seem unlikely there is an unidentified protein acting to destabilize OphMA[40,41,50]. Finally, such a hypothetical protein would be expected to be highly specific and therefore absent in *P. pastoris*[41,45,46], where the product can be made. Taken together, these observations led us to eliminate this explanation. The third explanation we considered, was the existence of another proteinase that cuts OphMA to expose the N-terminus of the substrate peptide. The structure of methylated OphMA at this presumed cleavage site is flexible and exposed to solvent,[50] thus accessible to a proteinase. In the segetalin A (a peptide macrocycle) pathway an additional proteinase, oligopeptidase (OLP1), cleaves off a leader peptide from the precursor peptide to generate the substrate for the POP macrocyclase PCY1[18], thus, establishing the precedent for this third hypothesis (albeit with a peptidase rather than a proteinase) However, no candidate for such a proteinase has been identified in the gene clusters reported for the biosynthesis of omphalotin A in *O. olearius* (or homologs in *L. edodes* and *D. bispora*[40,41,51]) and an absolutely required, specific protease is implausible given the heterologous production of the macrocycle in the *P. pastoris*[41,45,46]. It remains possible that there is a specific protease in these filamentous fungi that is (partially) compensated for by an unspecific protease in *P. pastoris*[41,45,46].

Substrate entry to the active site

396 Substrate binding by POP family enzymes has been proposed to occur by two different
397 mechanisms. The original one, based on the study of porcine muscle prolyl oligopeptidase[52,53],
398 involves the opening of the central tunnel of the β-propeller domain with blades 1 and 7
399 acting as the gate. An alternative mechanism with a hinge between the two domains giving
400 rise to an open (substrate binding/product release) and closed (catalysis) form of the enzyme,
401 was put forward based on the discovery of open conformation structures of several POP
402 enzymes [17,54–56] and molecular dynamics studies[57]. Apo S580A crystallized in a closed
403 conformation in the absence of ligand (**Figure 4a**). Nevertheless, we obtained both Oph-
404 18mer^{NL} and Oph-15mer co-complexes by soaking the peptide substrates into crystals where
405 packing would seem to prevent the conformational changes proposed in either mechanism.
406 The possibility of large-scale conformational change and annealing in the crystal seems
407 unlikely. Inspection of the electrostatic surface of the protein revealed only two plausible
408 routes for these peptides to reach the active site. The first is an entrance between the two α/β
409 and β-propeller domains (the side cavity) (**Figure 4-Figure supplement 1**). Such side entry
410 was observed in dipeptidyl peptidase IV, a prolyl-specific exopeptidase[54,58,59]. However, this
411 side cavity was much larger than that of apo OphP. In OphP, this side cavity is likely to be
412 further obscured by the disordered loops Pro222–Gly230 and Leu697–Gly704. Moreover, the
413 side cavity is charged and thus a poor match for a hydrophobic substrate (**Figure 4-Figure**
414 **supplement 1**). The second and more favored route is the central hydrophobic tunnel (**Figure**
415 **5a, Figure 4-Figure supplement 1**). Compared to the other POP enzymes (1QFS, 5O3U and
416 5N4B), this tunnel is wider and can accommodate e.g. a tryptophan side chain (**Figure 4-**
417 **Figure supplement 1)**. This route of substrate entry is new for the POP family.
418
419 ***Structural basis of substrate promiscuity***
420 PCY1 and GmPOPB recognize a six-residue sequence (follower peptide) at the C-terminus of
421 the precursor peptide located adjacent to the core peptide[17,19,20]. The crystal structures show
422 no specific interaction of OphP with follower residues in either 15- or 18-residue substrates.
423 The six follower residues of the presumed substrate when added as a stand-alone peptide
424 showed no binding by ITC (**Figure 2-Figure supplement 5**) nor gave a complex (soaking or
425 co-crystallization). Moreover, a comparison of the various substrate peptides processed by
426 OphP (**Figure 2a**) shows no conservation of the length or amino acid sequence of the
427 follower peptides. We conclude that OphP does not utilize the C-terminal follower peptide as
428 a recognition sequence, in contrast to GmPOPB and PCY1[16,19,20,26]. OphP tolerated sequence
429 variations within the core peptide, demonstrated by the incorporation of different leader
430 residues, the ability to choose an alternate ^{me}Gly in the core peptide and to produce
431 omphalotin A, lentinulin A, dendrothelin. Structural data which show no recognition at all of
432 the residues at the N-terminus of the substrates reveal that the interactions between OphP and
433 the substrate side chain (**Figure 4d)** are dominated by unspecific hydrophobic contacts. This
434 is reminiscent of the promiscuity of the peptide auto-α-N-methyltransferase activity of
435 OphMA[45,46].
436
437 ***The P1 pocket favors N-methyl glycine***
438 In the 18mer^{NL} complex, Tyr499 hydrogen bonds to the carbonyl of ^{me}G12 that becomes the
439 tetrahedral intermediate (P1 residue) (**Figure 4d**). A different conformer of the side chain of
440 Arg667 would contribute to the stabilization of the negatively charged intermediate. Both of
441 these residues are found in other members of the POP family where they play a similar role[52].
442 Analysis of the products from the various substrates revealed that ^{me}Gly was the point of
443 macrocyclization (P1 site) with one exception. Using the Oph-15mer substrate, a variant with
444 a non-methylated glycine was converted but only after all ^{me}Gly species was processed and
445 only with a high concentration of OphP (**Figure 3b, c**). In contrast to the requirement for Pro

at P1 which defines the POP family, OphP utilises methylated glycine (**Figure 3b, d, Figure 4-Figure supplement 3**). This substrate preference is consistent with the inability to cleave residues at the N-terminus. Analysis of ^{me}Gly12 in the crystal structure Φ and Ψ dihedral angles are similar to the prolines (P1 site) in structures of PCY1 (PDB 5O3U) and GmPOPB (5N4C) (**Figure 5b**). ^{me}Gly at P1 has additional hydrophobic contacts with Trp621 and Ile606 as a consequence of the N-methyl group (**Figure 4d**), these favourable interactions are not present for unmethylated glycine. Glycine residues are well known structurally for their wider range of permissible Φ and Ψ angles [60,61]. Since N-methylation profoundly reduces the array of favourable conformations[62] (**Figure 5b**), the entropic penalty for immobilisation of ^{me}Gly would be expected to be lower than for glycine.

^{me}Gly12 binds to a hydrophobic pocket formed by Trp621, Tyr625, Val668, Asn581, Phe502 and Ile606 (**Figure 5c**). The methyl group interacts with Trp621 consistent with the preference for methylated substrates, and W621A expectedly showed abolished cyclization activity (**Figure 4g**). All of these residues except for Ile606 are strictly conserved in POP enzymes as they are also involved in the coordination of Pro at P1 (**Figure 4-Figure supplement 3, Figure 5-Figure supplement 1**). In over one thousand prolyl oligopeptides sequences identified by a BLAST search mostly valine is found at the 606 position which creates a larger pocket and isoleucine is almost exclusively found in OphP and closely related methylated peptide macrocyclases (**Figure 4-Figure supplement 3, Figure 5-Figure supplement 1)**. A simple model of the Oph-18mer^{NL} complex which places a proline residue (or equivalently bulky side chain) at P1 will clash (distance < 2.5 Å) with Ile606 (**Figure 5d**). The OphP:ZPP complex has a proline group at the P1 site which results in Ile606 adopting an unfavorable conformation (**Figure 5d**). In the two subunits where there is weak density for ZPP, which attributes to low occupancy, Ile606 has remained in the preferred conformation. The requirement for the structural re-arrangement of Ile606 correlates with the lower-than-expected potency of ZPP as an inhibitor against OphP. In fact, only Gly and Ala would fit in this pocket without structural re-arrangement, consistent with the observed selectivity of the enzyme (**Figure 5e**).

In summary, we show that OphP is not a dual function proteinase/macrocyclase and that *in vivo* a third enzyme is almost certainly required for the production of ribosomally synthesized, backbone N-methylated peptide macrocycles from auto-α-N-methylating precursor proteins like OphMA. In addition, OphP recognises an N-methylated glycine rather than a proline residue at the P1 site of macrocyclization using a hydrophobic pocket that selects against residues larger than alanine whilst selecting for methylated amides. The hydrophobic and spacious nature of the substrate-binding pocket results in few specific contacts endowing OphP with substrate promiscuity and the unique ability to cyclize multiply methylated substrates. These unique properties of OphP may turn this enzyme into a valuable tool for producing highly α-N-methylated cyclic peptides for pharmaceutical applications.

Materials and methods

Cells, antibodies, and reagents

ProAlanase (mass spec grade) was ordered from Promega. Vectors for the expression of GmPOPB (plasmid PMA 1237: pJ414-GmPOPB) was previously described[17] and TEV (pRK793_MBP-TEV site-His6-TEV-C4) provided by Alvar Gossert (ETH Zurich, Switzerland). Phusion high-fidelity DNA polymerase was ordered from ThermoFisher Scientific (USA). Peptides AMA1 and PHA1 were chemically synthesized by GenScript Biotech (USA). The chromogenic substrate Gly-Pro-pNA and the POP inhibitor Z-Pro-prolinal were ordered from Sigma-Aldrich. Follower peptides and leader peptides were synthesized from Genscript.

Plasmid construction

The plasmids expressing OphP or LedP were constructed from pPIC3.5K-strepII-SUMO*Oph (PMA1382) and pPIC3.5K-StrepII-SUMO*LedP (PMA1379) that were previously used in omphalotin A production in *P. pastoris*[45]. The His-tag was introduced by PCR amplification to SUMO* using PMA1379 as a template, with primers His-SUMOSTAR-FW and His-SUMOSTAR-RV. The obtained fragment was cloned into *Spe*I and *BamH*I on plasmids PMA1382 and PMA1379 to generate pPIC3.5K-His8-SUMO*OphP (PMA1596) and pPIC3.5K- His8-SUMO*LedP (PMA1595), respectively. *ophP* S580A mutant obtained from PMA1374 (pCDFDuet-sMBP-OphP-S580A) by digestion with *Not*I and *Spe*I enzymes and exchanging it with *ophP* gene into PMA1596 using the same restriction sites. For most of the OphMA-TEV constructs, one common primer OphMA-Fw was used. For plasmids expressing OphMA-TEV-18mer, -DbiCterm and -LedCterm, primers ΔVIG-RV, DbiCterm-RV, LedCterm-RV were used together with OphMA-FW on PMA1488, respectively. The obtained PCR fragments were digested with *Not*I and *Nde*I and inserted in the respective sites on the pET24b vector. For OphMA-TEV-24mer, primer 24mer-RV was used, while for the OphMA-TEV-31mer and -38mer, primer pairs 31mer-RV1/31mer-RV2 and 38mer-RV1/38mer-RV2, respectively, were used on PMA1004. The PCR fragments were inserted into *Nde*I and *Nco*I of PMA1488. To generate OphMA-18mer-W400A and 18mer-intermediate, primers 18mer-W400A-RV1, 18mer-inter-RV were used on PMA1004, respectively. The PCR products were digested either with enzyme pair *Nde*I/*Not*I or *Nde*I/*EcoR*I and ligated into respective sites on the pET24b vector. In all cases, the plasmids were amplified in *E. coli* DH5α. Plasmid sequences were confirmed by Sanger sequencing. OphP-I606A and OphMAΔC6-G408A, OphMAΔC6-G408V, OphMAΔC6-G408L were created using reported protocols[66]. The used primers are listed in Table 1.

Plasmids PMA1488 (OphMA-21mer), PMA1304 (OphMA-15mer), pMA1498 (pCDFDuet-1_His_8-MBP-M378-TEVcs-core-SVMSTE, PJK54) were part of our plasmid library. They were used to generate 21mer, 15mer, non-methylated 21mer peptides, respectively. PMA1304 and PMA1488 were constructed from the plasmid PMA1004 (pET24-His_8-OphMA_cDNA) that was described earlier for expressing OphMA in *E. coli*[40]. PMA1498 was constructed by fusing the His_8MBP with the OphMA-TEV-21mer C-terminus (M378-E417). The hybrid gene was ligated into restriction sites *EcoR*I and *Hind*III of the vector pCDFDuet-1.

Production of recombinant OphP in *P. pastoris*

*Pichia pastori*s GS115 cells were transformed by electroporation using the plasmids pPIC3.5K-His8-SUMO*OphP or pPIC3.5K-His8-SUMO*LedP, linearized by *Bsp*EI for the integration into the *HIS4* locus. Transformants were selected first on a standard SD-HIS

538 minimal medium and then on 250 µg/ml geneticin for high-copy number screening. To
539 produce OphP, cells were cultured at 20 °C in a standard methanol-containing complex
540 medium (BMMY) for three days following the recommendations for *Pichia* protein
541 expression[67]. For harvesting, cells were separated from the culture medium by centrifugation,
542 and cell pellets were washed with cold lysing buffer (2xPBS) or double-distilled water (dd
543 H_2O) and centrifuged again at 8000 × *g* for 10 min at 4 °C. Cell pellets were resuspended in
544 cell lysis buffer [2xPBS, 10% glycerol, 1 mM DTT, 20 mM imidazole, and protease inhibitor
545 cocktail (PIC) (Roche)]. Cells lysis was performed on a planetary mill (Pulverisette 7) as
546 previously[67]. Cell debris are removed by spinning down the cell lysate at 16, 000 *x g* for 30
547 min at 4 °C. The cell lysate supernatant was collected and subjected to purification via a Ni^{2+}-
548 based immobilized metal affinity chromatography (Ni-IMAC) system using the washing
549 buffer (50 mM HEPES pH 8.0, 10% glycerol and 20 mM imidazole), and elution buffer
550 (50mM HEPES pH 8.0, 10% glycerol and 400 mM imidazole). The purified proteins were
551 stored in storage buffer (50 mM HEPES pH 8.0 + 10% glycerol + 5 mM DTT) at -80 °C. The
552 His_8SUMO* tag was cleaved off by incubation with TEV protease (1:10, w/w) in assay
553 buffer [300 mM NaCl, 50 mM TRIS pH 8.0, 1mM DTT and 10% Glycerol] overnight, at 25
554 °C. The reaction mixture was reloaded on a Ni-IMAC system to remove the His_8-SUMO*
555 tag. The fractions containing OphP were collected and concentrated using an Amicon filter
556 column (50 kDa cut-off). OphP was further polished across an Äkta FPLC system for size
557 exclusion chromatography (SEC) equipped with a Superdex 200 Increase column. For the
558 this final purification step, HEPES buffer [50 mM HEPES pH 8, 1 mM DTT, 10% glycerol
559 (v/v)] was used, as previously described[67].
560
561 **Protein expression in *E. coli***
562 OphMA, OphMA-TEV, GmPOPB, and TEV protease were produced in *E. coli* BL21 as
563 previously described[17,67]. Briefly, chemically competent BL21 cells were transformed with
564 respective expression plasmids and selected on appropriate antibiotics. A pre-culture was
565 incubated overnight in 10 ml at 37ºC, 180 rpm. 5 ml of the preculture was used to inoculate 1
566 L of terrific broth (TB) medium. The culture was maintained at 37ºC, 160 rpm until OD_{600} of
567 1.5 to 2.0. The culture was chilled on ice for 30 min before the addition of 200 µM isopropyl
568 β-D-thiogalactopyranoside (IPTG) and maintained at 16 ºC, 160 rpm for 2 days (GmPOPB
569 and TEV) and 3-5 days for OphMA and OphMA-TEV mutants. Cells were harvested by
570 centrifugation at 8000 × *g* for 20min, at 4ºC. Cells pellets were resuspended in 100 mL ice-
571 cold lysis buffer [300 mM NaCl, 50 mM Tris pH 8.0, 10% glycerol, 1 mM DTT, DNase I, 20
572 mM Imidazole and protease inhibitor cocktail (Roche)]. For OphMA and OphMA-TEV
573 mutants, NaCl and Tris in the buffer above, were replaced by 50mM HEPES pH 8.0, 0.1%
574 Triton x-100. Cells were lysed by a cold French press, two passages, and clearing of cell
575 debris by centrifugation at 12 000 rpm, 30 min at 4 ºC. The cell lysate supernatant was
576 subjected to protein purification either by Ni-IMAC systems (for TEV and GmPOPB) or by
577 Ni-NTA beads (Macherey Nagel). Elution and wash buffers and the SEC method were the
578 same as for OphP purification above. The protein concentration was determined by BCA
579 assay (Thermo Scientific). To confirm the protein quality, 10 µg of each protein was loaded
580 on a 12% SDS gel and run by electrophoresis and stained by coomassie brilliant blue. The
581 purified proteins were shock-frozen in liquid nitrogen and then stored at -80 ºC. Peptide
582 constructs that we tried but failed to obtain are listed in Table 2.
583
584 **Peptide production and purification**
585 To produce OphMA-C-terminal fragments, purified and TEV-cleavable OphMA proteins
586 were mixed with TEV protease (1:10) to a concentration of 10 mg/ml in assay buffer [300
587 mM NaCl, 50 mM TRIS pH 8.0, 1 mM DTT and 10 % glycerol]. The reaction was mixed

well by pipetting and kept overnight at 25 °C. The reaction mixture was loaded on a pre-equilibrated C8 or C18-SepPak cartridge following the user instruction and recommendations. The peptides were eluted in 1-3 ml 100% methanol depending on the concentration. 5 µl of the eluate was used for HPLC-MS/MS analysis before further purification on an Agilent 1260 infinity preparative HPLC harboring a C18 column (Luna 5 µm C18(2) 100Å, 250X10 mm. The mobile phase consisted of a gradient between water (A) and acetonitrile (B), both supplemented with 0.1% formic acid. The flow rate was set at 1.2 ml/min, and one collection each minute. The method started with a system equilibration for 5 min at 5% B, followed by a linear gradient up to 40 % B in 10 min, then increased to 98% B in 30 min. The column was finally washed with 98% B for 5 min before gradually dropping to 5% B in a 5 min span. Fractions corresponding to the expected products were collected, and 5 µl of each fraction are tested by HPLC-MS/MS for the presence of peptides. To determine the concentration, samples were analysed by an Agilent 1100 series UV-HPLC calibrated to the bovine albumin serum (BSA) as an internal standard, at $\lambda = 210$ nm.

For TEV non-cleavable OphMA, trypsin digestion was performed. 100 µg of the substrate were digested using 1.25 mg trypsin in 25 µl HEPES buffer pH 8.0, 37 °C, 650 rpm, overnight. 3 µl of the reaction was used for MS analysis.

Protein sequences (the portion used after TEV cleavage is underlined, TEV site is in bold)

His_8OphMA-Tev-21mer.

MEHHHHHHHHTSTQTKAGSLTIVGTGIESIGQMTLQALSYIEAAAKVFYCVIDPATE
AFILTKNKNCVDLYQYYDNGKSRLNTYTQMSELMVREVRKGLDVVGVFYGHPGVF
VNPSHRALAIAKSEGYRARMLPGVSAEDCLFADLCIDPSNPGCLTYEASDFLIRDRPV
SIHSHLVLFQVGCVGIADFNFTGFDNNKFGVLVDRLEQEYGAEHPVVHYIAAMMPH
QDPVTDKYTVAQLREPEIAKRVGGVSTFYIPPKARKASNLDIIRRLELLPAGQVPDKK
ARIYPANQWEPDVPEVEPYRPSDQAAIAQLADHAPPEQYQPLATSKAMSDVMTKLA
LDPKALADYKADHRAFAQSVPDLTPQERAALELGDSWAIRCAMKNMPSSLLDAAR
ESG**ENLYFQG**FPWVIVVGVIGVIGSVMSTE

His_8OphMA-Tev-15mer.

MEHHHHHHHHTSTQTKAGSLTIVGTGIESIGQMTLQALSYIEAAAKVFYCVIDPATE
AFILTKNKNCVDLYQYYDNGKSRLNTYTQMSELMVREVRKGLDVVGVFYGHPGVF
VNPSHRALAIAKSEGYRARMLPGVSAEDCLFADLCIDPSNPGCLTYEASDFLIRDRPV
SIHSHLVLFQVGCVGIADFNFTGFDNNKFGVLVDRLEQEYGAEHPVVHYIAAMMPH
QDPVTDKYTVAQLREPEIAKRVGGVSTFYIPPKARKASNLDIIRRLELLPAGQVPDKK
ARIYPANQWEPDVPEVEPYRPSDQAAIAQLADHAPPEQYQPLATSKAMSDVMTKLA
LDPKALADYKADHRAFAQSVPDLTPQERAALELGDSWAIRCAMKNMPSSLLDAAR
ESG**ENLYFQG**FPWVIVVGVIGVIG

His_8OphMA-Tev-24mer.

MEHHHHHHHHTSTQTKAGSLTIVGTGIESIGQMTLQALSYIEAAAKVFYCVIDPATE
AFILTKNKNCVDLYQYYDNGKSRLNTYTQMSELMVREVRKGLDVVGVFYGHPGVF
VNPSHRALAIAKSEGYRARMLPGVSAEDCLFADLCIDPSNPGCLTYEASDFLIRDRPV
SIHSHLVLFQVGCVGIADFNFTGFDNNKFGVLVDRLEQEYGAEHPVVHYIAAMMPH
QDPVTDKYTVAQLREPEIAKRVGGVSTFYIPPKARKASNLDIIRRLELLPAGQVPDKK
ARIYPANQWEPDVPEVEPYRPSDQAAIAQLADHAPPEQYQPLATSKAMSDVMTKLA
LDPKALADYKADHRAFAQSVPDLTPQERAALELGDSWAIRCAMKNMPSSLLDAA**E**
NLYFQGSQNGFPWVIVVGVIGVIGSVMSTE

His_8OphMA-Tev-30mer.

MEHHHHHHHHTSTQTKAGSLTIVGTGIESIGQMTLQALSYIEAAAKVFYCVIDPATE
AFILTKNKNCVDLYQYYDNGKSRLNTYTQMSELMVREVRKGLDVVGVFYGHPGVF
VNPSHRALAIAKSEGYRARMLPGVSAEDCLFADLCIDPSNPGCLTYEASDFLIRDRPV
SIHSHLVLFQVGCVGIADFNFTGFDNNKFGVLVDRLEQEYGAEHPVVHYIAAMMPH
QDPVTDKYTVAQLREPEIAKRVGGVSTFYIPPKARKASNLDIIRRLELLPAGQVPDKK
ARIYPANQWEPDVPEVEPYRPSDQAAIAQLADHAPPEQYQPLATSKAMSDVMTKLA
LDPKALADYKADHRAFAQSVPDLTPQERAALELGDSWAIRCAMKNMPS**ENLYFQG**
ESGEEASQNGFPWVIVVGVIGVIGSVMSTE

His_8SUMOTEV-OphP.

MGHHHHHHHHGGSDSEVNQEAKPEVKPEVKPETHINLKVSDGSSEIFFKIKKTTPLR
RLMEAFAKRQGKEMDSLTFLYDGIEIQADQTPEDLDMEDNDIIEAHREQIGG**ENLYF**
QGTSMSFPGWGPYPPVERDETSAITYSSKLHGSVTVRDPYSQLEVPFEDSEETKAFV
HSQRKFARTYLDENPDREAWLETLKKSWNYRRFSALKPESDGHYYFEYNDGLQSQL
SLYRVRMGEEDTVLTESGPGGELFFNPNLLSLDGNAALTGFVMSPCGNYWAYGVSE
HGSDWMSIYVRKTSSPHLPSQERGKDPGRMNDKIRHVRFFIVSWTSDSKGFFYSRYP
PEDDEGKGNAPAMNCMVYYHRIGEDQESDVLVHEDPEHPFWISSVQLTPSGRYILFA
ASRDASHTQLVKIADLHENDIGTNMKWKNLHDPWEARFTIVGDEGSKIYFMTNLKA
KNYKVATFDANHPDEGLTTLIAEDPNAFLVSASIHAQDKLLLVYLRNASHEIHIRDLT
TGKPLGRIFEDLLGQFMVSGRRQDNDIFVLFSSFLSPGTVYRYTFGEEKGYRSLFRAIS
IPGLNLDDFMTESVFYPSKDGTSVHMFITRPKDVLLDGTSPVLQYGYGGFSLAMLPT
FSLSTLLFCKIYRAIYAIPNIRGGSEYGESWHREGMLDKKQNVFDDFNAATEWLIAN
KYASKDRIAIRGGSNGGVLTTACANQAPGLYRCVITIEGIIDMLRFPKFTFGASWRSE
YGDPEDPEDFDFIFKYSPYHNIPPPGDTVMPAMLFFTAAYDDRVSPLHTFKHVAALQ
HNFPKGPNPCLMRIDLNSGHFAGKSTQEMLEETADEYSFIGKSMGLTMQTQGSVDSS
RWSCVTV

Enzyme activity assays

For the chromogenic substrate and the POP inhibitor, stocks of 50 mM and 10 mM, respectively, were prepared in methanol following the user information. Before the reaction, the substrate was solubilized at 40 °C and then the required amounts were mixed with the standard assay buffer [50 mM HEPES pH 6.0 + 10 mM DTT]. The enzyme was added last, to make the total reaction volume 50 µL. The reaction mixture was kept at 30°C while shaking at 600 rpm. The reaction was quenched by the addition of 50 µl methanol. The enzymatic activity was monitored by absorbance measurement at 410 nm (for *p*-nitroanilide) on an Infinite 200Pro M Plex spectrophotometer (Tecan). Continuous reaction monitoring was ensured by incubating the 96-well plates at 30°C, with absorbance measurements each 30 min.

For peptide substrates, reactions were also carried out in 50 µl with a standard buffer [50 mM HEPES pH 7.0, 10 mM DTT], at 30°C, 600 rpm unless stated otherwise. The peptide was first mixed with the buffer before adding the enzymes. Both substrate and enzyme concentrations varied up to 100 µM. The reaction was stopped by the addition of 50 µl methanol, then spun down at the highest speed (20,000 *x g*), 4ºC. For HPLC-MS/MS analysis, 5 µl supernatant was used. For the synthetic peptides, PHA1 and AMA1 were stored in 1 mg/ml. For the reaction, 20 µM substrate was used with 1 µM of protease. For ProAlanase, a 1:50 enzyme/substrate (w/w) was used in a 25 µl reaction volume, in either 50 mM HEPES (pH 6.0) or 50 mM sodium acetate (pH 4.0). These reactions were carried out at 37°C for 4 h

688 and stopped by adding 25 µl methanol. After centrifugation at the highest speed at 4 °C, 5 µl
689 supernatant was used for HPLC-MS/MS analysis.
690
691 For assays of OphP variants with Oph-15mer (almost pure 7-fold methylations), the reactions
692 were performed in buffer containing 50 mM HEPES (pH 7.0), 100 mM NaCl, and 5 mM
693 DTT at a concentration of 200 μM Oph-15mer and 20 μM OphP. The reaction mixtures in
694 Eppendorf tubes were incubated at 25 ^{o}C and 1000 rpm using a ThermoMixer C for 18 hours.
695 Reactions were quenched by adding an equal amount of methanol and protein precipitation
696 was removed by centrifugation. The supernatant was analysed using Waters Acquity H-Class
697 plus UPLC equipped with SQ, PDA and ELS detectors. Buffer A (water with 0.1% FA) and
698 buffer B (acetonitrile with 0.1% FA) are used as mobile phase. Typically, 10 µL of
699 supernatant was loaded and separated on a ACQUITY UPLC BEH C18 column (1.7 µM, 2.1
700 x 100 mm) at a flow rate of 0.6 ml/min with following gradient: 0-0.25 min for 5% buffer B,
701 0.25-0.4 min from 5% to 40% buffer B, 0.4-3.6 min from 40% to 55% buffer B, 3.6-3.7 min
702 from 55% to 60% buffer B, 3.7-6.0 min from 60% to 70% buffer B, 6.0-6.15 min from 70%
703 to 95% buffer B, 6.15-7.6 min for 95% buffer B.
704
705 **LC-ESI-MS/MS analysis**
706 Peptide analysis was performed by following previous protocols[67] for HPLC-MS/MS analysis
707 of borosins. Briefly, data were generated from Dionex Ultimate 3000 UHPLC HPLC coupled
708 to an MS/MS system (Thermo Scientific Q Exactive classic). A list of expected masses
709 (inclusion list) was always included in the HPLC-MS/MS method. The peptide was applied
710 on a C18 column (Phenomenex Kinetex ®µm XB-C18 100 Å (150 x 2.1 mm)) pre-heated at
711 50 °C. For UV-vis spectra, the signals were recorded by a diode array detector (DAD) set at
712 210, 230, 250, and 280 nm. Water (solvent A) and acetonitrile (solvent B) both containing 0.1%
713 FA served as a mobile phase, with a 0.5 ml/min flow rate. The HPLC method started by
714 equilibrating the system for 2 min at 5% B, followed by a linear gradient up to 70 % B in 13
715 min, and then increased to 100% B in 3 min. The column was rinsed first with 100% B for 1
716 min and then with 5% B for 5 min. The MS/MS system used the heated electrospray
717 ionization in a positive ion mode. The full MS was set as follows: an automatic gain control
718 (AGC) target of 70,000 [AGC target 1e6, maximum ion trap (IT), 120 ms, and scan range of
719 200-2500m/z]. Data-dependent (dd) MS/MS was performed at a resolution of 17,500 [AGC
720 target at 1e5, maximum IT 120 ms, and isolation window of 3.0 m/z]. The normalized
721 collision energy (NCE) was set at 30% for macrocycles, and 18% or stepped NCE (16, 18,
722 22%) for linear peptides.
723
724 **ESI-TOF MS and intact mass measurement**
725 Intact protein mass analysis was performed using a Waters Xevo G2-QS QToF MS coupled
726 to an ACQUITY UPLC I-Class LC system (Waters Corporation). The spectrometer was auto-
727 calibrated throughout the experiment using an internal lock-spray mass calibrant (at 556.2771
728 m/z of leucine enkephalin, 1 s scan every 120 s interval). The data was acquired in
729 Continuum format, in a 300 – 2500 m/z spectral window with a scan time of 1 s and an
730 interscan time of 0.014 s. The mass spectrometer and ESI ionization source were operated
731 under the following parameters: capillary voltage at 3 kV, cone voltage at 20 V, source offset
732 voltage at 40 V, source temperature at 100 °C, desolvation temperature at 400 °C and
733 desolvation gas (nitrogen) flow at 650 L/h, cone gas flow at 30 L/h. In a typical analysis, 1
734 µL (30 ng) of the protein sample was injected and desalted on a ProSwift™ RP-1S HPLC
735 (250 x 4.6 mm x 5 µm, Thermo Scientific™) column maintained at 60 ^{o}C. The elution was
736 performed using solvent A (water with 0.1% formic acid) and solvent B (acetonitrile with 0.1%
737 formic acid) with a gradient elution using isocratic 95% solvent A (0 - 1 min), linear gradient

738 to 95% solvent B (1.1 – 7 min), and isocratic 95% solvent A (7.1 – 10 min) at a flowrate of
739 0.2 ml/min. Combined mass spectra from the total chromatographic protein peak were used
740 for intact mass reconstruction using MassLynx (Waters) Max(imum) Ent(ropy) 1
741 deconvolution algorithm (Resolution: 0.5 Da/channel, Width at half-height: ion
742 series/protein-dependent, Minimum intensity ratios: 33% Left and Right). Spectra were
743 deconvoluted between 40000 and 55000 for OphMA.
744
745 **ITC studies of OphP with peptides**
746 Isothermal titration calorimetry (ITC) experiments were performed using a MicroCal PEAQ-
747 ITC (Malvern). Leader peptides and follower peptides (SVMSTE and VIGSVMSTE) were
748 dissolved in DMSO at sufficient concentration as a stock. A typical ITC experiment was
749 performed by injecting 0.4 mL of peptide solution from a syringe followed by repeatedly
750 injecting 2 mL of peptide solution in syringe eighteen times into a cell solution containing
751 S580A. The measurements were done at 25 ^{o}C at a stirring rate of 750 rpm with a reference
752 power (DP) of 5 mcal/s or 10 mcal/s. Control titrations were performed similarly except for
753 the absence of protein in the cell solution. Data processing and fitting were performed using
754 MicroCal PEAQ-ITC analysis software (Malvern).
755
756 **Crystallization, data collection, reduction, and refinement**
757 Freshly purified OphP and S580A proteins were screened for apo crystals using the sitting
758 drop method using commercial screening kits from Hampton Research or Molecular
759 Dimensions. OphP and S580A were eventually crystallized at 40-50 mg/ml by mixing 0.3 µL
760 of proteins with 0.3 µL of the reservoir (0.2 M sodium acetate, 0.1 M Bis-Tris propane (pH
761 6.0-6.5) and 28% PEG 3350). Crystals appeared within eight days and grew to full size
762 within three weeks at room temperature. Crystals were fished, transferred to cryo-protectant
763 (reservoir solution supplemented with 40% PEG 3350) and flash-frozen in liquid nitrogen.
764 The structure of the OphP-ZPP complex was determined by soaking OphP crystals with 5
765 mM Z-Pro-prolinal overnight at room temperature. Crystals were in similar cryoprotectant
766 with 1 mM ZPP. For the S580A:Oph-15mer complex, apo S580A crystals were soaked with
767 1 mM purified Oph-15mer overnight at room temperature. Due to the poor solubility of Oph-
768 18mer^{NL}, apo OphP(S580A) crystals were soaked with a cloudy reservoir solution containing
769 18mer overnight to obtain the OphP(S580A)-18mer^{CF} complex. More than 50 crystals dataset
770 were collected for each complex and screened based on the density.
771 All the X-ray diffraction data were recorded at Diamond Light Source beamlines (I03, I04,
772 I04-1, and I24). The diffraction images were reduced, integrated, and scaled using xia2[68],
773 DIALS[69], Apo structures of S580A were determined by molecular replacement using a
774 Phaser[70] with GmPOPB structure (PDB entry 5N4C) as the initial model. Autobuilding was
775 performed using Buccanner from the molecular replacement solutions and further refined
776 using Refmac5[71] and manually built with Coot[72], and improved using PDB-redo[73]. Simulated
777 omit maps for the ligands were calculated using Phenix[74]. All the other structures were solved
778 by molecular replacement using apo S580A structure as initial models, refined, manually
779 built and improved similarly. All crystallographic figures were generated using Pymol
780 (Schrödinger LLC), CCP4mg[75] or Chimera[65]. Structure-based sequence alignment was
781 created using MUSCLE[76] and ESPript 3.0[77]. Full crystallographic details are given in Table 3.
782
783
784 **Acknowledgements**
785 We would like to thank Prof. Jörn Piel and his staff, in particular, Dr. Clara Chepkirui and Dr.
786 Silke Probst for their support in the HPLC purification, and Philip Rößler for supplying TEV
787 protease and helping with protein purification. We are grateful to Dr. Chris Arter from

Rosalind Franklin Institute for the assistance with the MS experiments and Dr. Xiaping Fu for the assistance with the purification of peptides. We would also like to thank Diamond Light source for the access to the synchrotron. This work was funded by the Swiss National Science Foundation (Grant no. 31003A-173097), ETH Zürich and UK BBSRC (BB/R018189/1).

Competing interests

MK is an inventor on a patent application filed by ETH Zurich (no. WO2017174760A1, priority date: 7 April 2016). The authors declare no other competing interests.

Data availability

Crystallographic and structural data reported in the paper are available from the RCSB; 7ZB2 (apo), 7ZAZ (ZPP complex). 7ZB0 (15 mer) 7ZB1 (18 mer). Raw data for the Figures are shown in Supporting Information.

FIGURES

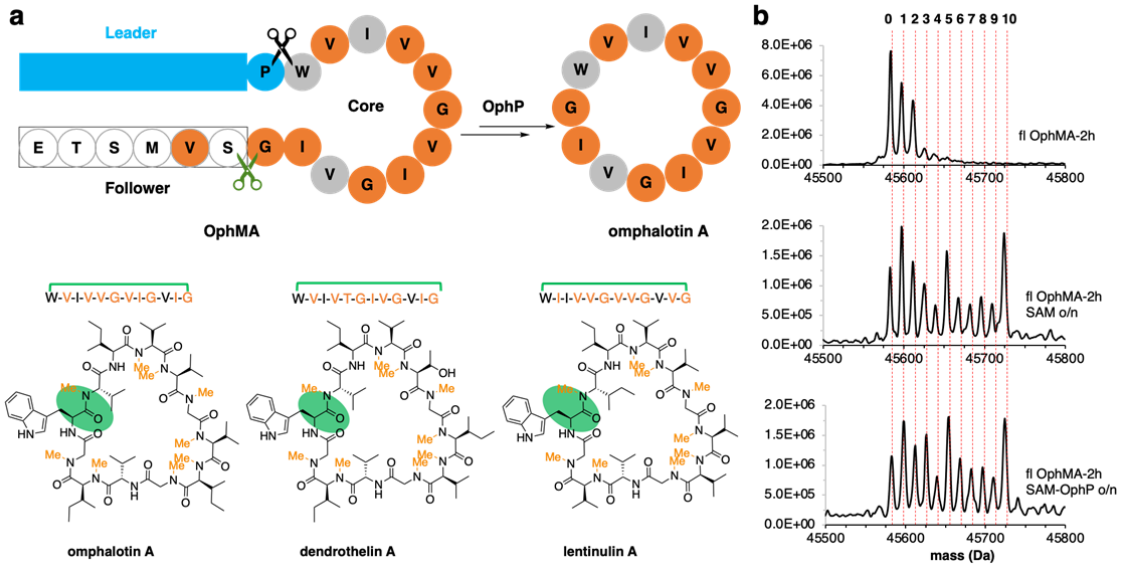

Figure 1. Biosynthesis of omphalotin A inferred from the heterologous co-production of OphMA and OphP in *Pichia pastoris*. (**a**). Proposed biosynthetic pathway of omphalotin A, where scissors indicate proteolytic cleavage (black) and macrocyclization sites (green). Below, sequences and chemical structure of omphalotin A, and homologous peptide natural products dendrothelin A and lentinulin A are shown with methylation sites in orange and the cyclization site in green. These peptide macrocycles were heterologously produced in *Pichia pastoris* by co-producing OphP and OphMA variants with respective C-termini. (**b**) ESI-MALDI-ToF analysis of purified OphMA co-incubated with methyl donor substrate SAM and purified OphP *in vitro*. Full spectra can be found in the Supplementary Information. Numbers indicate the various methylation states of OphMA.

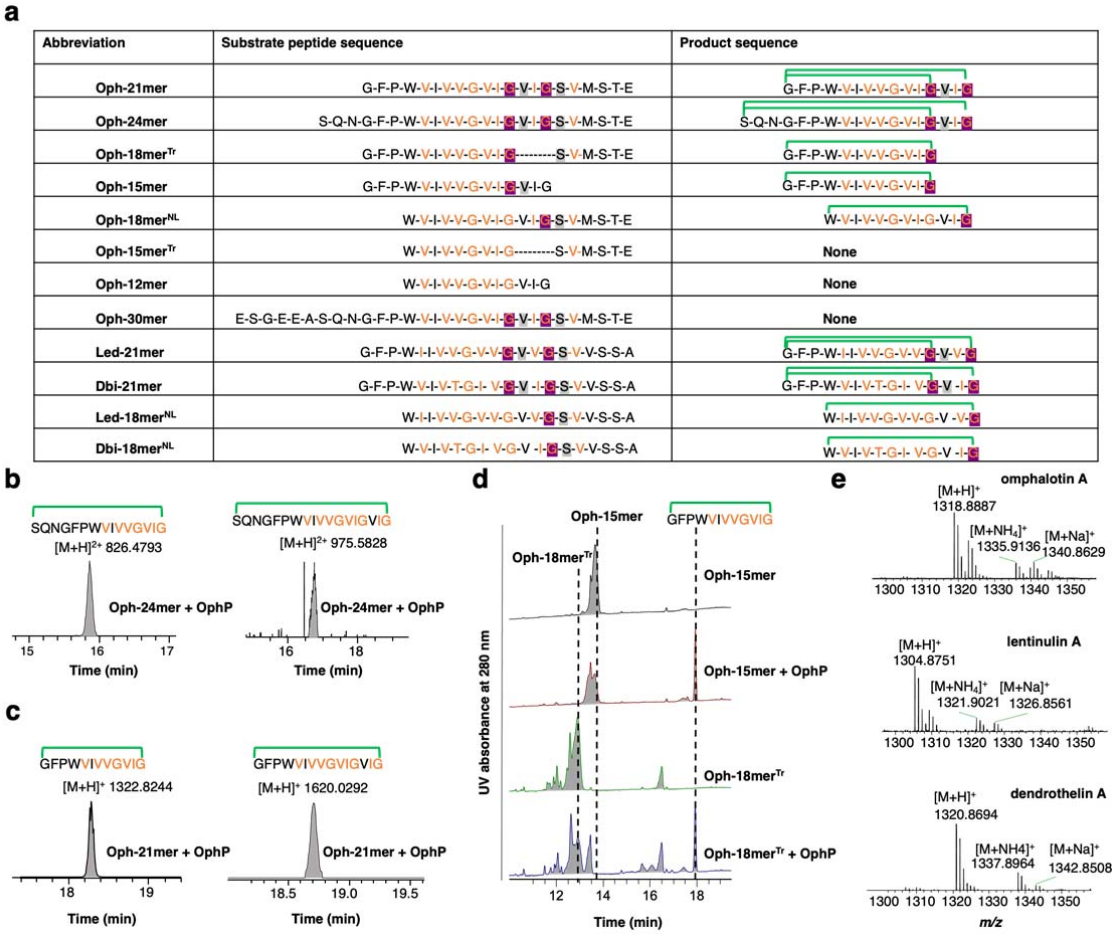

Figure 2. ***In vitro*** **macrocyclization assays of OphP using purified peptide substrates.** (**a**) Sequences of purified peptides used in this work. The residues, which are N-methylated in the fully methylated peptide, are highlighted in orange. Note that methylation of the core peptide by OphMA proceeds directionally from N- to C-terminus. The P1 site residue recognized by OphP is highlighted in purple and the P1' site residue in grey. Macrocycles formed by OphP are shown with green brackets. Leader peptide removal was achieved by incubating OphMA variants with TEV and GmPOPB or ProAlanase. (**b and c**) Extracted ion chromatograms (EICs) of macrocyclic products when Oph-24mer **(b)** or Oph-21mer (**c**) were incubated with OphP. (**d**) RP-HPLC UV absorption profiles at 280 nm for Oph-15mer or Oph-18mer^{Tr} in the absence and presence of OphP show the production of the same macrocycle. **(e)** Production of omphalotin A and its orthologues lentinulin A and dendrothelin A using OphP and Oph-18mer^{NL}, Led-18mer^{NL} and Dbi-18mer^{NL}. Sodium and ammonium adducts of the compounds are indicated.

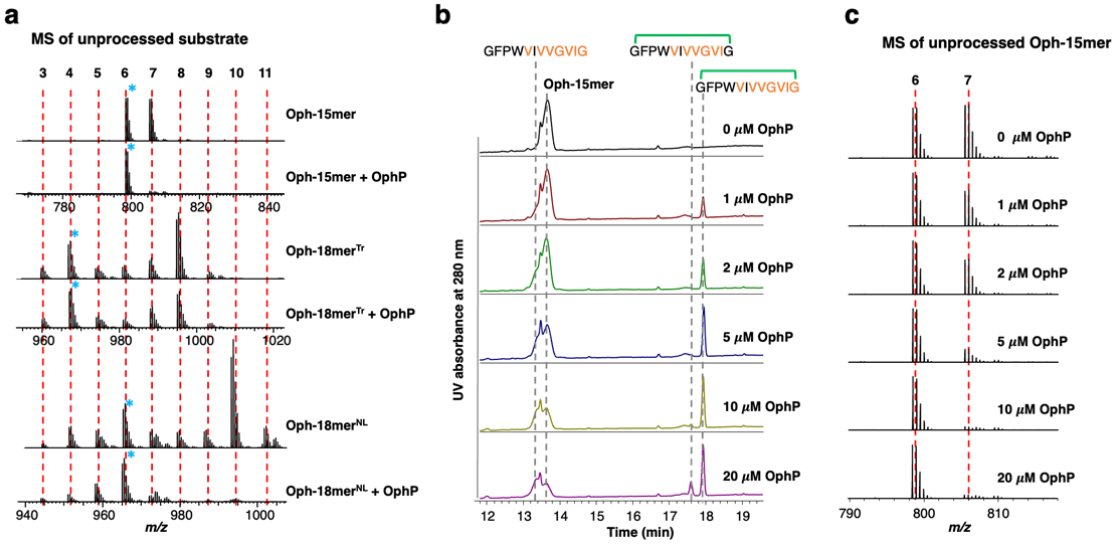

Figure 3. Preference of OphP towards highly backbone N-methylated peptides. (**a**) Mass spectrometric analysis showing ion chromatograms of the unprocessed substrates used in the assays (panels (**b**) and (**c**)). The relative abundance in assays with or without OphP demonstrates the preference of OphP for fully methylated substrates. Red broken lines indicate the number of methylations. For comparison, the peak height of the most abundant non-reactive species was drawn at the same level (6-fold methylation in Oph-15mer, 4-fold in Oph-18mer^{Tr}, and 6-fold in Oph-18mer^{NL}. These species were marked with blue asterisks. (**b**) RP-HPLC UV absorption profile of 100 µM of 15mer with varying concentrations of OphP (0, 1, 2, 5, 10, 20 μM). Linear products resulting from the peptidase activity of OphP can be detected but overlapped with starting material. Cyclo(G-F-P-W-^{me}V-I-^{me}V-^{me}V-^{me}G-^{me}V-^{me}I-G) can only be detected when high concentrations of OphP are used. Broken black lines show the retention times of the various peptide species. (**c**) Mass spectrometric analysis showing ion chromatograms of the unprocessed substrate in Figure 3b. The 7-fold methylated Oph-15mer is depleted at high concentrations of OphP (10 and 20 μM). After the depletion of this species, OphP started to process the 6-fold methylated species.

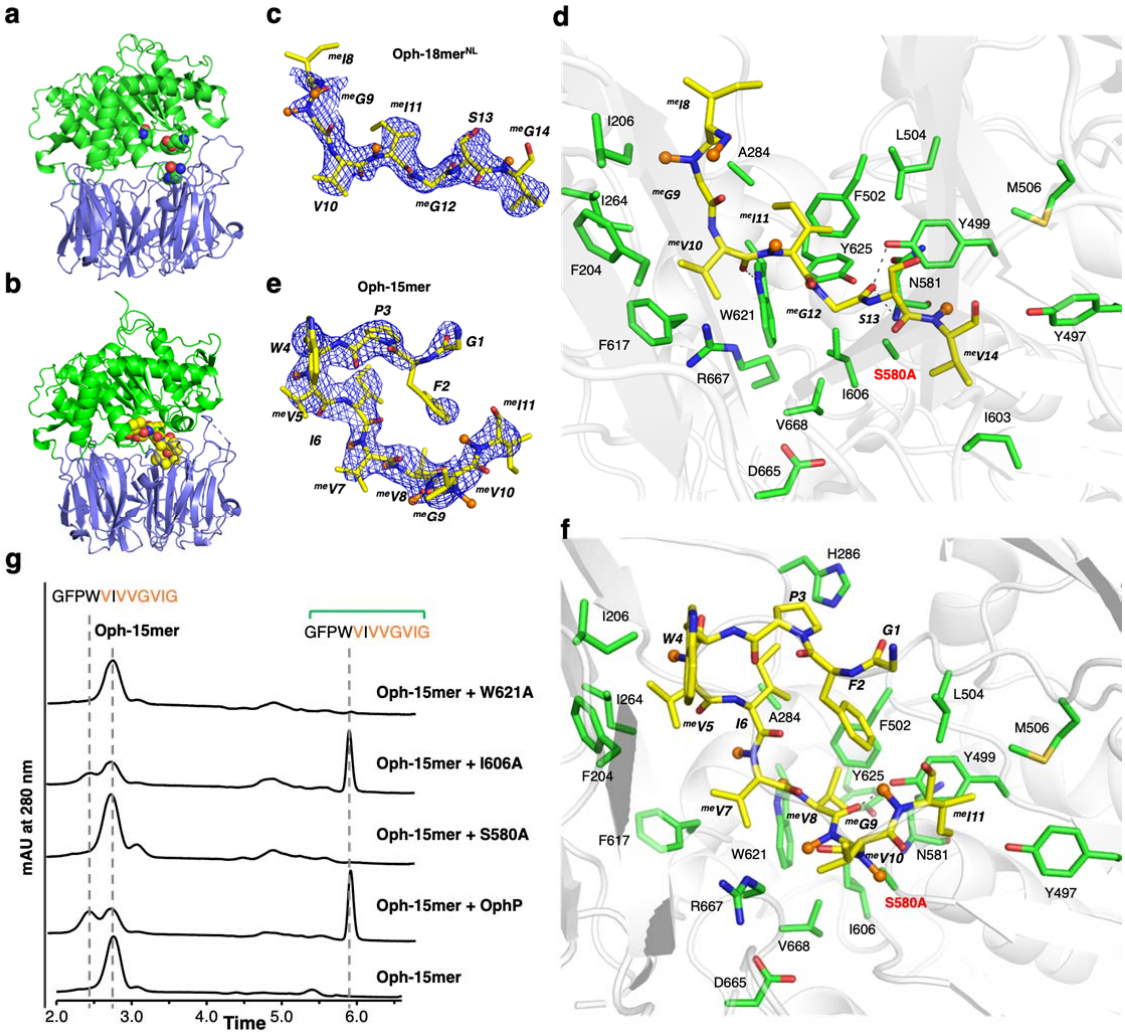

Figure 4. Crystal structures of OphP in apo form and in complex with Oph-18mer^{NL} and Oph-15mer. (**a**) Overall structure of apo OphP S580A. The catalytic triad is shown in spheres and colored as oxygen in red and nitrogen in blue. (**b**) Overall structure of the OphP S580A:Oph-18mer^{NL} complex. The peptide substrate Oph-18mer^{NL} is shown in spheres and colored as carbon in yellow, oxygen in red, and nitrogen in blue. σ_A-weighted 2mFo-DFc map (contoured at 1) for Oph-18mer^{NL} (**c**) and Oph-15mer (**e**) complexed with OphP S580A. Active site view of OphP:Oph-18mer^{NL} (**d**) and OphP:Oph-15mer (**f**) in the complex structure showing the interactions. Side chains of the active site residues are shown in sticks with carbon green, nitrogen blue, oxygen red and the methyl groups orange. Broken lines show hydrogen bonds. (**g**) HPLC analysis of assays using almost pure 7-methylated Oph-15mer as substrate for OphP and its variants. The control reaction without OphP shows the absorption profile of the starting material. While the W621A mutation abolished macrocyclization, I606A showed an activity comparable to wild type OphP. The I606A variant shows a better ratio of macrocyclic to linear peptide than the wild type enzyme. The reactions were performed at 25 °C in buffer containing 50 mM HEPES pH 7.0, 100 mM NaCl and 5 mM DTT at a concentration of 20 µM enzymes and 200 µM Oph-15mer.

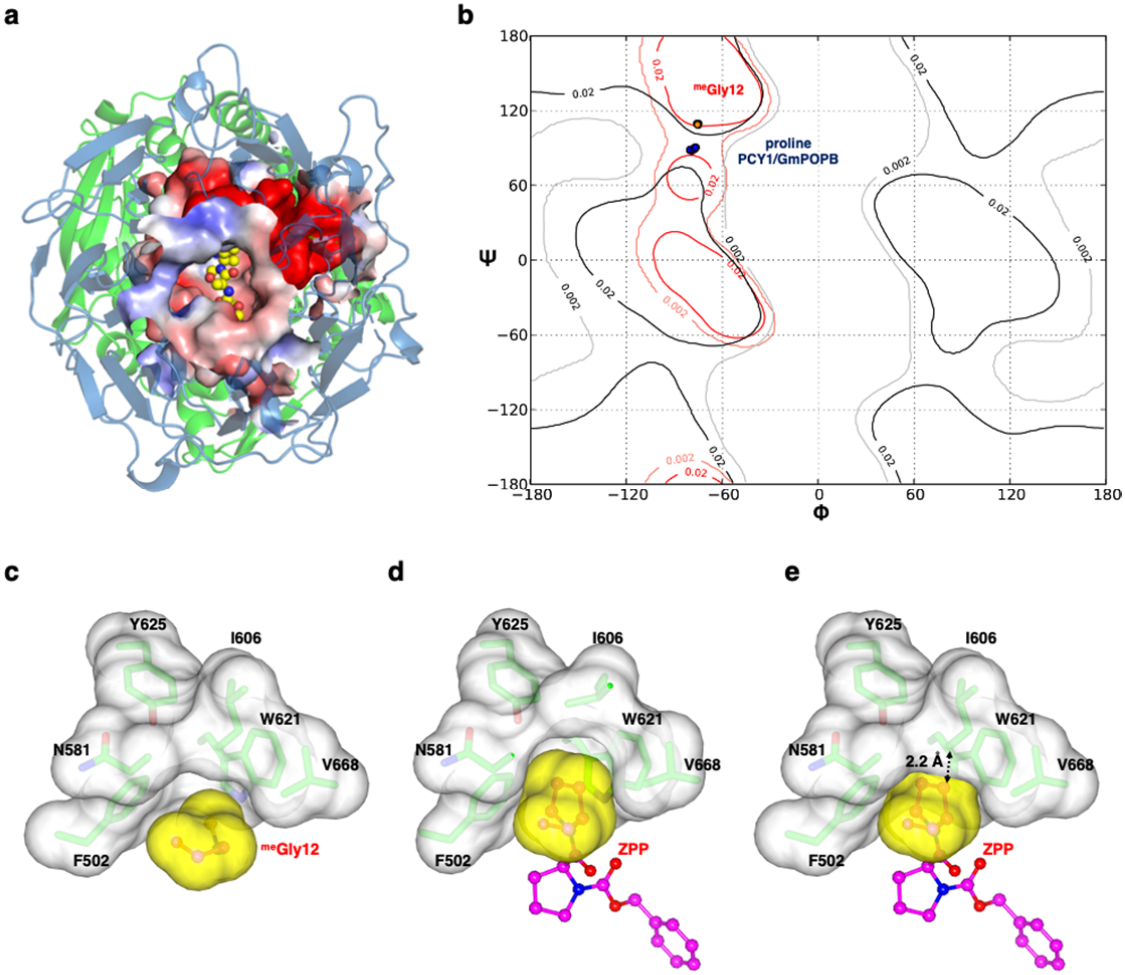

Figure 5. Substrate tunnel and ^{me}Gly12 recognition site of OphP. (a) Top view of the electrostatic surface of the tunnel and cavity of OphP. Electrostatic calculation was performed using the APBS-PDB2PQR software suite[63] under the default setting and drawn in PyMol. The surface of the central tunnel cavity of OphP is calculated with the program Hollow[64] using default parameters and the central axes of the cylinder (radius of 22 Å) are defined by the C-atoms of Met171 (offset 0 Å) and Ser384 (offset -5.0 Å). The electrostatic potential is set at ± 3 kT/e. **(b)** Ramachandran plot of P1 residues, ^{me}Gly12 in OphP and prolines in PCY1 and GmPOPB. All the residues fall into the preferred (red line with probability contoured at 0.02) or allowed regions (red line probability contoured at 0.002) for proline. Ramachandran plots for normal glycine residues are shown in grey (allowed region with probability contoured at 0.002) and black lines (preferred region with probability contoured at 0.02). ^{me}Gly12 has very similar dihedral angles to those of proline residues at P1 site in PCY1 (5O3U) and GmPOPB (5N4C). Ramachandran plot was drawn using Chimera[65]and colored in Adobe Illustrator**. (c)** Surfaces of ^{me}Gly12 and its surrounding hydrophobic pocket in Oph-18mer^{NL} complex. The pocket is composed of Tyr625, Trp621, Val668, Phe502, Asn581 and Ile606. (**d**) Surfaces of proline (P1) of ZPP and P1 hydrophobic pocket in ZPP covalent complex structure. **(e)** Surfaces of proline (P1) of ZPP and the hydrophobic pocket from apo S580A. Structure of OphP:ZPP is superimposed to apo S580A. C_δ of Ile606 is only 2.3 Å away from C_β of proline in ZPP leading to a steric clash. ZPP and ^{me}Gly12 colored as carbon in magenta, oxygen in red, and nitrogen in blue. Surface of P1 proline is shown in yellow.

895

896 **Tables**

897

898 **Table 1**. List of oligonucleotides

899

His-SUMOSTAR-FW	GAAGGATCCGAAACTATGGGTCATCATCATCATCATCATCATCATGGTGGT TCTGACTCCGAGGTC
SUMOSTAR-RV	AGACATACTAGTACCTTGGAAGTACAAGTTTTC
OphMA-NotI-Rv	GAGTGCGGCCGCTTATTCCGTGCTCATGACTGATC
OphP_FW	AAGGTACTAGTATGTCGTTTCCAGGATGGGGACCAT
OphMA-Fw	ATATACATATGGAGCATCATCATCATCATCATCATCATACTTCCACTC
31mer-RV1	TCGCCGGATTGGAAGTACAAGTTTTCACGAGCAGCGTCCAAGAGCGACG
31MER-RV2	GACCCATGGGAAACCGTTTTGGGATGCCTCTTCGCCGGATTGGAAGTAC
38mer-Rv1	TTCGCCGGATTCACGATGATGATGATGATGATGACCTTGGAAGTACAAG
38mer-Rv2	GACCCATGGGAAACCGTTTTGGGATGCCTCTTCGCCGGATTCACGATG
DbiCterm_RV:	GCTCGAATTCTTACGCGCTGCTAACCACGCTTCCGATGACCCCAA CGATACCCGTGACGATGACCCATGGGAAACC
LedCterm_RV:	CTCGAATTCTTACGCGCTGCTAACCACGCTACCAACC ACGCCAACCACACCAACCACAATGATCCATGGGAAACCTTGGAAGTAC
ΔVIG Rv	GTAGCAGCAACCACAATAGCCAAGTCAGTACTCGTGCCTTATTCGCCG GCGGTC
24mer_Rv1	TGACCCATGGGAAACCGTTTTGGGATTGGAAGTACAAGTTTTCACGAG CAGCGTCCAAGAGCGACG
18mer- W400A-Rv1	ACCGATAACACCAACGACGATGACCGCTTGGAAGTACAAGTTTTCCTC TTCGCCGGATTCACGAG
18mer-inter-Rv1	ACCGATAACACCAACGACGATGACCCATTGGAAGTACAAGTTTTCCTC TTCGCCGGATTCACGAG
OphP-I606A-FW	GAGGGTGCAATTGATATGCTTAGATTTCCTAAGTTTACATTTG
OphP-I606A-RV	CATATCAATTGCACCCTCAATTGTGATCACACAACGGTAGAG
OphMAΔC6-G408A-FW	GTCGTTGGTGTTATCGCT GTCATCGGATAAGCGGCCGC
OphMAΔC6-G408A-RV	AGCGATAACACCAACGACGATGACCCATGGGAAACCGTTT
OphMAΔC6-G408V-FW	GTCGTTGGTGTTATCGTCGTCATCGGATAAGCGGCCGC
OphMAΔC6-G408V-RV	GACGATAACACCAACGACGATGACCCATGGGAAACCGTTT
OphMAΔC6-G408L-FW	GTCGTTGGTGTTATCCTCGTCATCGGATAAGCGGCCGC
OphMAΔC6-G408L-RV	GAGGATAACACCAACGACGATGACCCATGGGAAACCGTTT

900

901

902 **Table 2**. List of peptides that were NOT successfully produced

903

Construct	TEV-cleavable OphMA C-terminal fragment	Description
OphMA wt	PSSLLDAARESGEEASQNGFP**WVIVVGVIGVIG**SVMSTE	WT peptide with longer leader
OphMA R72A-TEV-21mer	**G**FP**WVIVVGVIGVIG**SVMSTE	Non-methylated 21mer
OphMA-TEV-31mer	**G**ESGEEASQNGFP**WVIVVGVIGVIG**SVMSTE	Methylated 31mer
OphMA S129A-TEV-31mer	**G**ESGEEASQNGFP**WVIVVGVIGVIG**SVMSTE	Non-methylated 31mer
OphMA-TEV-His6-38mer	**G**HHHHHHRESGEEASQNGFP**WVIVVGVIGVIG**SVMSTE	His-tagged 38mer
OphMA-TEV-21mer I407F	**G**FP**WVIVVGVFGVIG**SVMSTE	21mer with I407F core mutation
OphMA-TEV-21mer I407T	**G**FP**WVIVVGVTGVIG**SVMSTE	21mer with I407T core mutation
OphMA-TEV-18mer W400A	**AV**I**VVGVIG**V**IG**SVMSTE	18mer with W400A mutation
OphMA R72A-TEV-15mer noFl	**G**FP**WVIVVGVIGVIG**---------	Non-methylated 15mer w/o follower

904

905

906

907 **Table 3**. Data collection, phasing and refinement statistics for all the structures.
908

	Apo S580A	OPhP-ZPP	S580A:Oph-15mer	S580A:Oph-18mer
PDB Entry				
Data collection				
Space group	P 1	P 1	P 1	P 1
Cell dimensions				
a, *b*, *c* (Å)	69.86, 113.43, 186.32	69.68, 102.65, 110.27	70.22,106.18, 114.79	70.01, 104.61, 110.65
α, β, γ (°)	83.97, 82.09, 76.93	116.23, 101.09, 92.18	113.04, 101.67, 93.24	115.81, 98.87, 93.79
Wavelength (Å)	0.9795	0.9763	0.9763	0.9762
Resolution (Å)	66.00-1.94 (1.97-1.94)	67.71-2.00 (2.03 -2.00)	64.35-2.47 (2.51-2.47)	55.84 -2.00 (2.03-2.00)
R_{merge}	0.075 (0.993)	0.115 (1.099)	0.120 (1.375)	0.090 (1.234)
$I / \sigma I$	7.3 (0.9)	14.3 (1.2)	13.0 (0.9)	15.0 (1.0)
Completeness (%)	97.6 (96.6)	97.6 (92.3)	98.6(97.96)	98.0 (96.9)
Redundancy	2.5 (2.4)	3.5 (3.4)	3.6 (3.6)	3.3 (3.5)
No. Unique reflections	999365 (397483)	611334 (175661)	370936 (104483)	598522 (182773)
$CC_{1/2}$	0.996 (0.315)	0.990 (0.580)	0.993 (0.530)	0.996 (0.545)
Refinement				
Resolution (Å)	66.00-1.94 (1.97-1.94)	67.71-2.0 (2.03-2.0)	64.35-2.47 (2.51-2.47)	55.84-2.0 (2.03 -2.0)
R_{work} / R_{free}	0.214/0.241	0.210/0.245	0.227/0.263	0.201/0.235
No. atoms				
Protein	46235	22799	22933	23204
Ligand/ion	89	257	276	251
Water	898	1328	53	682
B-factors (Å^2)				
Protein	45.91	36.6	76.66	47.46
Ligand/ion	60.91	56.4	103.09	76.67
Water	36.98	36.6	61.90	39.54
R.m.s deviations				
Bond lengths (Å)	0.007	0.006	0.007	0.006
Bond angles (°)	1.354	1.317	1.421	1.332
Ramachandran				
Allowed (%)	99.75	99.72	99.79	99.83
Outliers (%)	0.25	0.28	0.21	0.17

909 *Values in parentheses are for highest-resolution shell.

910
911
912

References

(1) Lipinski, C. A.; Lombardo, F.; Dominy, B. W.; Feeney, P. J. Adv. Drug Deliv. Rev. 2001, 46, 3.

(2) Marsault, E.; Peterson, M. L. J. Med. Chem. 2011, 54, 1961.

(3) Martí-Centelles, V.; Pandey, M. D.; Burguete, M. I.; Luis, S. V. Chem. Rev. 2015, 115, 8736.

(4) Giordanetto, F.; Kihlberg, J. J. Med. Chem. 2014, 57, 278.

(5) Driggers, E. M.; Hale, S. P.; Lee, J.; Terrett, N. K. Nat. Rev. Drug Discov. 2008, 7, 608.

(6) Surade, S.; Blundell, T. L. Chem. Biol. 2012, 19, 42.

(7) Arnison, P. G.; Bibb, M. J.; Bierbaum, G.; Bowers, A. A.; Bugni, T. S.; Bulaj, G.; Camarero, J. A.; Campopiano, D. J.; Challis, G. L.; Clardy, J.; Cotter, P. D.; Craik, D. J.; Dawson, M.; Dittmann, E.; Donadio, S.; Dorrestein, P. C.; Entian, K.-D.; Fischbach, M. A.; Garavelli, J. S.; Göransson, U.; Gruber, C. W.; Haft, D. H.; Hemscheidt, T. K.; Hertweck, C.; Hill, C.; Horswill, A. R.; Jaspars, M.; Kelly, W. L.; Klinman, J. P.; Kuipers, O. P.; Link, A. J.; Liu, W.; Marahiel, M. A.; Mitchell, D. A.; Moll, G. N.; Moore, B. S.; Müller, R.; Nair, S. K.; Nes, I. F.; Norris, G. E.; Olivera, B. M.; Onaka, H.; Patchett, M. L.; Piel, J.; Reaney, M. J. T.; Rebuffat, S.; Ross, R. P.; Sahl, H.-G.; Schmidt, E. W.; Selsted, M. E.; Severinov, K.; Shen, B.; Sivonen, K.; Smith, L.; Stein, T.; Süssmuth, R. D.; Tagg, J. R.; Tang, G.-L.; Truman, A. W.; Vederas, J. C.; Walsh, C. T.; Walton, J. D.; Wenzel, S. C.; Willey, J. M.; van der Donk, W. A. Nat Prod Rep 2013, 30, 108.

(8) Montalbán-López, M.; Scott, T. A.; Ramesh, S.; Rahman, I. R.; van Heel, A. J.; Viel, J. H.; Bandarian, V.; Dittmann, E.; Genilloud, O.; Goto, Y.; Grande Burgos, M. J.; Hill, C.; Kim, S.; Koehnke, J.; Latham, J. A.; Link, A. J.; Martínez, B.; Nair, S. K.; Nicolet, Y.; Rebuffat, S.; Sahl, H.-G.; Sareen, D.; Schmidt, E. W.; Schmitt, L.; Severinov, K.; Süssmuth, R. D.; Truman, A. W.; Wang, H.; Weng, J.-K.; van Wezel, G. P.; Zhang, Q.; Zhong, J.; Piel, J.; Mitchell, D. A.; Kuipers, O. P.; van der Donk, W. A. Nat Prod Rep 2021, 38, 130.

(9) Cyclic peptides: from bioorganic synthesis to applications; Koehnke, J.; Naismith, J.; van der Donk, W. A., Eds.; Chemical Biology; Royal Society of Chemistry: Cambridge, 2017.

(10) Lee, H.; van der Donk, W. A. Annu. Rev. Biochem. 2022.

(11) Kohli, R. M.; Trauger, J. W.; Schwarzer, D.; Marahiel, M. A.; Walsh, C. T. Biochemistry 2001, 40, 7099.

(12) Gao, X.; Haynes, S. W.; Ames, B. D.; Wang, P.; Vien, L. P.; Walsh, C. T.; Tang, Y. Nat. Chem. Biol. 2012, 8, 823.

(13) Zhang, J.; Liu, N.; Cacho, R. A.; Gong, Z.; Liu, Z.; Qin, W.; Tang, C.; Tang, Y.; Zhou, J. Nat. Chem. Biol. 2016, 12, 1001.

(14) Donia, M. S.; Ravel, J.; Schmidt, E. W. Nat. Chem. Biol. 2008, 4, 341.

(15) McIntosh, J. A.; Robertson, C. R.; Agarwal, V.; Nair, S. K.; Bulaj, G. W.; Schmidt, E. W. J. Am. Chem. Soc. 2010, 132, 15499.

(16) Luo, H.; Hong, S.-Y.; Sgambelluri, R. M.; Angelos, E.; Li, X.; Walton, J. D. Chem. Biol. 2014, 21, 1610.

(17) Czekster, C. M.; Ludewig, H.; McMahon, S. A.; Naismith, J. H. Nat. Commun. 2017, 8, 1045.

(18) Barber, C. J. S.; Pujara, P. T.; Reed, D. W.; Chiwocha, S.; Zhang, H.; Covello, P. S. J. Biol. Chem. 2013, 288, 12500.

(19) Chekan, J. R.; Estrada, P.; Covello, P. S.; Nair, S. K. Proc. Natl. Acad. Sci. USA 2017, 114, 6551.

(20) Ludewig, H.; Czekster, C. M.; Oueis, E.; Munday, E. S.; Arshad, M.; Synowsky, S. A.; Bent, A. F.; Naismith, J. H. ACS Chem. Biol. 2018, 13, 801.

(21) Koehnke, J.; Bent, A.; Houssen, W. E.; Zollman, D.; Morawitz, F.; Shirran, S.; Vendome, J.; Nneoyiegbe, A. F.; Trembleau, L.; Botting, C. H.; Smith, M. C. M.; Jaspars, M.; Naismith, J. H. Nat. Struct. Mol. Biol. 2012, 19, 767.
(22) Koehnke, J.; Bent, A. F.; Houssen, W. E.; Mann, G.; Jaspars, M.; Naismith, J. H. Curr. Opin. Struct. Biol. 2014, 29, 112.
(23) Oueis, E.; Jaspars, M.; Westwood, N. J.; Naismith, J. H. Angew. Chem. Weinheim. Bergstr. Ger. 2016, 128, 5936.
(24) Oueis, E.; Stevenson, H.; Jaspars, M.; Westwood, N. J.; Naismith, J. H. Chem. Commun. 2017, 53, 12274.
(25) Oueis, E.; Nardone, B.; Jaspars, M.; Westwood, N. J.; Naismith, J. H. ChemistryOpen 2017, 6, 11.
(26) Czekster, C. M.; Naismith, J. H. Biochemistry 2017, 56, 2086.
(27) Nguyen, G. K. T.; Wang, S.; Qiu, Y.; Hemu, X.; Lian, Y.; Tam, J. P. Nat. Chem. Biol. 2014, 10, 732.
(28) Nguyen, G. K. T.; Kam, A.; Loo, S.; Jansson, A. E.; Pan, L. X.; Tam, J. P. J. Am. Chem. Soc. 2015, 137, 15398.
(29) Chatterjee, J.; Gilon, C.; Hoffman, A.; Kessler, H. Acc. Chem. Res. 2008, 41, 1331.
(30) Ovadia, O.; Greenberg, S.; Chatterjee, J.; Laufer, B.; Opperer, F.; Kessler, H.; Gilon, C.; Hoffman, A. Mol. Pharm. 2011, 8, 479.
(31) Sgambelluri, R. M.; Smith, M. O.; Walton, J. D. ACS Synth. Biol. 2018, 7, 145.
(32) Yu, X.; Sun, D. Molecules 2013, 18, 6230.
(33) Cohen, D. J.; Loertscher, R.; Rubin, M. F.; Tilney, N. L.; Carpenter, C. B.; Strom, T. B. Ann. Intern. Med. 1984, 101, 667.
(34) Dreyfuss, M.; H□rri, E.; Hofmann, H.; Kobel, H.; Pache, W.; Tscherter, H. European J. Appl Microbiol. 1976, 3, 125.
(35) el Tayar, N.; Mark, A. E.; Vallat, P.; Brunne, R. M.; Testa, B.; van Gunsteren, W. F. J. Med. Chem. 1993, 36, 3757.
(36) Alex, A.; Millan, D. S.; Perez, M.; Wakenhut, F.; Whitlock, G. A. Medchemcomm 2011, 2, 669.
(37) Dittmann, J.; Wenger, R. M.; Kleinkauf, H.; Lawen, A. J. Biol. Chem. 1994, 269, 2841.
(38) Lawen, A.; Zocher, R. J. Biol. Chem. 1990, 265, 11355.
(39) Mayer, A.; Anke, H.; Sterner, O. Nat Prod Lett 1997, 10, 25.
(40) van der Velden, N. S.; Kälin, N.; Helf, M. J.; Piel, J.; Freeman, M. F.; Künzler, M. Nat. Chem. Biol. 2017, 13, 833.
(41) Ramm, S.; Krawczyk, B.; Mühlenweg, A.; Poch, A.; Mösker, E.; Süssmuth, R. D. Angew. Chem. Int. Ed. 2017, 56, 9994.
(42) Song, H.; Fahrig-Kamarauskaitė, J. R.; Matabaro, E.; Kaspar, H.; Shirran, S. L.; Zach, C.; Pace, A.; Stefanov, B.-A.; Naismith, J. H.; Künzler, M. ACS Chem. Biol. 2020, 15, 1901.
(43) Song, H.; Naismith, J. H. Curr. Opin. Struct. Biol. 2020, 65, 79.
(44) Song, H.; Burton, A. J.; Shirran, S. L.; Fahrig-Kamarauskaitė, J.; Kaspar, H.; Muir, T. W.; Künzler, M.; Naismith, J. H. Angew. Chem. Int. Ed. 2021, 60, 14319.
(45) Matabaro, E.; Kaspar, H.; Dahlin, P.; Bader, D. L. V.; Murar, C. E.; Staubli, F.; Field, C. M.; Bode, J. W.; Künzler, M. Sci. Rep. 2021, 11, 3541.
(46) Matabaro, E.; Song, H.; Chepkirui, C.; Kaspar, H.; Witte, L.; Naismith, J. H.; Freeman, M. F.; Künzler, M. Meth. Enzymol. 2021, 656, 429.
(47) Vogt, E.; Künzler, M. Appl. Microbiol. Biotechnol. 2019, 103, 5567.
(48) Nagatsu, T.; Hino, M.; Fuyamada, H.; Hayakawa, T.; Sakakibara, S.; Nakagawa, Y.; Takemoto, T. Anal. Biochem. 1976, 74, 466.

(49) Yoshimoto, T.; Kawahara, K.; Matsubara, F.; Kado, K.; Tsuru, D. J. Biochem. 1985, 98, 975.
(50) Song, H.; van der Velden, N. S.; Shiran, S. L.; Bleiziffer, P.; Zach, C.; Sieber, R.; Imani, A. S.; Krausbeck, F.; Aebi, M.; Freeman, M. F.; Riniker, S.; Künzler, M.; Naismith, J. H. Sci. Adv. 2018, 4, eaat2720.
(51) Quijano, M. R.; Zach, C.; Miller, F. S.; Lee, A. R.; Imani, A. S.; Künzler, M.; Freeman, M. F. J. Am. Chem. Soc. 2019, 141, 9637.
(52) Fülöp, V.; Böcskei, Z.; Polgár, L. Cell 1998, 94, 161.
(53) Fülöp, V.; Szeltner, Z.; Polgár, L. EMBO Rep. 2000, 1, 277.
(54) Shan, L.; Mathews, I. I.; Khosla, C. Proc. Natl. Acad. Sci. USA 2005, 102, 3599.
(55) Canning, P.; Rea, D.; Morty, R. E.; Fülöp, V. PLoS One 2013, 8, e79349.
(56) Li, M.; Chen, C.; Davies, D. R.; Chiu, T. K. J. Biol. Chem. 2010, 285, 21487.
(57) Kaushik, S.; Etchebest, C.; Sowdhamini, R. Proteins 2014, 82, 1428.
(58) Thoma, R.; Löffler, B.; Stihle, M.; Huber, W.; Ruf, A.; Hennig, M. Structure 2003, 11, 947.
(59) Aertgeerts, K.; Ye, S.; Tennant, M. G.; Kraus, M. L.; Rogers, J.; Sang, B.-C.; Skene, R. J.; Webb, D. R.; Prasad, G. S. Protein Sci. 2004, 13, 412.
(60) Ramachandran, G. N.; Ramakrishnan, C.; Sasisekharan, V. J. Mol. Biol. 1963, 7, 95.
(61) Lovell, S. C.; Davis, I. W.; Arendall, W. B.; de Bakker, P. I. W.; Word, J. M.; Prisant, M. G.; Richardson, J. S.; Richardson, D. C. Proteins 2003, 50, 437.
(62) Simon, R. J.; Kania, R. S.; Zuckermann, R. N.; Huebner, V. D.; Jewell, D. A.; Banville, S.; Ng, S.; Wang, L.; Rosenberg, S.; Marlowe, C. K. Proc. Natl. Acad. Sci. USA 1992, 89, 9367.
(63) Jurrus, E.; Engel, D.; Star, K.; Monson, K.; Brandi, J.; Felberg, L. E.; Brookes, D. H.; Wilson, L.; Chen, J.; Liles, K.; Chun, M.; Li, P.; Gohara, D. W.; Dolinsky, T.; Konecny, R.; Koes, D. R.; Nielsen, J. E.; Head-Gordon, T.; Geng, W.; Krasny, R.; Wei, G.-W.; Holst, M. J.; McCammon, J. A.; Baker, N. A. Protein Sci. 2018, 27, 112.
(64) Ho, B. K.; Gruswitz, F. BMC Struct Biol 2008, 8, 49.
(65) Pettersen, E. F.; Goddard, T. D.; Huang, C. C.; Couch, G. S.; Greenblatt, D. M.; Meng, E. C.; Ferrin, T. E. J. Comput. Chem. 2004, 25, 1605.
(66) Liu, H.; Naismith, J.H. BMS Biotechnology, 2009, 8, 9.
(67) Matabaro, E.; Song, H.; Chepkirui, C.; Kaspar, H.; Luca Witte, L.; Naismith, J.H.; Freeman, M.F.; Markus Künzler, M.; Meth. Enzymol. 2021, 429-458
(68) Winter, G. Appl. Cryst. 2010, 43, 186-190.
(69) Winter, G.; Waterman, D. H.; Parkhurst, J. M.; Brewster, A. S.; Gildea, R.J.; Gerstel, M.; Fuentes-Montero, L.; Vollmar, M.; Michels-Clark, T.; Young, I.D.; Sauter, N.K; G. Evans, G.; Acta Cryst., 2018, D74, 85-97
(70) McCoy A.; Grosse-Kunstleve R.; Adams P.; Winn M.; Storoni L.; Read R.J.; Appl. Cryst. 2007. 40, 658-674
(71) Murshudov, G.N.; Vagin, A.A.; Dodson, E.J.; Acta Cryst., 1997, D53, 240-255.
(72) Emsley, P., Lohkamp, B., Scott, W.G., Cowtan, K.; Acta Cryst., 2010 66, 486-501.
(73) Joosten R.P.; Joosten K.; Murshudov G.N.; Perrakis A.; Acta Cryst. 2012; D68:484-496.
(74) McNicholas, S.; Potterton, E.; Wilson, K.S.; Noble, M.E.M.; Acta Cryst. 2011, 67, 386-39
(75) Liebschner, D.; Afonine, P.V.; Baker, M.L.; Bunkóczi, G.; Chen, V.B.; Croll, T.I.; Hintze, B.; Hung, L.W., Jain, S.; McCoy, A.J.; Moriarty, N.W.; Oeffner, R. D.; Poon, B. K.; Prisant, M. G.; Read, R. J.; Richardson, J.S.; Richardson, D. C.; Sammito, M.D; Sobolev, O.V.; Stockwell, D.H.; Terwilliger, T.; Urzhumtsev, A.G.; Videau, L.L.; Williams, C.J.; Adams, P.D.; Acta Cryst. 2019 D75, 861–877

1062 (76) Edgar, R.C.; Nuc. Acid. Res. 2004, 32, 1792–1797.
1063 (76) Robert, X.; Gouet, P., Nuc. Acid. Res. 2014, 42,W320-324.

Supplementary figures

Figure 1-Figure supplement 1. **OphP production in *Pichia pastoris*.** (**a**) OphP was fused to a His_8SUMO* via a TEV cleavage site (in red). Residues Thr and Ser after the TEV cleavage site resulted from the insertion of the restriction site *Spe*I between OphP and the tag. The arrow indicates the cleavage site for TEV protease. (**b**) Purification of OphP. After purification of His_8SUMO*-OphP, the tag was cleaved off by TEV protease. (The tag appeared to be slowly cleaved off at room temperature without the addition of TEV protease after residue Thr117, the number corresponds to the as expressed fusion protein, not the final purified protein.) The cleaved protein was further purified by size exclusion chromatography (SEC) over an Akta FPLC system. (**c**) OphP peak from SEC purification. mAU: Milli Absorbance Unit. (**d**) Production of OphP homologs LedP and GmPOPB. LedP was recombinantly produced in *P. pastoris* and GmPOPB in *E. coli*. Arrow indicates purified POP.

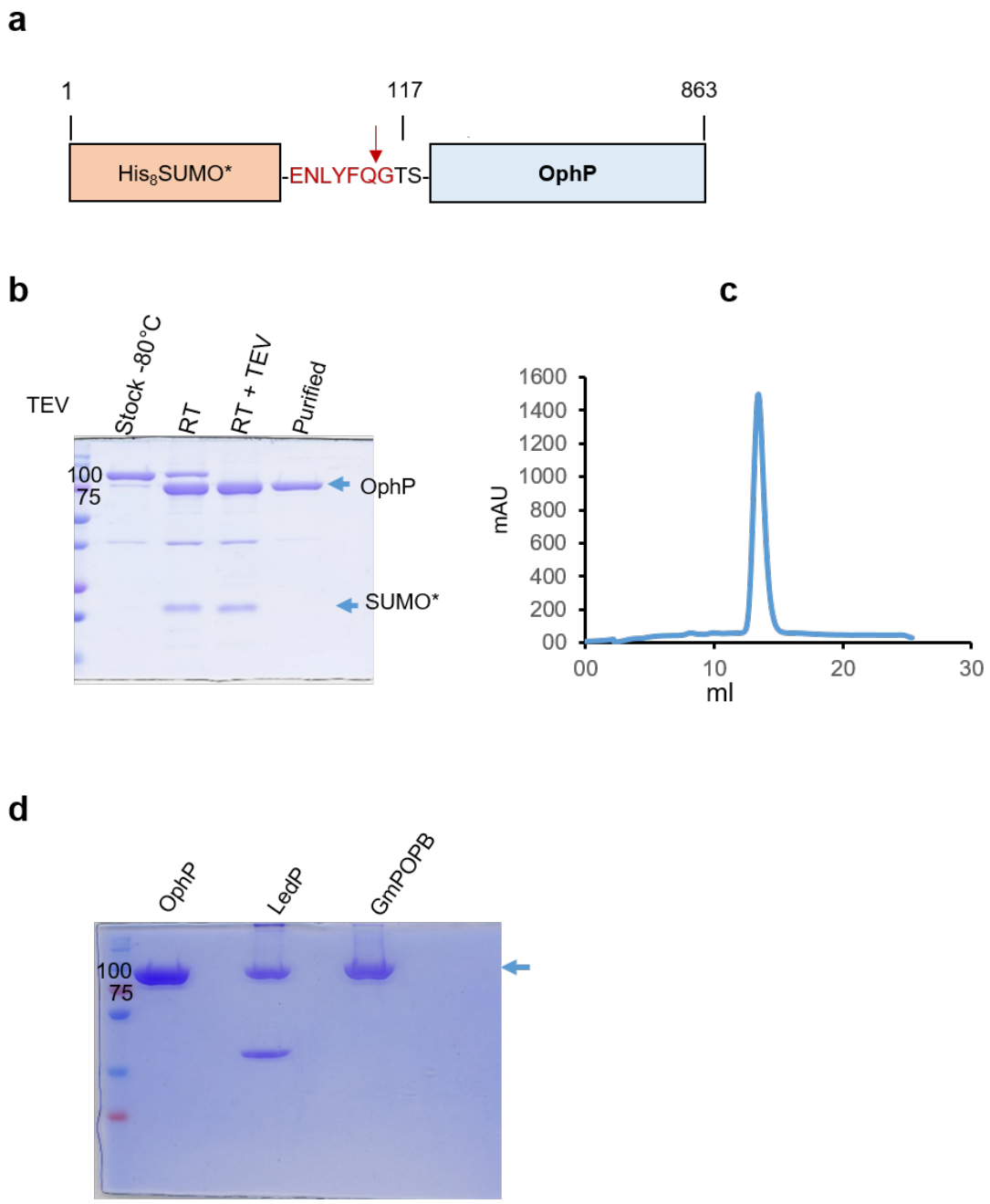

Figure 1-Figure supplement 2. OphP activity on the chromogenic substrate Z-Gly-Pro-pNA. (**a**) The effect of temperature on OphP activity. (**b**) The effect of pH on OphP activity. In both assays, the concentration of the substrate and the enzyme was 1mM and 8uM, respectively. (**c**) The inhibitory effect of Z-Pro-prolinal on OphP. The assays were performed in triplicates. OphP was incubated with Z-Pro-prolinal for 30min at 30°C before adding the chromogenic substrate.

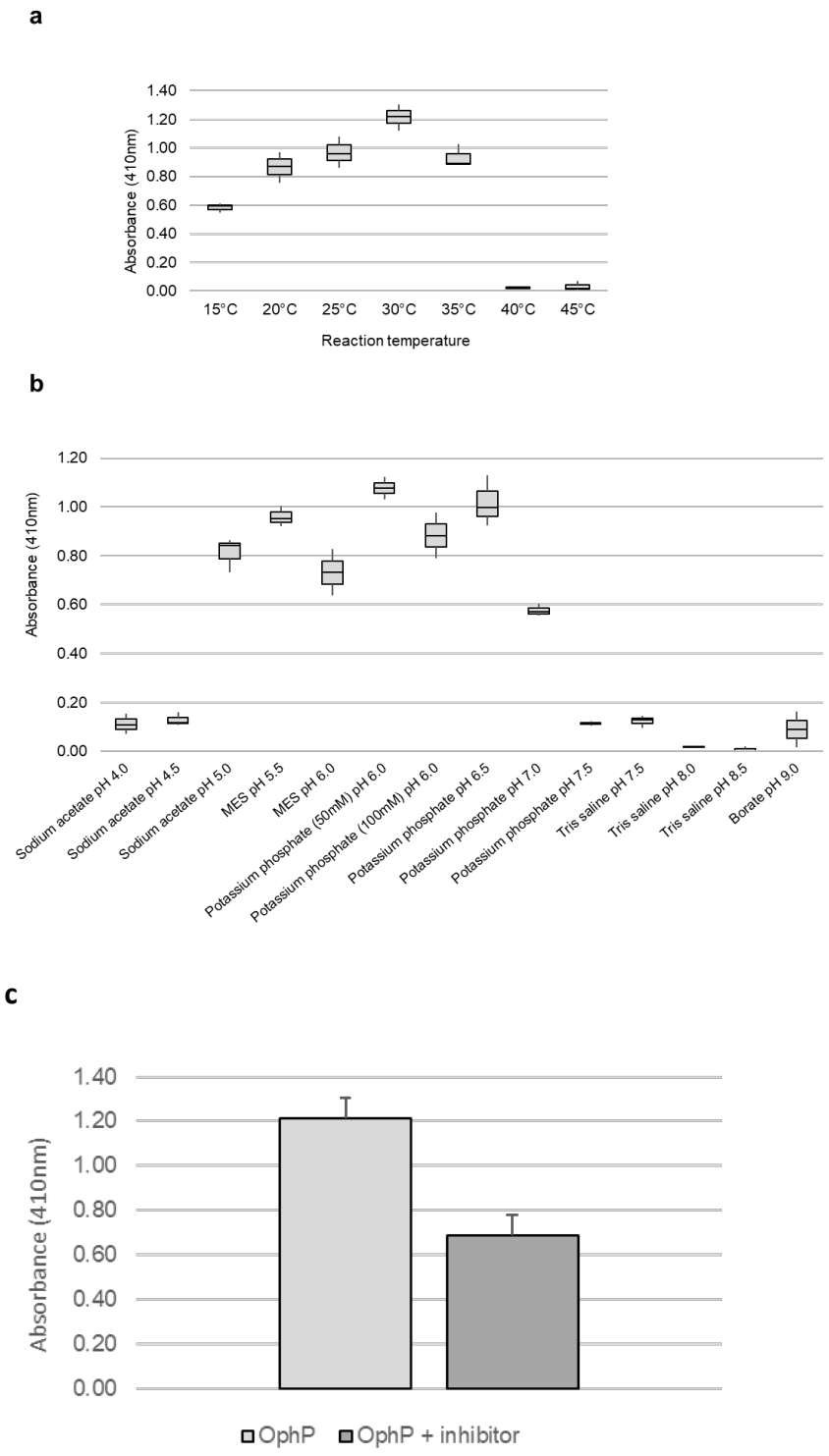

Figure 1-Figure supplement 3. **Intact mass of full-length OphMA-2h incubated with OphP with or without SAM**. (a) Intact mass of full length OphMA-2h expressed for only 2 hours in *E. coli* at 16 ºC. (b) Intact mass of full length OphMA-2h when incubated at 4 mg/ml with 5 mM SAM at room temperature in 50 mM Tris pH 8.0, 100 mM NaCl and 1 mM TCEP. (**c**) Intact mass of full length OphMA-2h incubated at 4 mg/ml with 5 mM SAM and 0.9 mg/ml OphP (10 mM) at room temperature in 50 mM Tris pH 8.0, 100 mM NaCl and 1 mM TCEP. The molecular mass of OphP (after TEV cleavage) is 84611 Da and the peak at 42303 Da corresponds to doubly charged OphP.

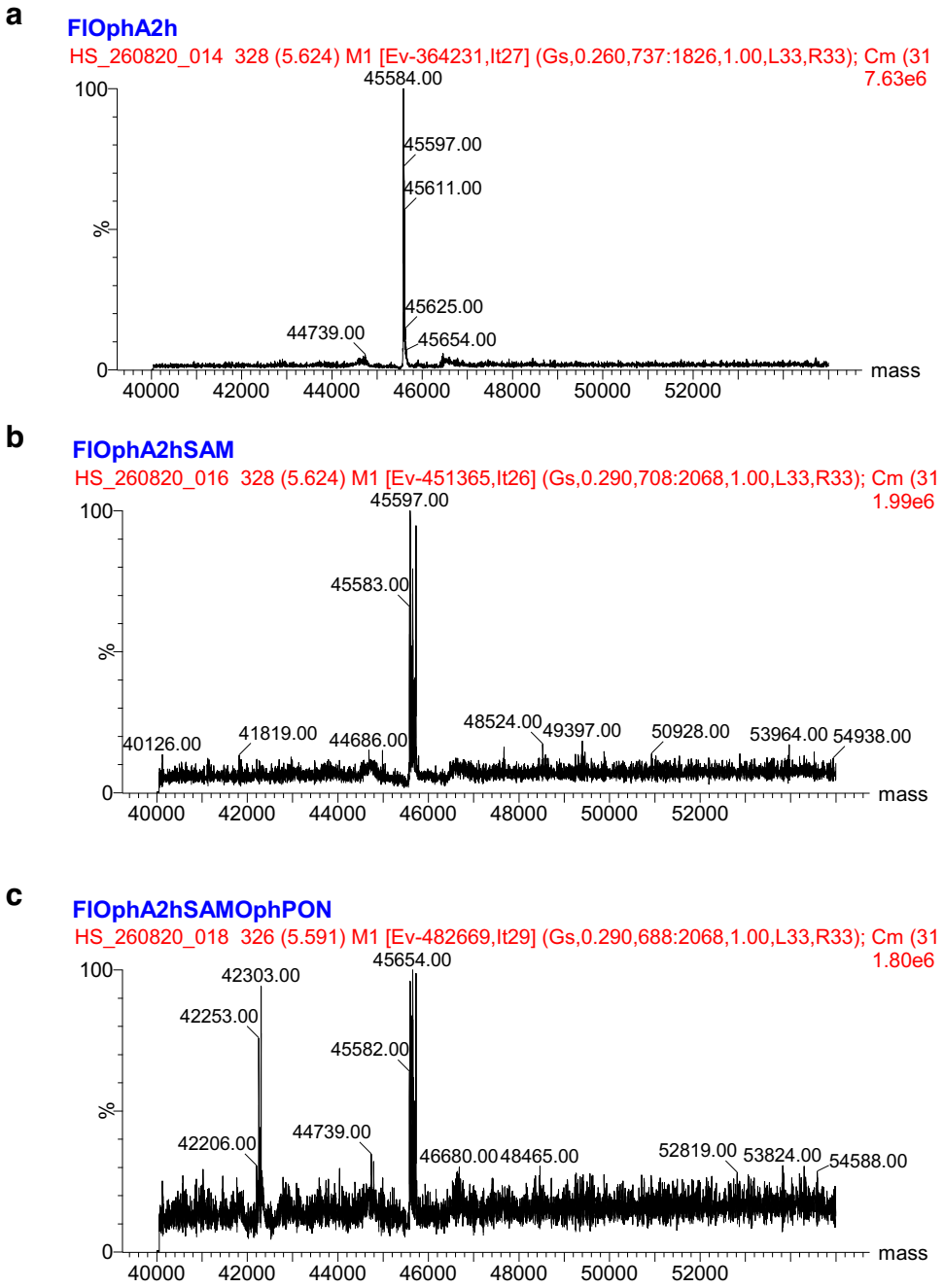

Figure 1-Figure supplement 4. Co-purification following the first metal affinity step of His_8OphMA and His_8SUMO*-OphP(S580A) heterologously co-expressed in *Pichia pastoris*. (**a**) Size exclusion chromatography (HiLoad 16/600 Superdex S200 pg) of His_8OphMA and His_8SUMO*OphP(S580A). (**b**) SDS-PAGE gel of the corresponding fractions from the gel filtration. (**c**) Intact protein mass determination of His_8OphMA confirming integrity and methylation. (**d-e**) Size exclusion chromatography of TEV protease cleaved OphP(S580A) lacking the His_8SUMO* tag and corresponding SDS-PAGE gels. This was not co-expressed with His_8OphMA and is used as a control.

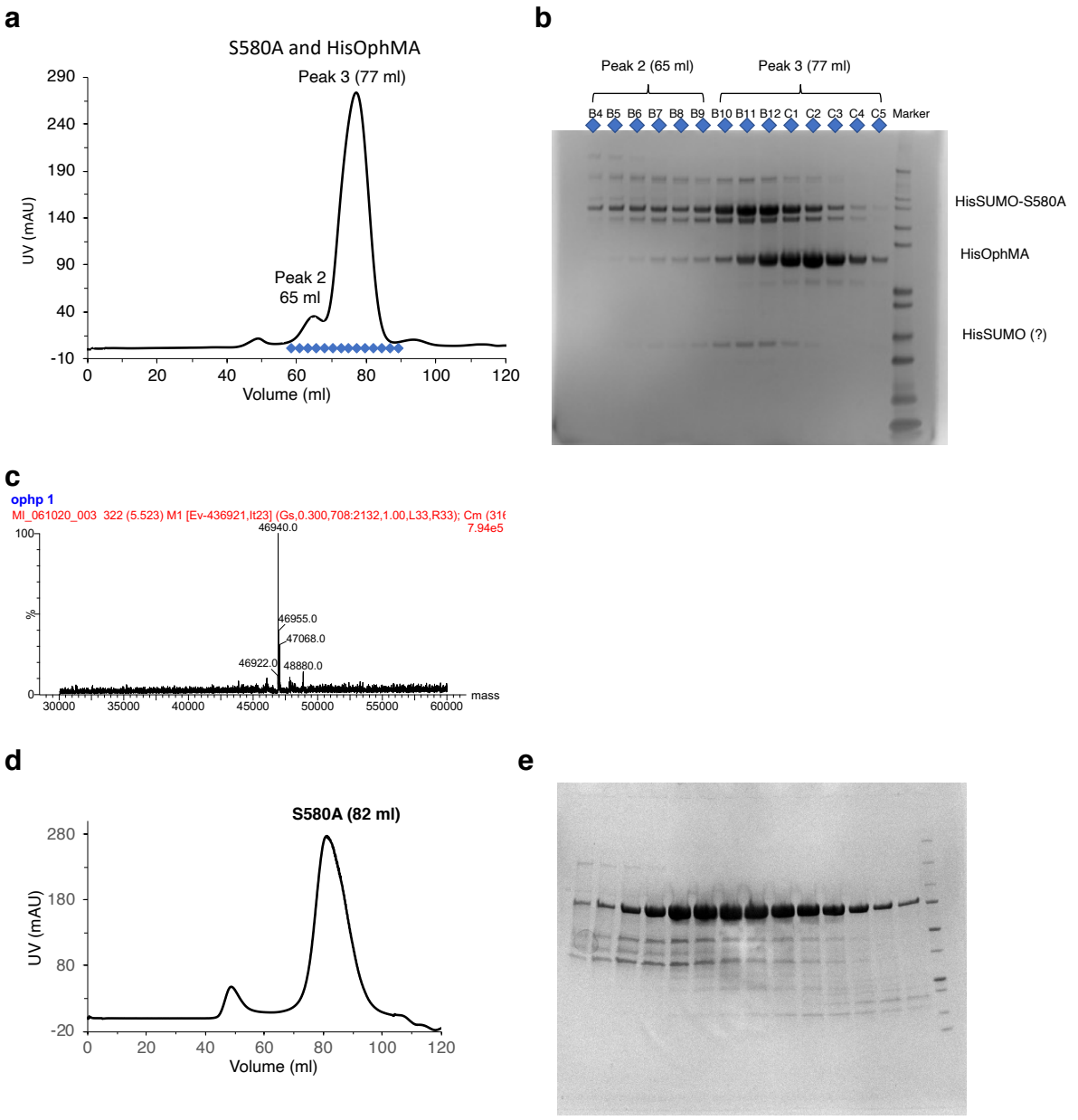

Figure 1-Figure supplement 5. Co-purification following the first metal affinity step of His_8OphMA and His_8SUMO*OphP heterologously co-expressed in *Pichia pastoris*. (**a**) Size exclusion chromatography (HiLoad 16/600 Superdex S200 pg) of His_8OphMA and His_8SUMO*OphP. (**b**) SDS-PAGE gel of the corresponding fractions from the gel filtration. (**c**) Intact protein mass determination of His_8OphMA confirming integrity and methylation.

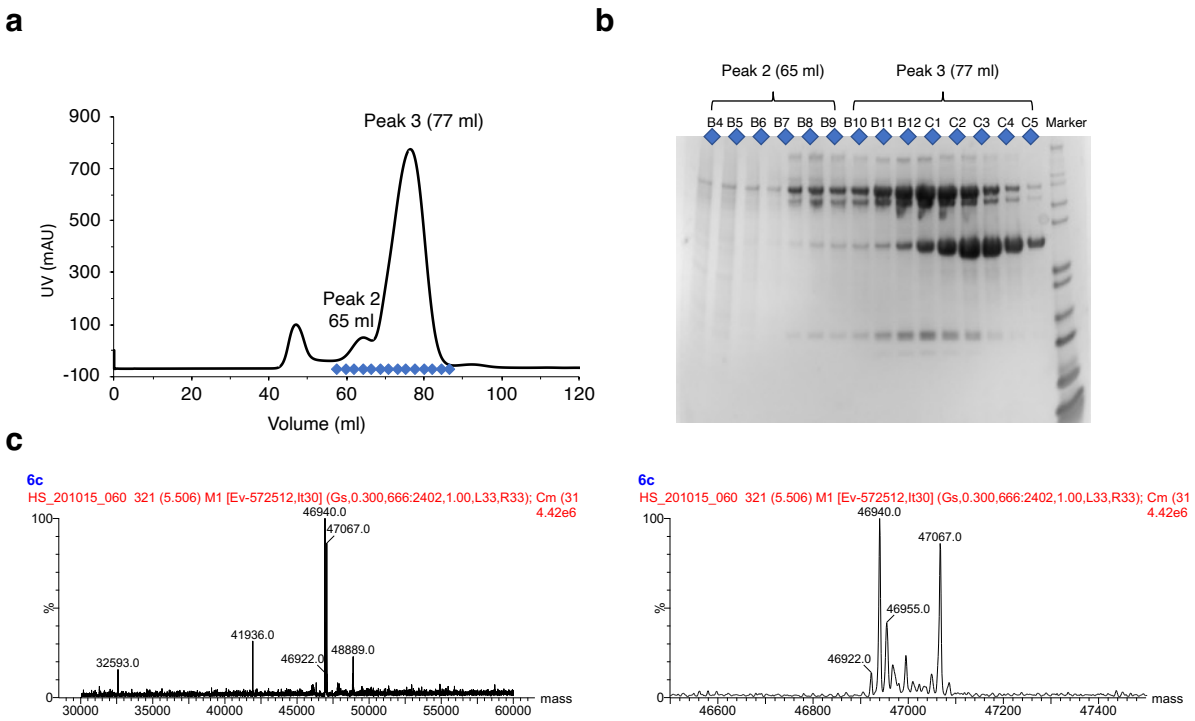

Figure 2-Figure supplement 1. **HPLC-MS analysis of peptide substrates.** (**a, b**) Ion chromatograms of OphMA-TEV-derived backbone N-methylated peptide substrates produced using TEV protease only (a) or in combination with GmPOPB (b). The number of methylated residues is indicated by green numbers and red dashed lines. The different peptides have been aligned by extent of methylation rather than by absolute mass, to aid comparison. The core peptide is underlined. Note that the follower peptide is different for the non-omphalotin peptides.

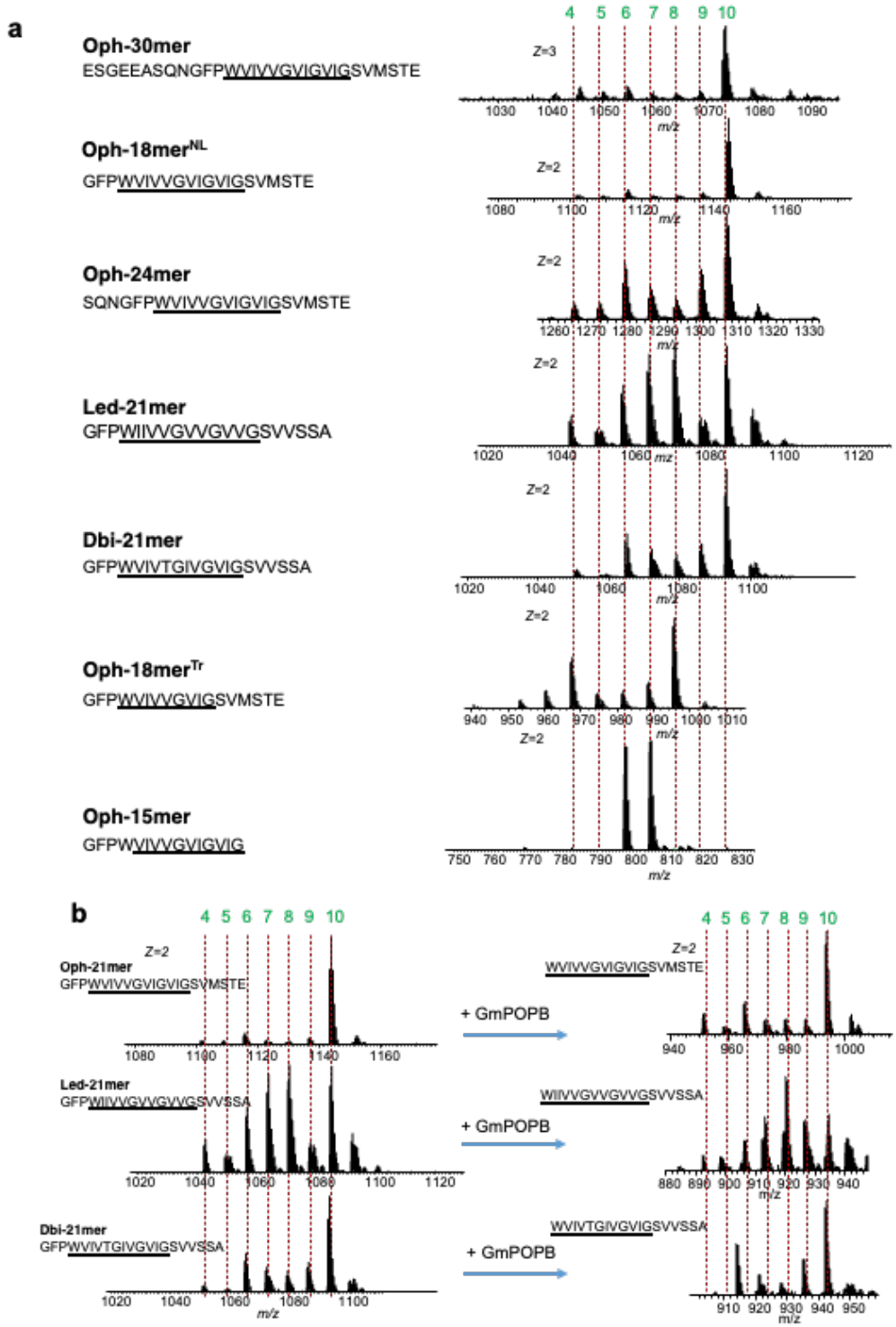

Figure 2-Figure supplement 2. LC-MS/MS spectra of OphMA-TEV C-terminal peptides. (**a-g**) Peptides substrates obtained by cleaving OphMA-TEV variants with the TEV protease: Oph-21mer, Led-21mer, Dbi- Oph-21mer, Oph-18mer^{NL}, Oph-18mer^{Tr}, Oph-24mer, non-methylated peptide Oph-21mer, and Oph-15mer, respectively. **(h-m)** Peptide products obtained by incubation of peptide substrates with OphP: 12-residue cyclic peptide from Oph-21mer (**h**), 12-residue and 15-residue cyclic peptides obtained from Led-21mer, respectively (**i-j**), 15-residue cyclic peptide obtained from Dbi-21mer (**k**), 15-residue and 18-residue cyclic peptides from Oph-24mer (**l-m**). **(n-p)** Omphalotin A, lentinulin A and dendrothelin A intermediates. Methylated residues are highlighted in green color. B-ions and y-ions are shown in blue color. Mass tolerance between observed masses and the theoretical masses was set at 10 ppm. This difference is indicated in parentheses. Mass precision was set at 4 decimals.

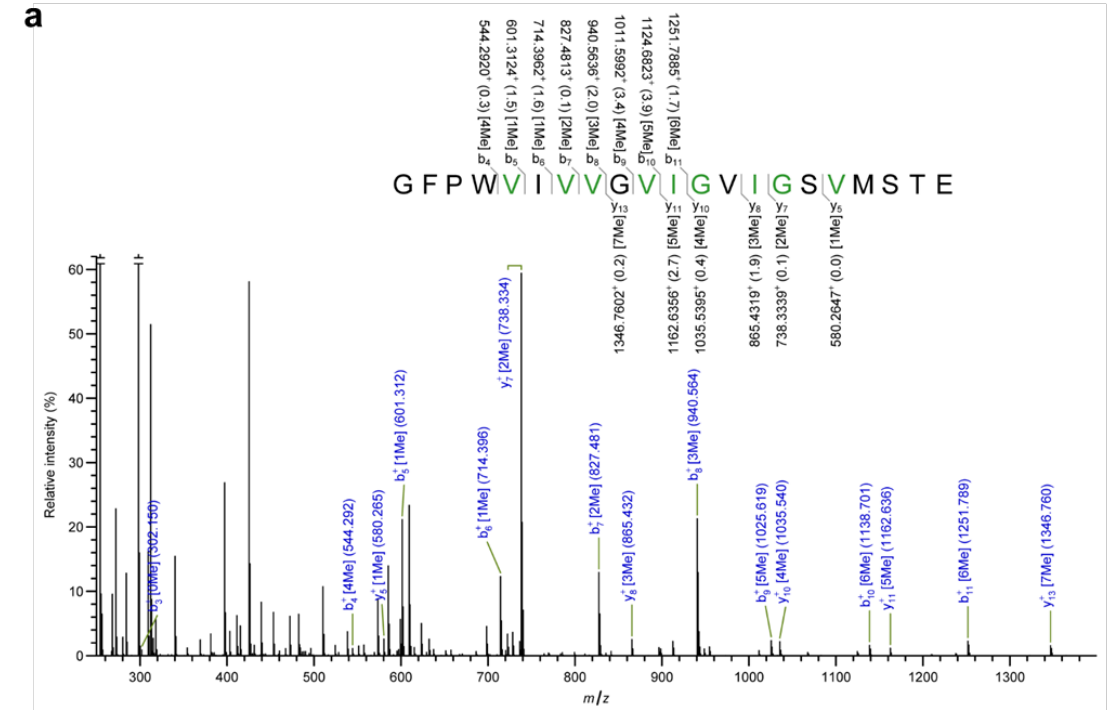
a
544.2920+ (0.3) [4Me] b4
601.3124+ (1.5) [1Me] b5
714.3962+ (1.6) [1Me] b6
827.4813+ (0.1) [2Me] b7
940.5636+ (2.0) [3Me] b8
1011.5992+ (3.4) [4Me] b9
1124.6823+ (3.9) [5Me] b10
1251.7885+ (1.7) [6Me] b11
GFPWVIVVGVIGVIGSVMSTE
1346.7602+ (0.2) [7Me] y13
1162.6356+ (2.7) [5Me] y11
1035.5395+ (0.4) [4Me] y10
865.4319+ (1.9) [3Me] y8
738.3339+ (0.1) [2Me] y7
580.2647+ (0.0) [1Me] y5
Relative intensity (%)
m/z
b2+ [4Me] (544.292)
y5+ [1Me] (580.265)
b5+ [1Me] (601.312)
b6+ [1Me] (714.396)
y7+ [2Me] (738.334)
b7+ [2Me] (827.481)
y8+ [3Me] (865.432)
b8+ [3Me] (940.564)
b9+ [5Me] (1025.619)
y10+ [4Me] (1035.540)
b10+ [6Me] (1138.701)
y11+ [5Me] (1162.636)
b11+ [6Me] (1251.789)
y13+ [7Me] (1346.760)

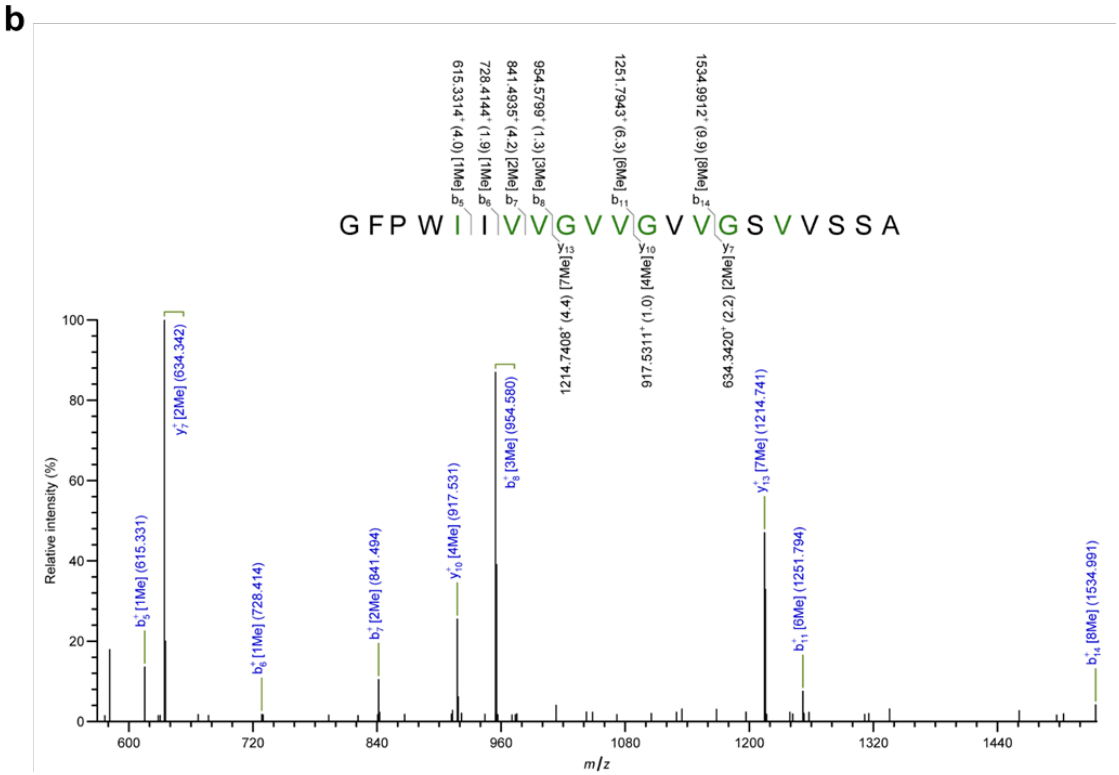
b
615.3314+ (4.0) [1Me] b5
728.4144+ (1.9) [1Me] b6
841.4935+ (4.2) [2Me] b7
954.5799+ (1.3) [3Me] b8
1251.7943+ (6.3) [6Me] b11
1534.9912+ (9.9) [8Me] b14
GFPWIIVVGVVGVVGSVVSSA
1214.7408+ (4.4) [7Me] y13
917.5311+ (1.0) [4Me] y10
634.3420+ (2.2) [2Me] y7
Relative intensity (%)
m/z
b5+ [1Me] (615.331)
y7+ [2Me] (634.342)
b6+ [1Me] (728.414)
b7+ [2Me] (841.494)
y10+ [4Me] (917.531)
b8+ [3Me] (954.580)
y13+ [7Me] (1214.741)
b11+ [6Me] (1251.794)
b14+ [8Me] (1534.991)

c

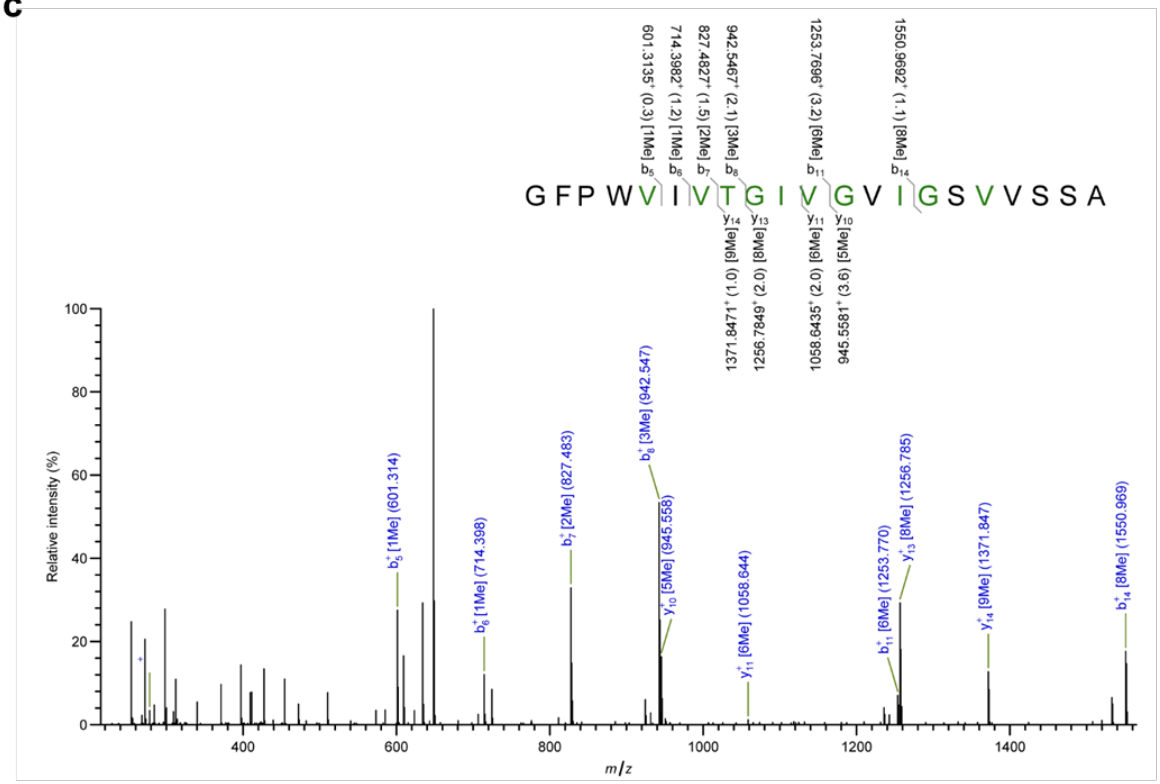
601.3135+ (0.3) [1Me] b5
714.3982+ (1.2) [1Me] b6
827.4827+ (1.5) [2Me] b7
942.5467+ (2.1) [3Me] b8
1253.7696+ (3.2) [6Me] b11
1550.9962+ (1.1) [8Me] b14
GFPWVIVTGIVGVIGSVVSSA
1371.8471+ (1.0) [9Me] y14
1256.7849+ (2.0) [8Me] y13
1058.6435+ (2.0) [6Me] y11
945.5581+ (3.6) [5Me] y10
Relative intensity (%)
m/z
b5+ [1Me] (601.314)
b6+ [1Me] (714.398)
b7+ [2Me] (827.483)
b8+ [3Me] (942.547)
y10+ [5Me] (945.558)
y11+ [6Me] (1058.644)
b11+ [6Me] (1253.770)
y13+ [8Me] (1256.785)
y14+ [9Me] (1371.847)
b14+ [8Me] (1550.969)

d

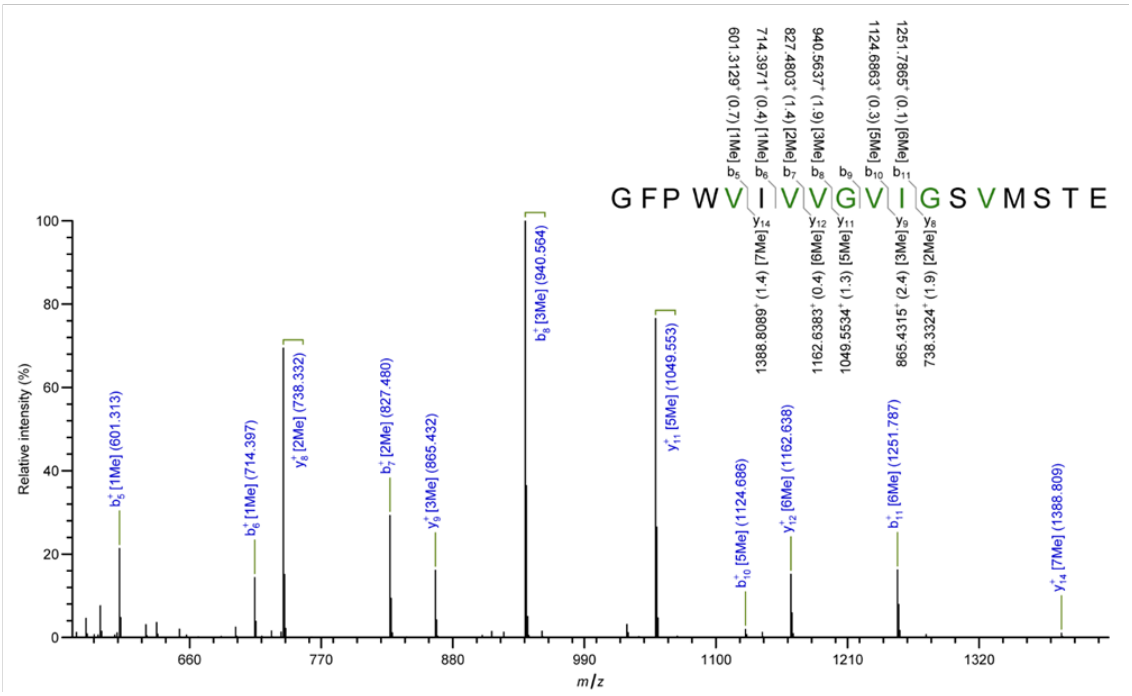
601.3129+ (0.7) [1Me] b5
714.3971+ (0.4) [1Me] b6
827.4803+ (1.4) [2Me] b7
940.5637+ (1.9) [3Me] b8
1124.6863+ (0.3) [5Me] b10
1251.7865+ (0.1) [6Me] b11
GFPWVIVVGVIGSVMSTE
1388.8089+ (1.4) [7Me] y14
1162.6383+ (0.4) [6Me] y12
1049.5534+ (1.3) [5Me] y11
865.4315+ (2.4) [3Me] y9
738.3324+ (1.9) [2Me] y8
Relative intensity (%)
m/z
b5+ [1Me] (601.313)
b6+ [1Me] (714.397)
y8+ [2Me] (738.332)
b7+ [2Me] (827.480)
y9+ [3Me] (865.432)
b8+ [3Me] (940.564)
y11+ [5Me] (1049.553)
b10+ [5Me] (1124.686)
y12+ [6Me] (1162.638)
b11+ [6Me] (1251.787)
y14+ [7Me] (1388.809)

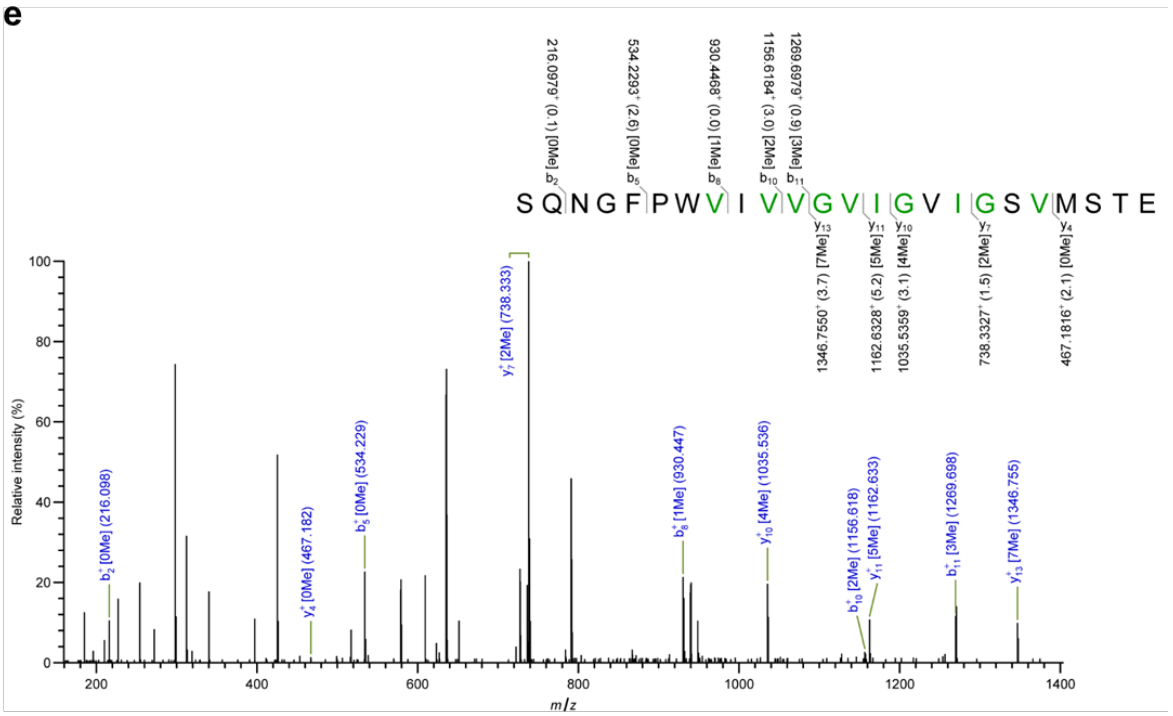
e
SQNGFPWVIVVGVIGVIGSVMSTE
Relative intensity (%)
m/z

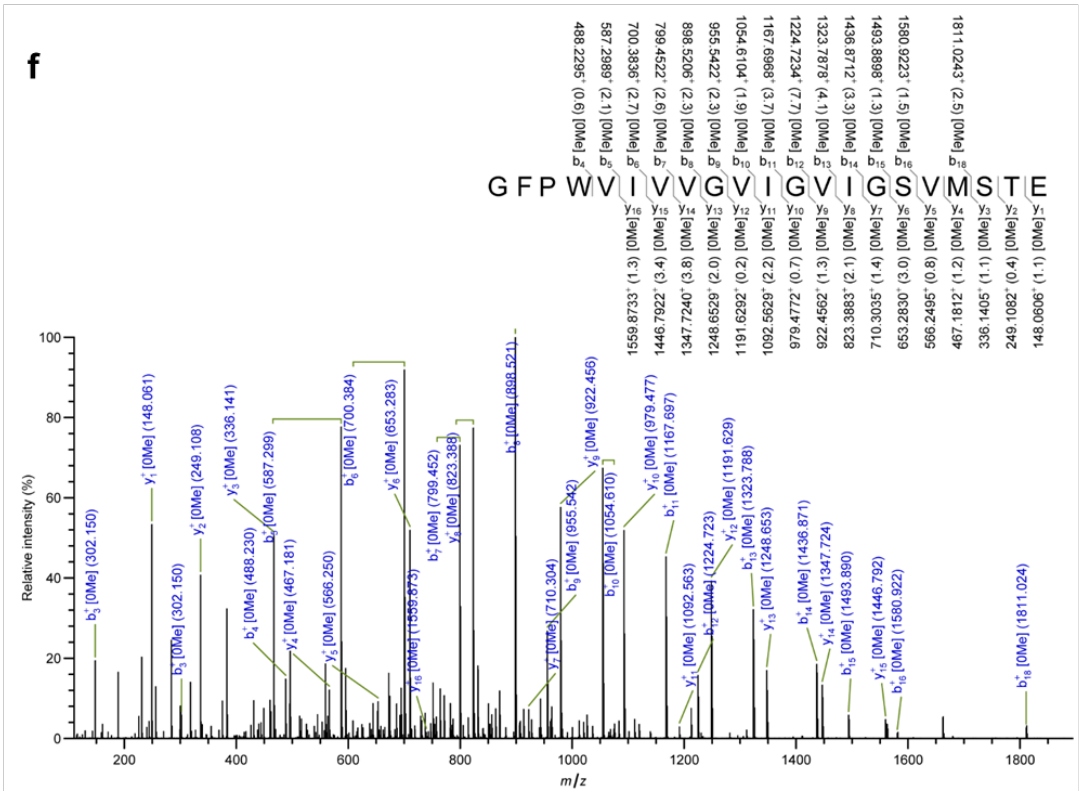
f
GFPWVIVVGVIGVIGSVMSTE
Relative intensity (%)
m/z

g

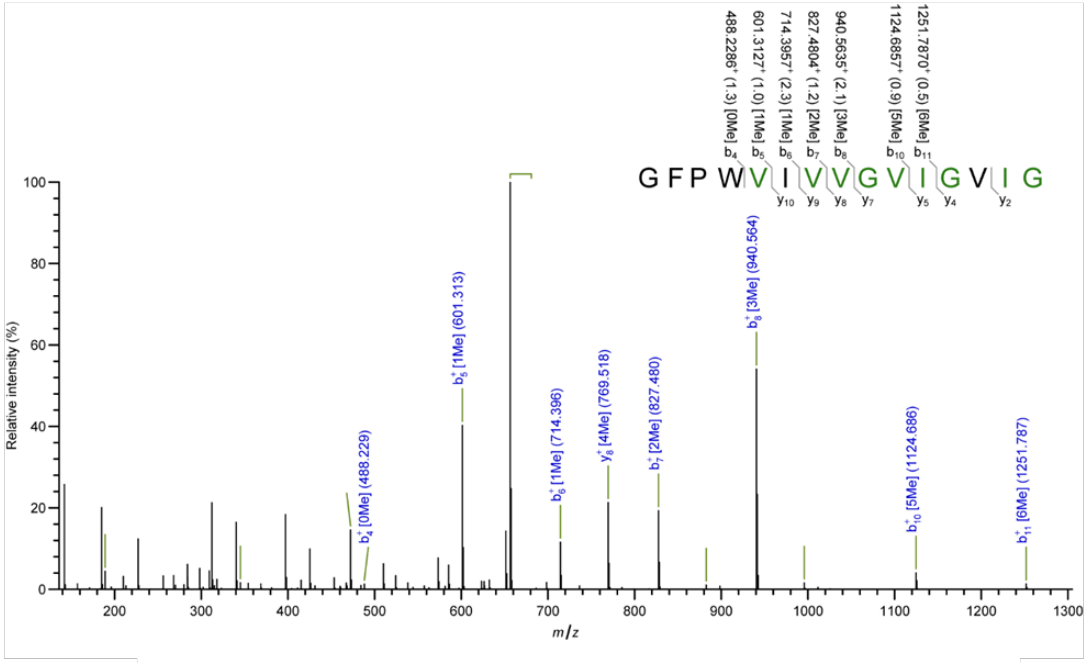
488.2286+ (1.3) [0Me]
601.3127+ (1.0) [1Me]
714.3957+ (2.3) [1Me]
827.4804+ (1.2) [2Me]
940.5635+ (2.1) [3Me]
1124.6857+ (0.9) [5Me]
1251.7870+ (0.5) [6Me]
GFPWVIVVGVIGVIG
b4+ [0Me] (488.229)
b5+ [1Me] (601.313)
b6+ [1Me] (714.396)
y8+ [4Me] (769.518)
b7+ [2Me] (827.480)
b8+ [3Me] (940.564)
b10+ [5Me] (1124.686)
b11+ [6Me] (1251.787)
Relative intensity (%)
m/z

h

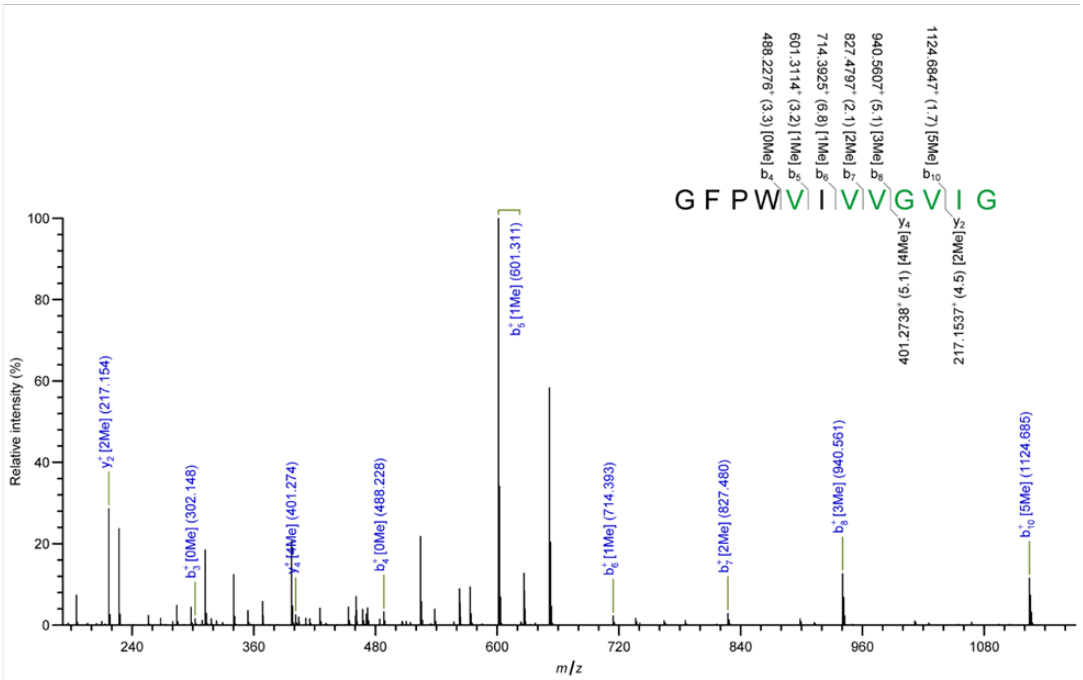
488.2276+ (3.3) [0Me]
601.3114+ (3.2) [1Me]
714.3925+ (6.8) [1Me]
827.4797+ (2.1) [2Me]
940.5607+ (5.1) [3Me]
1124.6847+ (1.7) [5Me]
GFPWVIVVGVIG
401.2738+ (5.1) [4Me]
217.1537+ (4.5) [2Me]
y2+ [2Me] (217.154)
b3+ [0Me] (302.148)
y4+ [4Me] (401.274)
b4+ [0Me] (488.228)
b5+ [1Me] (601.311)
b6+ [1Me] (714.393)
b7+ [2Me] (827.480)
b8+ [3Me] (940.561)
b10+ [5Me] (1124.685)
Relative intensity (%)
m/z

i

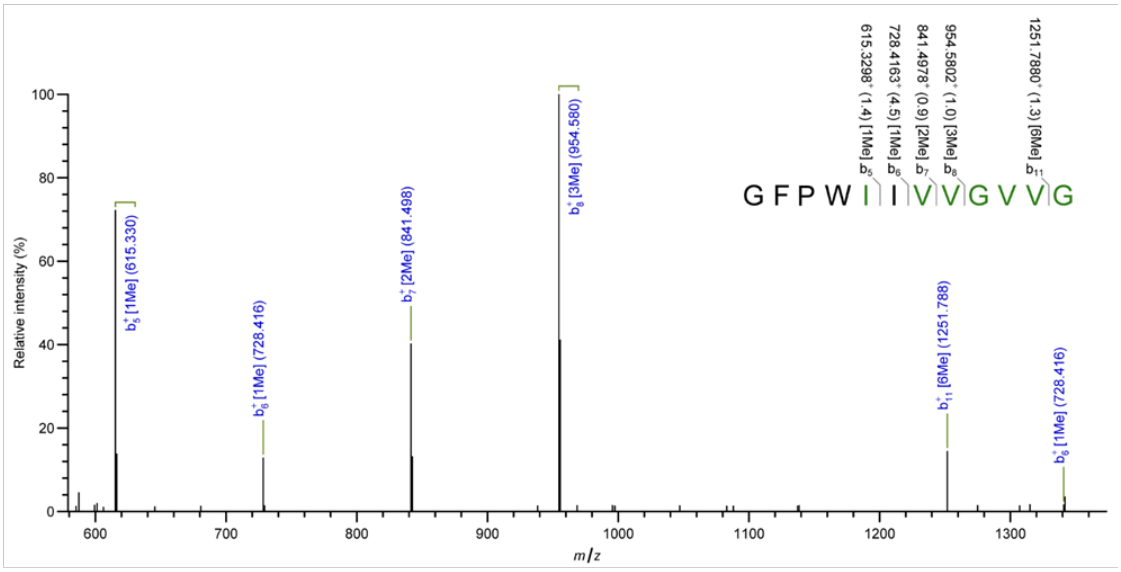
615.3298+ (1.4) [1Me] b5
728.4163+ (4.5) [1Me] b6
841.4978+ (0.9) [2Me] b7
954.5802+ (1.0) [3Me] b8
1251.7880+ (1.3) [6Me] b11
G F P W I I V V G V V G
b5+ [1Me] (615.330)
b6+ [1Me] (728.416)
b7+ [2Me] (841.498)
b8+ [3Me] (954.580)
b11+ [6Me] (1251.788)
b6+ [1Me] (728.416)
Relative intensity (%)
m/z

j

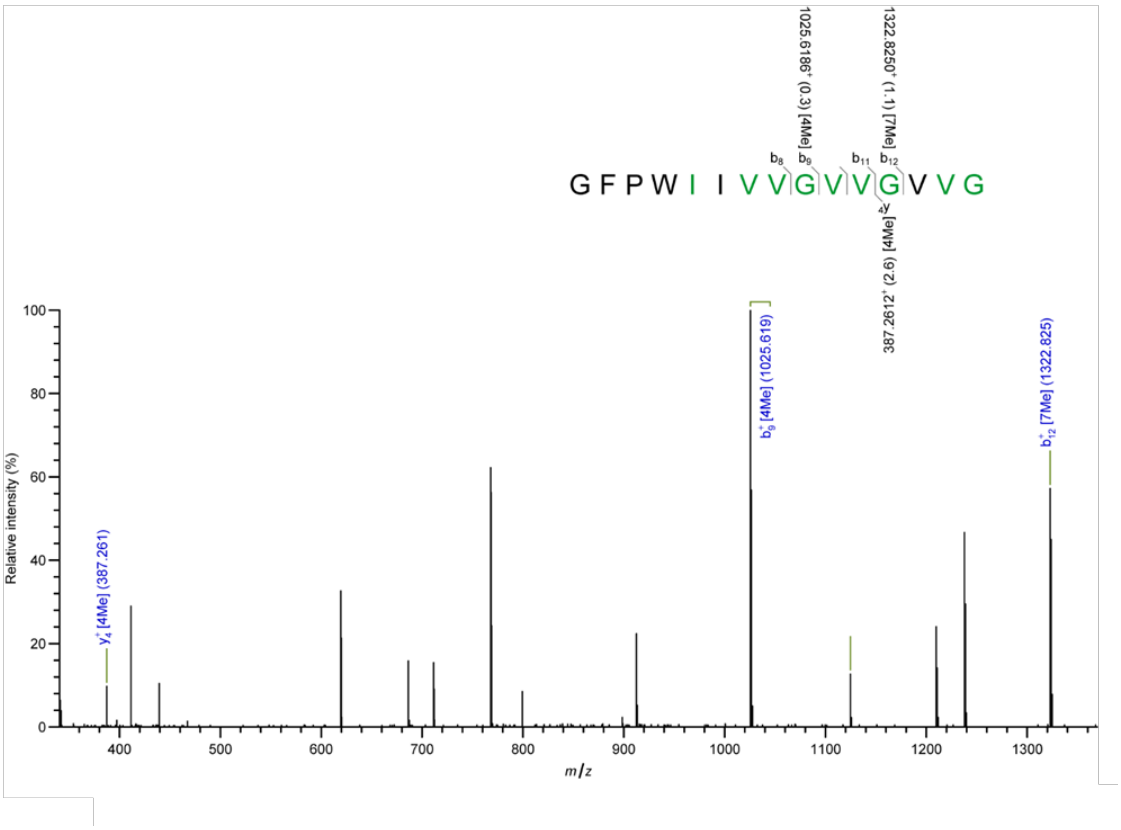
1025.6186+ (0.3) [4Me] b9
1322.8250+ (1.1) [7Me] b12
b8
b11
G F P W I I V V G V V G V V G
387.2612+ (2.6) [4Me] y4
b9+ [4Me] (1025.619)
b12+ [7Me] (1322.825)
y4+ [4Me] (387.261)
Relative intensity (%)
m/z

k

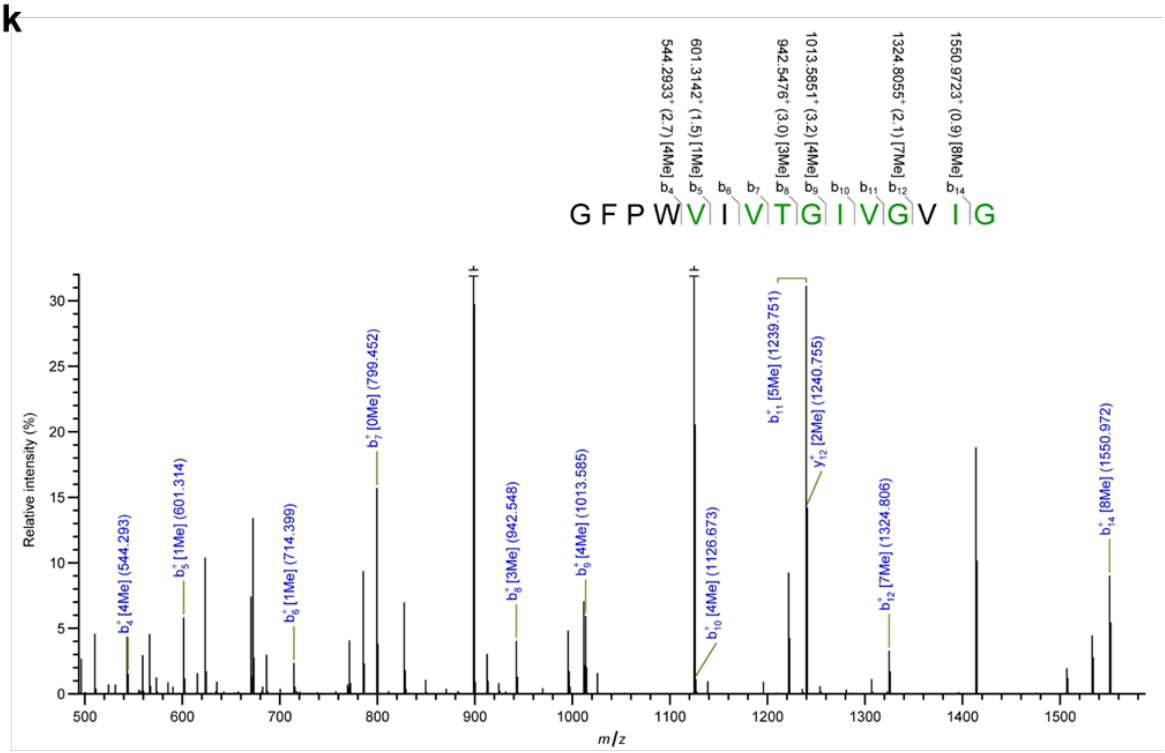
544.2933+ (2.7) [4Me] b4
601.3142+ (1.5) [1Me] b5
b6
b7
942.5476+ (3.0) [3Me] b8
1013.5851+ (3.2) [4Me] b9
b10
b11
1324.8055+ (2.1) [7Me] b12
1550.9723+ (0.9) [8Me] b14
G F P W V I V T G I V G V I G
b4+ [4Me] (544.293)
b5+ [1Me] (601.314)
b6+ [1Me] (714.399)
b7+ [0Me] (799.452)
b8+ [3Me] (942.548)
b9+ [4Me] (1013.585)
b10+ [4Me] (1126.673)
b11+ [5Me] (1239.751)
y12+ [2Me] (1240.755)
b12+ [7Me] (1324.806)
b14+ [8Me] (1550.972)
Relative intensity (%)
m/z

l

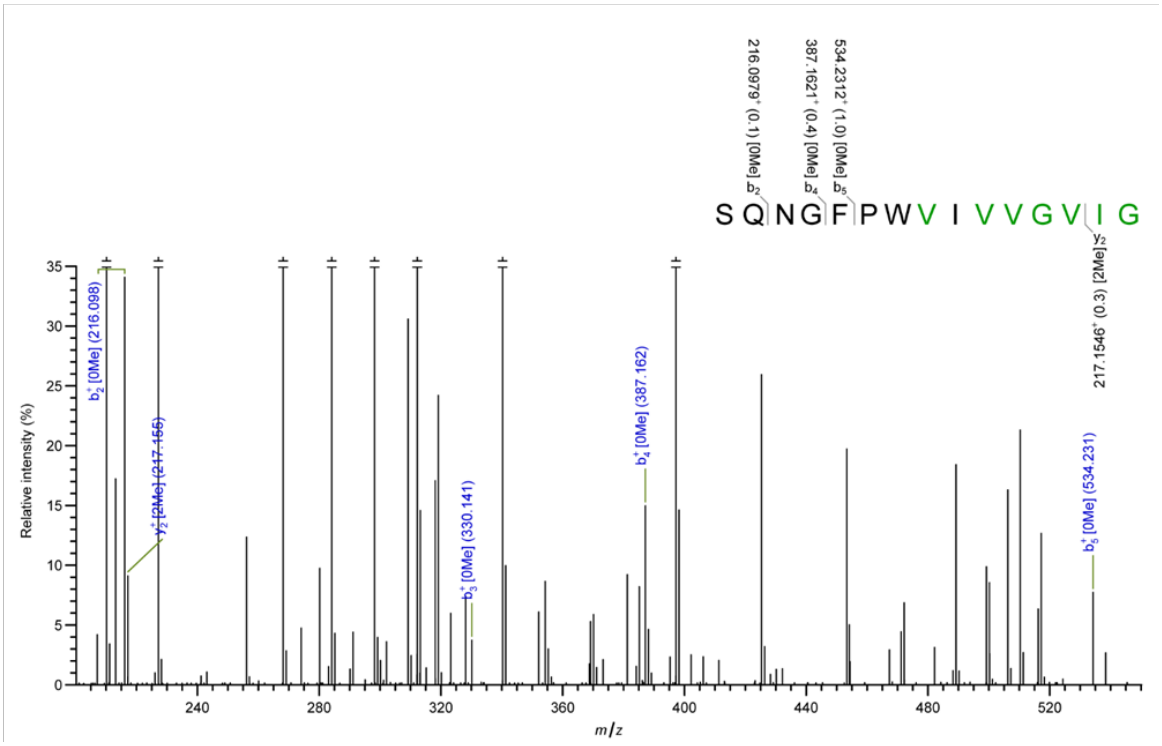
216.0979+ (0.1) [0Me] b2
387.1621+ (0.4) [0Me] b4
534.2312+ (1.0) [0Me] b5
S Q N G F P W V I V V G V I G
217.1546+ (0.3) [2Me] y5
b2+ [0Me] (216.098)
y2+ [2Me] (217.155)
b3+ [0Me] (330.141)
b4+ [0Me] (387.162)
b5+ [0Me] (534.231)
Relative intensity (%)
m/z

m

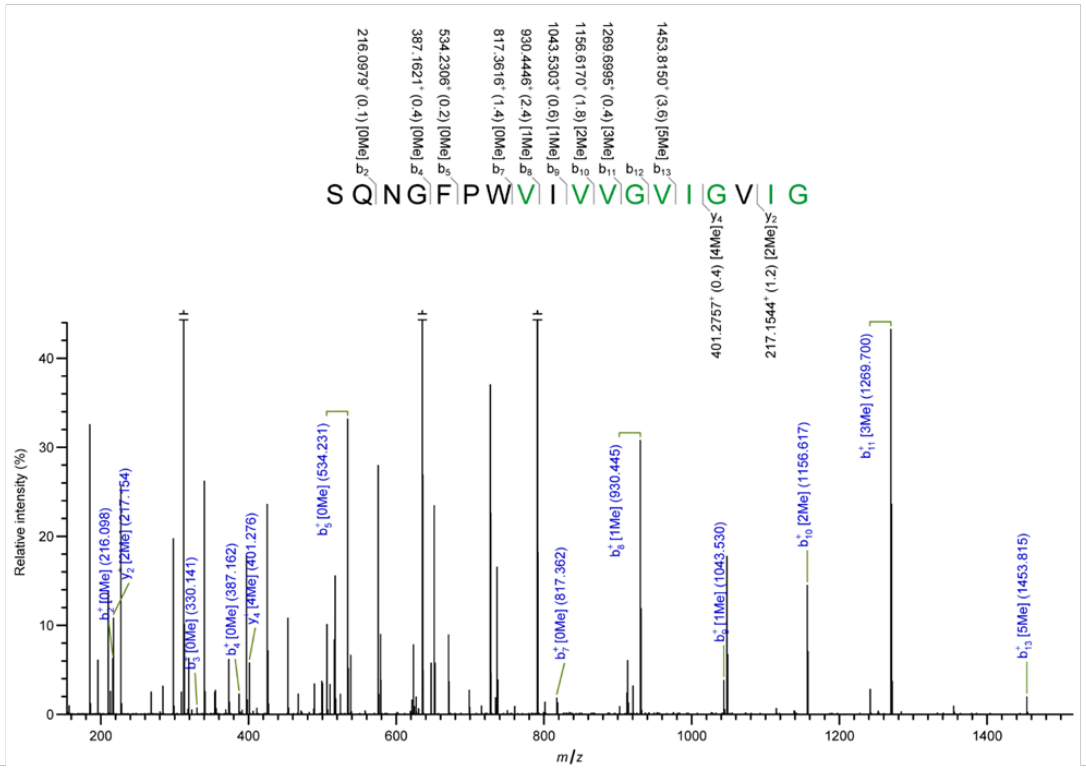
SQNGFPWVIVVGVIGVIG
216.0979+ (0.1) [0Me] b2+
387.1621+ (0.4) [0Me] b4+
534.2306+ (0.2) [0Me] b5+
817.3616+ (1.4) [0Me] b7+
930.4446+ (2.4) [1Me] b8+
1043.5303+ (0.6) [1Me] b9+
1156.6170+ (1.8) [2Me] b10+
1269.6995+ (0.4) [3Me] b11+
1453.8150+ (3.6) [5Me] b13+
401.2757+ (0.4) [4Me] y4+
217.1544+ (1.2) [2Me] y2+
b2+ [0Me] (216.098)
y2 [2Me] (217.154)
b3 [0Me] (330.141)
b4+ [0Me] (387.162)
y4 [4Me] (401.276)
b5+ [0Me] (534.231)
b7+ [0Me] (817.362)
b8+ [1Me] (930.445)
b9+ [1Me] (1043.530)
b10+ [2Me] (1156.617)
b11 [3Me] (1269.700)
b13+ [5Me] (1453.815)
Relative intensity (%)
m/z

n

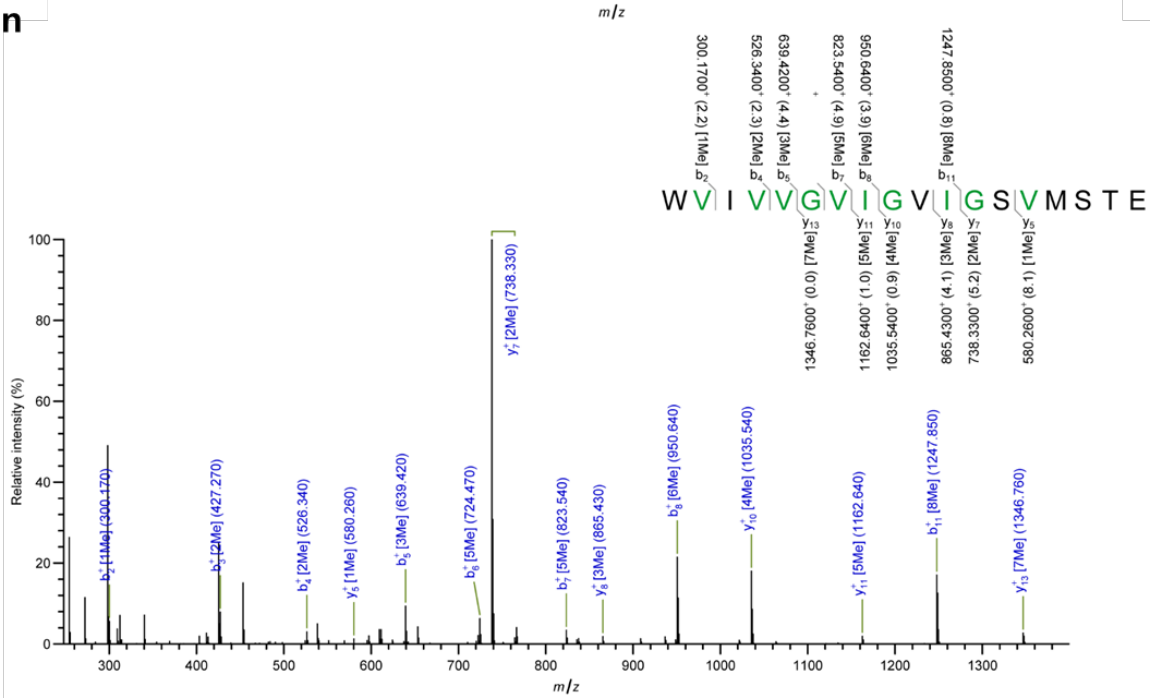
WVIVVGVIGVIGSVMSTE
300.1700+ (2.2) [1Me] b2+
526.3400+ (2.3) [2Me] b4+
639.4200+ (4.4) [3Me] b5+
823.5400+ (4.9) [5Me] b7+
950.6400+ (3.9) [6Me] b8+
1247.8500+ (0.8) [8Me] b11+
1346.7600+ (0.0) [7Me] y13+
1162.6400+ (1.0) [5Me] y11+
1035.5400+ (0.9) [4Me] y10+
865.4300+ (4.1) [3Me] y8+
738.3300+ (5.2) [2Me] y7+
580.2600+ (8.1) [1Me] y5+
b2+ [1Me] (300.170)
b3+ [2Me] (427.270)
b4+ [2Me] (526.340)
y5+ [1Me] (580.260)
b5+ [3Me] (639.420)
b6+ [5Me] (724.470)
y7+ [2Me] (738.330)
b7+ [5Me] (823.540)
y8+ [3Me] (865.430)
b8+ [6Me] (950.640)
y10+ [4Me] (1035.540)
y11+ [5Me] (1162.640)
b11+ [8Me] (1247.850)
y13+ [7Me] (1346.760)
Relative intensity (%)
m/z

o

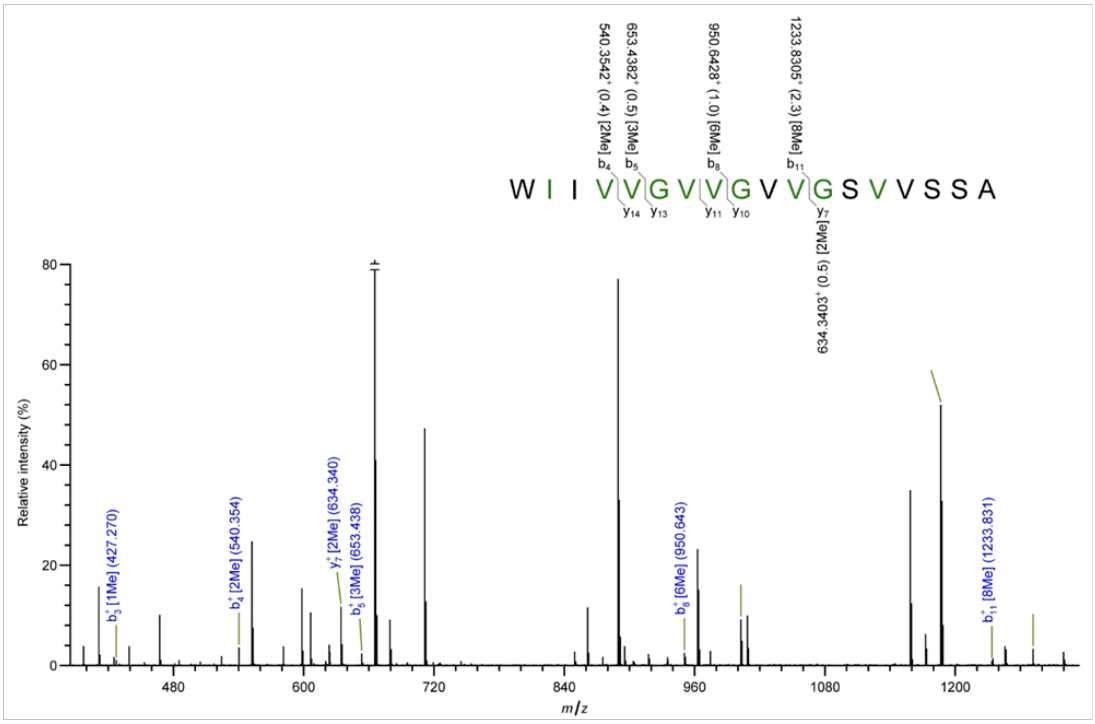
WIIVVGVVGVVGSVVSSA
540.3542+ (0.4) [2Me]
653.4382+ (0.5) [3Me]
950.6428+ (1.0) [6Me]
1233.8305+ (2.3) [8Me]
634.3403+ (0.5) [2Me]
Relative intensity (%)
m/z

p

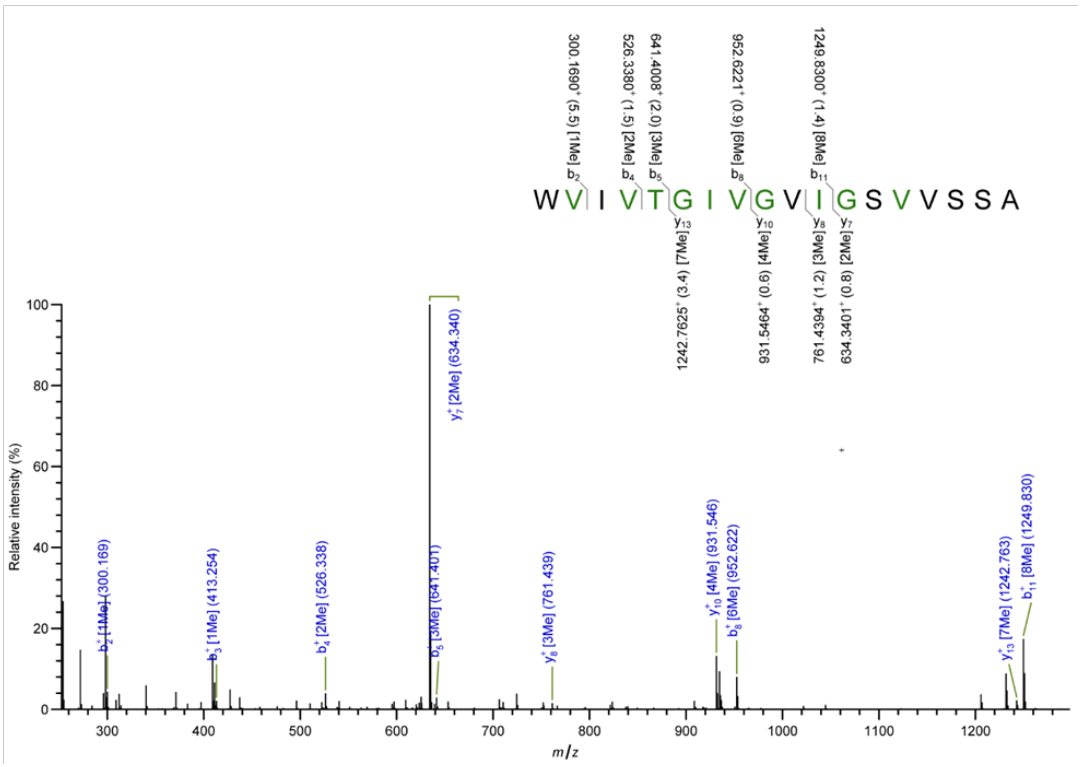
WVIVTGIVGVIGSVVSSA
300.1690+ (5.5) [1Me]
526.3380+ (1.5) [2Me]
641.4008+ (2.0) [3Me]
952.6221+ (0.9) [6Me]
1249.8300+ (1.4) [8Me]
1242.7625+ (3.4) [7Me]
931.5464+ (0.6) [4Me]
761.4394+ (1.2) [3Me]
634.3401+ (0.8) [2Me]
Relative intensity (%)
m/z

Figure 2-Figure supplement 3. HPLC-MS of peptide products. (a) Extracted ion chromatograms (EICs) of peptide products by the action of OphP on the Led-21mer and Dbi-21mer. Methylated residues are highlighted in a green color. (**b**) The EIC peak and mass spectra of the non-methylated Oph-21mer peptide. The core peptide is underlined.

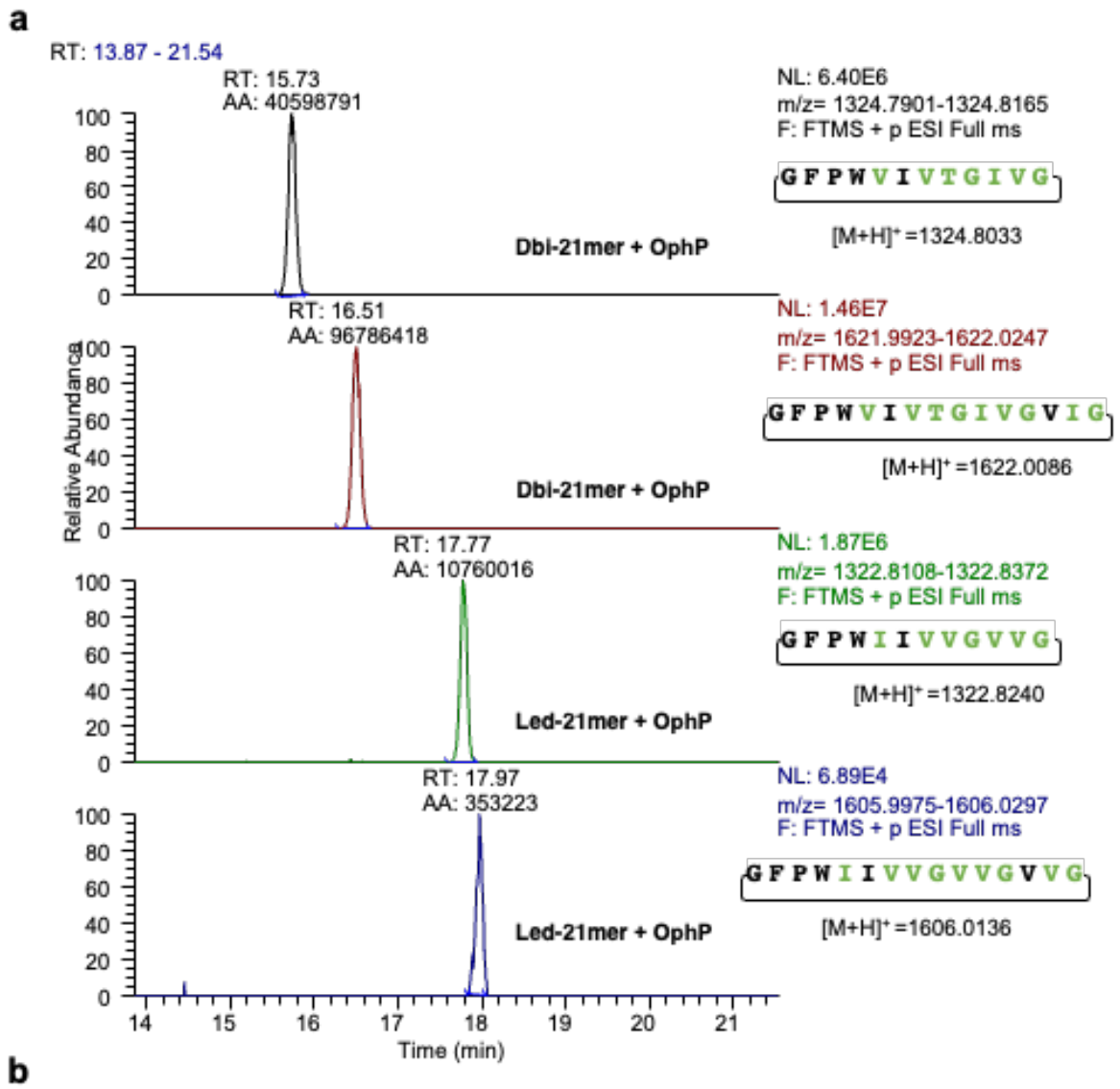

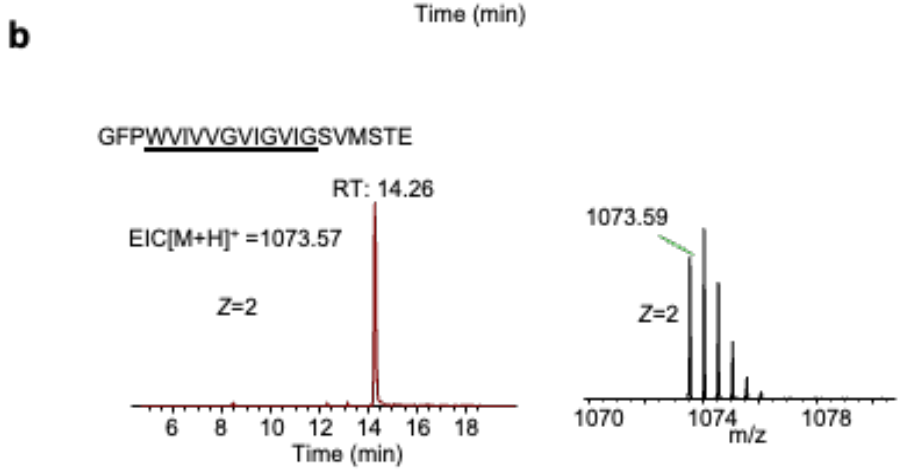

Figure 2-Figure supplement 4. Comparison of endopeptidase activities on the Oph-15mer peptide. (a) GmPOPB activity on the 15mer peptide as compared to OphP and LedP. (B) ProAlanase activity on the 15mer. The enzymatic activity was measured by UV absorbance at 280 nm.

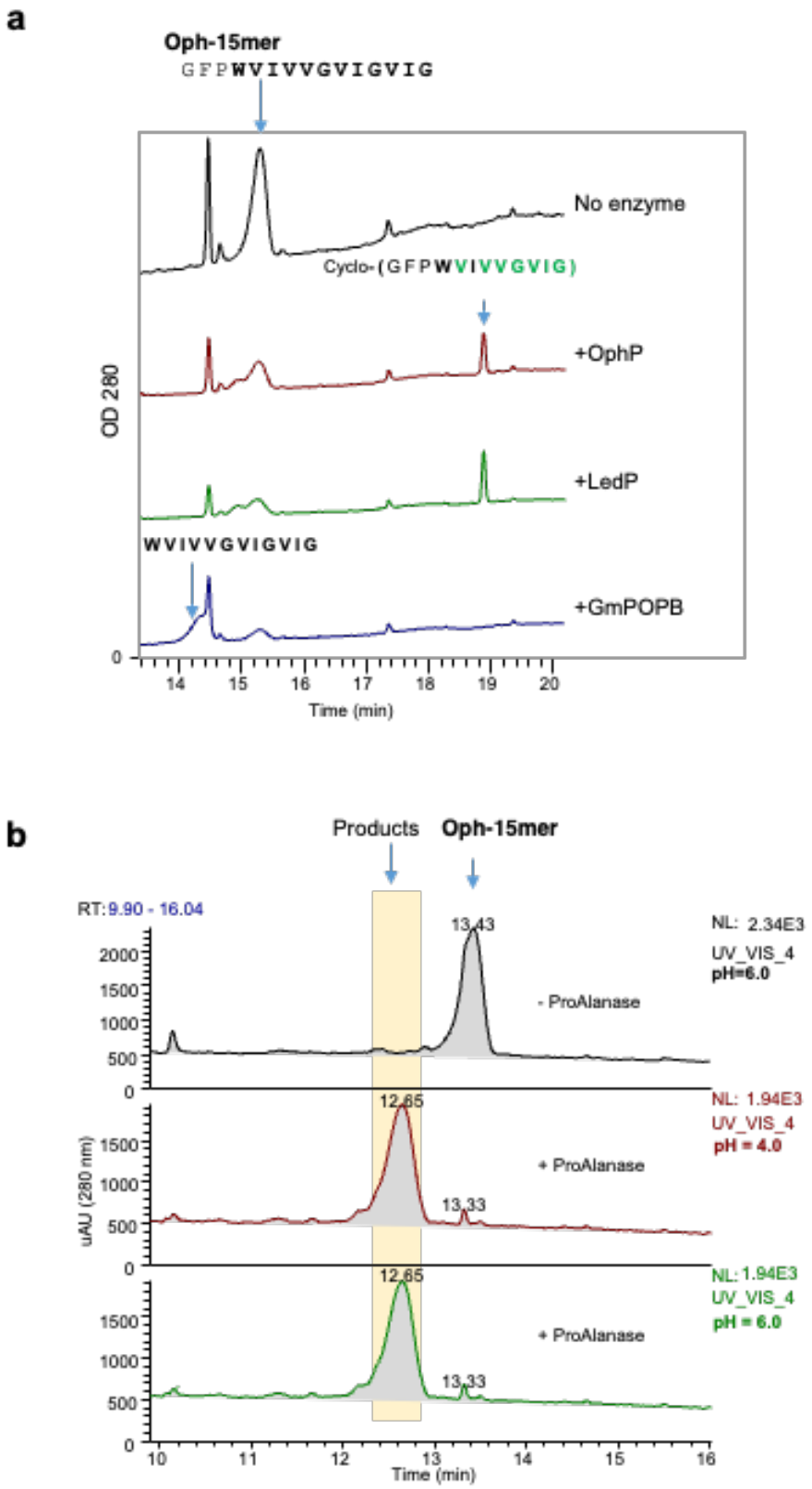

Figure 2-Figure supplement 5. ITC experiments of leader peptide (MPSSLLDAARESGEEASQNGFP), follower peptide (SVMSTE, and VIGSVMSTE), and 15mer. Leader peptide (**a**) and follower peptides (**b** and **c**) showed no binding up to 2 mM in the presence of 50 μM of S580A. 15mer binds to S580A with a K_D of 1.5 μM (**d**). The positive value of ΔH showed that the binding is endothermic suggesting the exclusion of water solvent during binding.

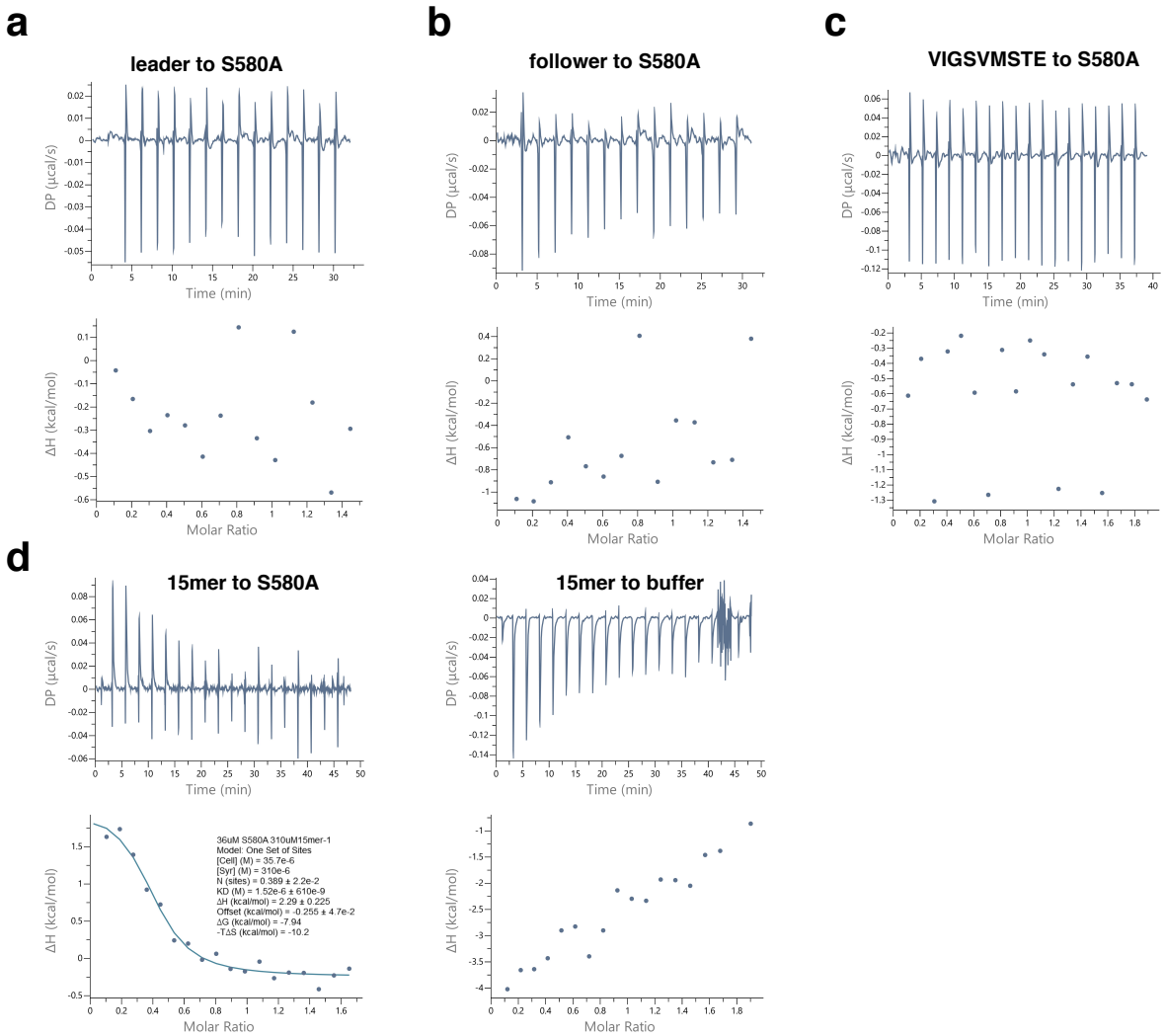

Figure 4-Figure supplement 1. Electrostatic surfaces of OphP, GmPOPB and PCY1 showing the central tunnel sizes. (**a-c**) Top view of the b-propeller domains of OphP, PCY1 (5O3U) and GmPOPB (5N4C). **(d-f)** Different views of the central tunnel of OphP focusing on the hydrophobic tunnel entrance and also a hydrophilic side cavity. Electrostatic calculation was performed using the APBS-PDB2PQR software suite[17] under the default setting and drawn in PyMol. The surface of the central tunnel cavity of OphP is calculated with the program Hollow[18] using default parameters and the central axes of the cylinder (radius of 22 Å) are defined by the Ca atoms of Met171 (offset 0 Å) and Ser384 (offset -5.0 Å). The electrostatic potential for all the figures is set at ± 3 kT/e.

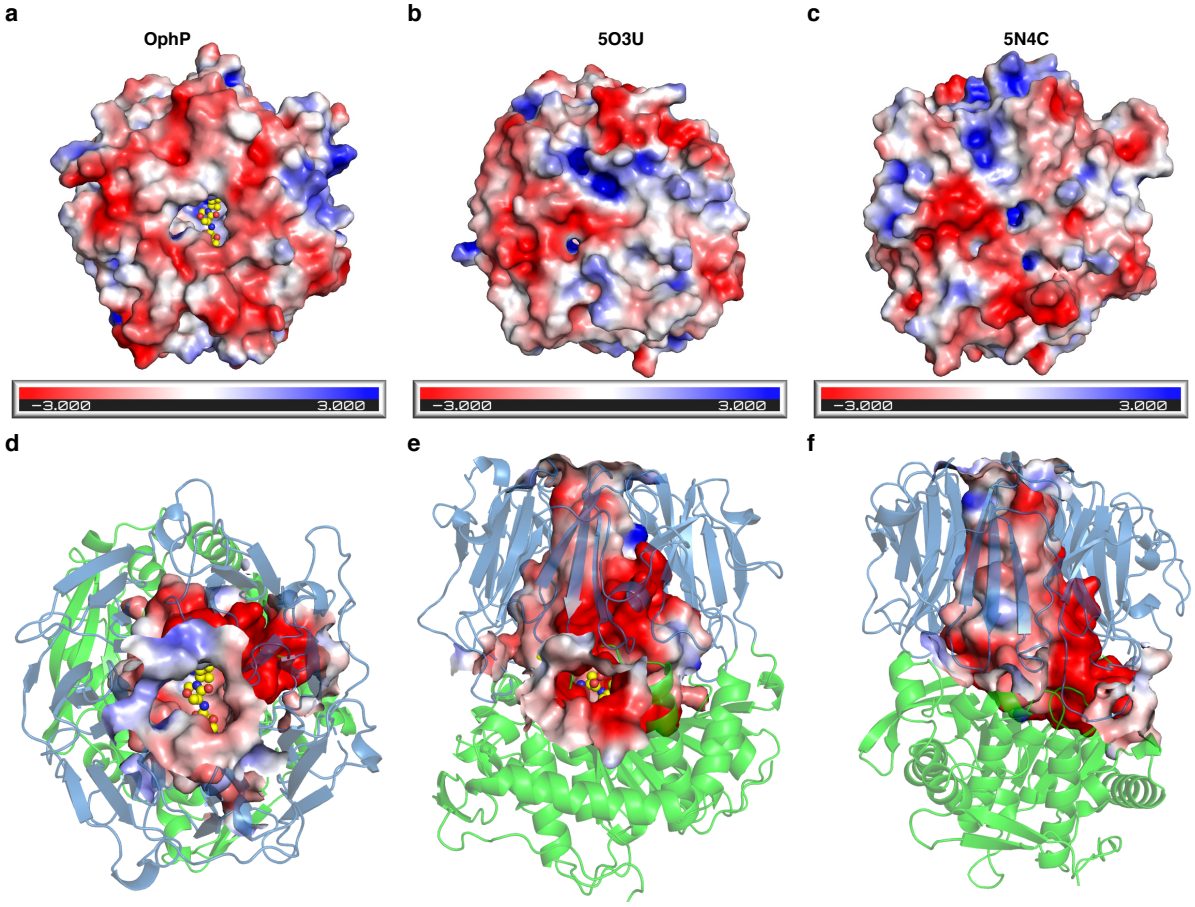

Figure 4-Figure supplement 2. Crystal structure of the OphP-ZPP covalent inhibitor complex. (a) Overall structure of the OphP-ZPP complex (b) σ_A-weighted electron density map (2mFo-DFc map contoured at 1 σ) showing the S580-acyl intermediate. (c). Superimposition of apo S580A (subunit A and H which have ordered loop region Leu697-Thr707) with OphP:ZPP complex (subunit A). The alignment shows the movement of two loops (Ser164-Met171, and Leu697-Thr707) with a salt bridge formed between D156 and R667 upon ZPP bound.

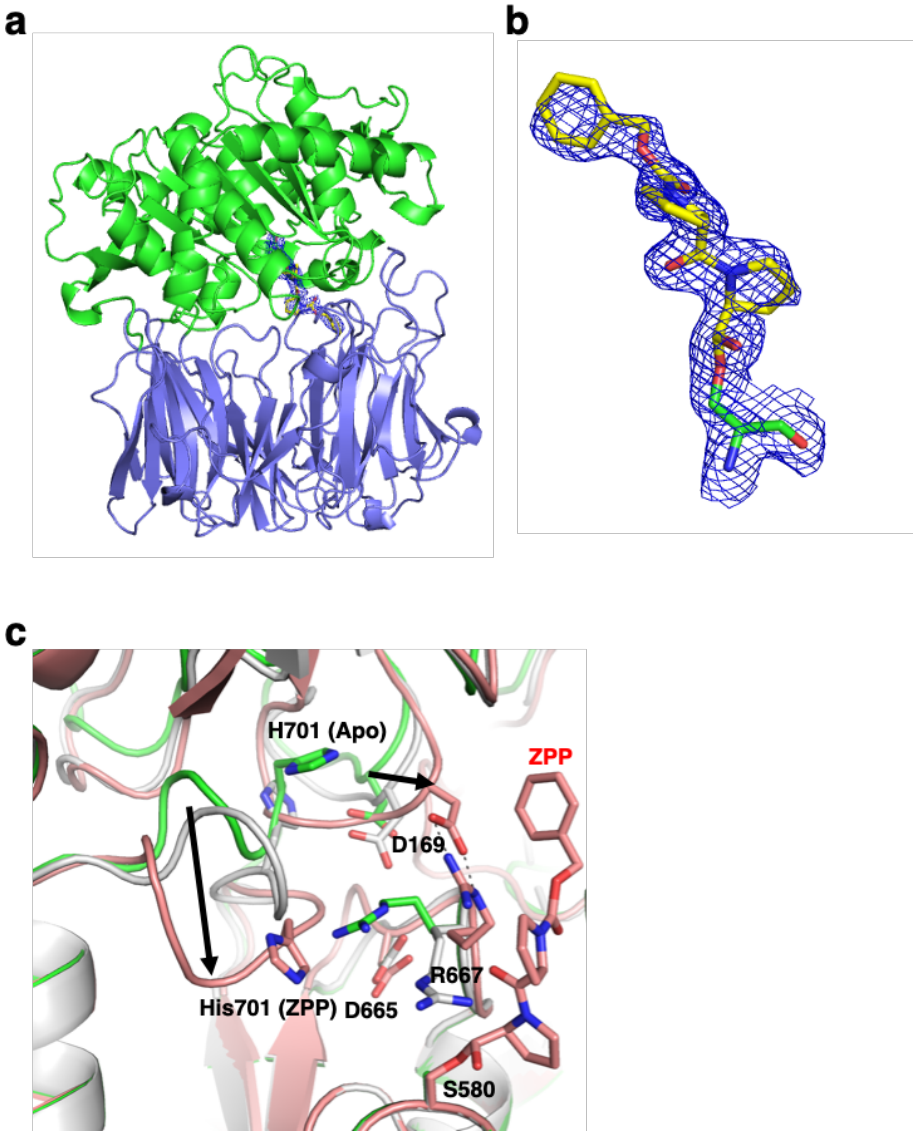

Figure 4-Figure supplement 3. Multiple sequence alignment of OphP with post-proline cleaving prolyl oligopeptidases (POPs). The sequence of OphP is used as a query and blasted (protein-protein BLAST) against the UniProtKB/SwissProt database. Sequences are further selected by removing all the dipeptidyl peptidase family enzyme sequences. Multiple sequence alignment was created with MUSCLE [15] and rendered as white and black with ESPript 3.0[16]. The hydrophobic pocket residues accommodating P1 proline are highlighted by underlying solid red triangles and catalytic triad residues are shown in solid purple triangles. Secondary structure elements of OphP are depicted above the aligned sequence. Black box with white character shows strict identity, bold black character similarity, and black frame similarity across groups. Names, UniProt ID and corresponding organisms are as follows: PCY1, R4P353, *Gypsophila vaccaria*; GmPOPB, H2E7Q8, *Galerina marginate*; GmPOPA, H2E7Q7, *Galerina marginate*; AbPOPB, E2JFG2, *Amanita bisporigera*; AbPOPA, E2JFG1, *Amanita bisporigera*; PfuPOP, Q51714 (PDB entry 5T88), *Pyrococcus furiosus*; AhPOP, Q06903, *Aeromonas hydrophila*; EmPOP1, P27028, *Elizabethkingia meningoseptica*; EmPOP2, P27195, *Elizabethkingia meningoseptica*; DbPOP, Q86AS5, *Dictyostelium discoideum*; MmPOP, Q9QUR6, *Mus musculus*; P48147, *Homo sapiens*; BtPOP, Q9XTA2, *Bos taurus*; SsPOP, P23687 (PDB entry 1QFS), *Sus scrofa*. Sequence of DbiP from *Dendrothele bispora* is retrieved from Joint Genome Institute website (name: gm1.24165_g, protein ID: 871165, location: scaffold_621:21283-24607). The sequence of LedP from *Lentinula* edodes is obtained from NCBI database (GAW09065).

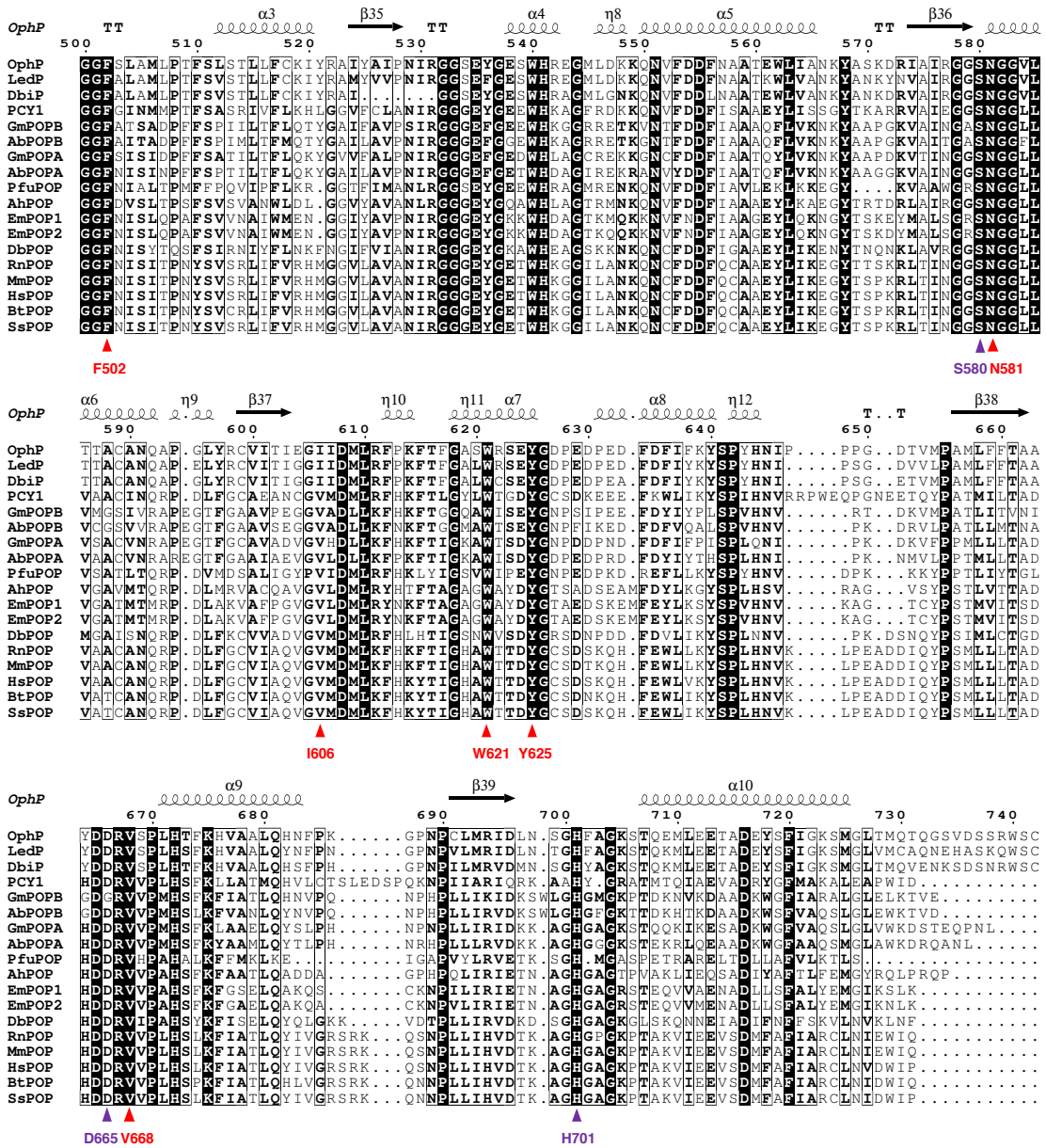
OphP
α3
β35
α4
η8
α5
β36
500 510 520 530 540 550 560 570 580
OphP
LedP
DbiP
PCY1
GmPOPB
AbPOPB
GmPOPA
AbPOPA
PfuPOP
AhPOP
EmPOP1
EmPOP2
DbPOP
RnPOP
MmPOP
HsPOP
BtPOP
SsPOP
F502
S580 N581
α6
η9
β37
η10
η11
α7
α8
η12
β38
590 600 610 620 630 640 650 660
I606
W621 Y625
α9
β39
α10
670 680 690 700 710 720 730 740
D665 V668
H701
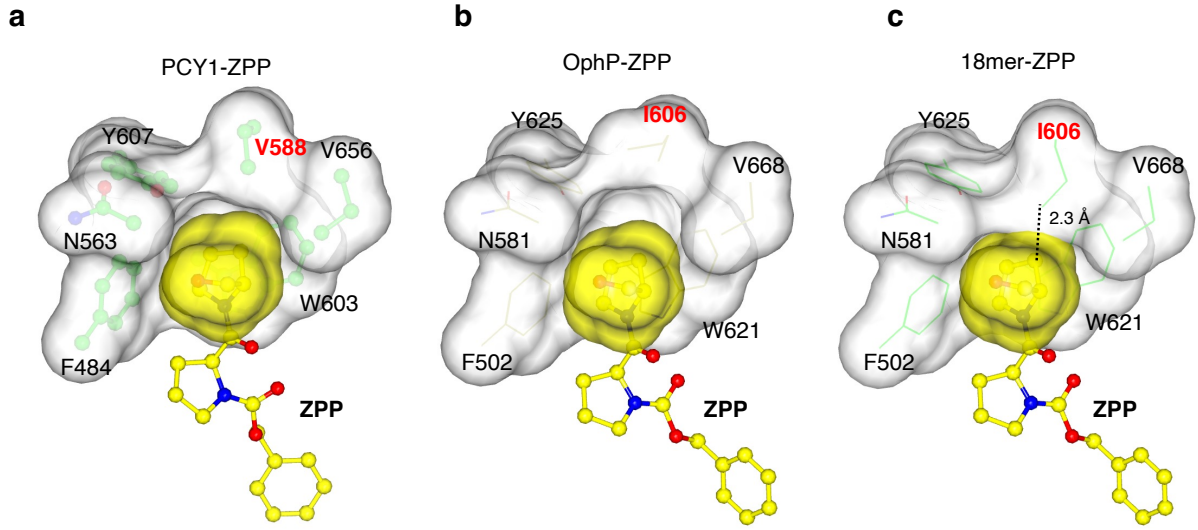
Figure 5-Figure supplement 1. Surface of P1 pocket accommodating the serine acyl intermediate for PCY1 and OphP. (**a**) The canonical P1 pocket of PCY1 can accommodate proline well at the cleavage P1 site. (**b**) Presence of covalently linked ZPP results in flipped Ile606. P1 pocket becomes larger to accommodate proline of ZPP. Flipped Ile606 clashes with Val584 with a 2.8 Å distance. (**c**) Surface showing clash between the proline of ZPP and Ile606. Cδ of I606 is only 2.3 Å away from Cβ of proline.